

Lawrence Berkeley National Laboratory

Recent Work

Title

EXPERIMENTS ON CHARGE IMBALANCE IN SUPERCONDUCTORS

Permalink

<https://escholarship.org/uc/item/9sz5c30g>

Author

Clarke, J.

Publication Date

1984-02-01

c. 2



Lawrence Berkeley Laboratory

UNIVERSITY OF CALIFORNIA

Materials & Molecular Research Division

RECEIVED
LAWRENCE
BERKELEY LABORATORY

NOV 1 1984

LIBRARY AND
DOCUMENTS SECTION

To be published as a chapter in Nonequilibrium
Superconductivity, Langenberg and Larkin, Eds.,
North-Holland Publishers

EXPERIMENTS ON CHARGE IMBALANCE IN SUPERCONDUCTORS

J. Clarke

February 1984

TWO-WEEK LOAN COPY
*This is a Library Circulating Copy
which may be borrowed for two weeks.*



LBL-17388
c. 2

DISCLAIMER

This document was prepared as an account of work sponsored by the United States Government. While this document is believed to contain correct information, neither the United States Government nor any agency thereof, nor the Regents of the University of California, nor any of their employees, makes any warranty, express or implied, or assumes any legal responsibility for the accuracy, completeness, or usefulness of any information, apparatus, product, or process disclosed, or represents that its use would not infringe privately owned rights. Reference herein to any specific commercial product, process, or service by its trade name, trademark, manufacturer, or otherwise, does not necessarily constitute or imply its endorsement, recommendation, or favoring by the United States Government or any agency thereof, or the Regents of the University of California. The views and opinions of authors expressed herein do not necessarily state or reflect those of the United States Government or any agency thereof or the Regents of the University of California.

EXPERIMENTS ON CHARGE IMBALANCE IN SUPERCONDUCTORS

John Clarke

Department of Physics
University of California
Berkeley, California 94720

and

Materials and Molecular Research Division
Lawrence Berkeley Laboratory
Berkeley, California 94720

CONTENTS

1. INTRODUCTION
2. THEORY OF CHARGE IMBALANCE
 - 2.1 Quasiparticle Charge and Charge Imbalance
 - 2.2 Tunneling Generation and Detection of Charge Imbalance
 - 2.3 Charge Imbalance Relaxation via Electron-Phonon Scattering
3. EXPERIMENTS ON TIN
4. EXPERIMENTS ON ALUMINUM
 - 4.1 Charge Relaxation via Elastic Scattering from Non-Magnetic Impurities
 - 4.2 Inelastic Scattering in Aluminum
5. CHARGE RELAXATION IN THE PRESENCE OF MAGNETIC IMPURITIES OR A SUPERCURRENT
 - 5.1 Elastic Scattering from Magnetic Impurities
 - 5.2 Elastic Scattering in the Presence of a Supercurrent
6. RESISTANCE OF THE NORMAL METAL-SUPERCONDUCTOR INTERFACE
7. PHASE-SLIP CENTERS
8. CHARGE IMBALANCE INDUCED BY A TEMPERATURE GRADIENT
 - 8.1 Thermoelectric Generation of Charge Imbalance at a NS Interface
 - 8.2 Spatial Dependence of Charge Imbalance Induced by a Temperature Gradient Near a Superconducting Boundary
 - 8.3 Supercurrent-Induced Charge Imbalance in the Presence of a Temperature Gradient
9. DYNAMICAL CHARGE IMBALANCE
10. CONCLUDING SUMMARY

1. INTRODUCTION

When a disequilibrium is created between the electron-like and hole-like excitations in a superconductor, a charge imbalance, Q^* , is created. Charge imbalance is of practical interest first, because it can be used to explain a wide variety of nonequilibrium processes that occur in superconductors, and, second, because it provides a valuable tool for measuring various electron-relaxation rates, most notably the electron-phonon scattering rate. The importance of the disequilibrium of the electron- and hole-like branches was first realized by Pippard et al. (1971) in their explanation of the excess resistance associated with the normal metal-superconductor (NS) boundary. However, the first quantitative understanding of charge imbalance was put forward by Tinkham and Clarke (1972) to explain the results of experiments in which electrons were injected via a tunnel junction into superconducting tin films (Clarke 1972). Among other results, these authors showed that the charge imbalance relaxation rate, $\tau_{Q^*}^{-1}$, due to inelastic scattering was of order $\tau_E^{-1}[\Delta(T)/k_B T]$ near T_c , where τ_E^{-1} is the electron-phonon scattering rate at T_c and at the Fermi energy.

The first detailed paper on the theory of charge imbalance was that of Tinkham (1972): This article laid the groundwork for a great deal of the subsequent theoretical development. The next major theoretical article was that of Schmid and Schön (1975) who used a Green's function approach to distinguish two different nonequilibrium modes, a transverse mode, in which the quasiparticle populations on the two branches differ (charge imbalance), and a longitudinal mode, in which the quasiparticle population on the two branches is equal but out of equilibrium, thereby modifying the energy gap, $\Delta(T)$. Subsequently, Pethick and Smith (1979a)

introduced a two-fluid approach to relaxation and collective motion in superconductors. This approach is conceptually simple, and produces the same results as the Schmid-Schön theory in the limit $\Delta(T)/k_B T \ll 1$ in which both theories are valid.

The purpose of the present chapter is to describe experiments in which charge imbalance plays a central role in our understanding of the physical mechanisms that are involved. It is, of course, necessary to present a theoretical framework, which appears in Sec. 2; however, I have given a minimum of theoretical discussion throughout the paper, but instead have quoted results and listed appropriate references. Section 3 describes the early work on Sn from which it was possible to extract an accurate value for τ_E^{-1} . Section 4 outlines work on Al in which both elastic scattering in the presence of gap anisotropy and electron-electron scattering may also relax charge imbalance. Section 5 is concerned with charge relaxation via elastic scattering in the presence of magnetic impurities or of a supercurrent. This section concludes the discussion of charge imbalance that has been generated by tunnel injection. Section 6 deals with the resistance of the NS interface in terms of charge imbalance, while Sec. 7 describes phase slip centers. Section 8 is concerned with charge imbalance in the presence of a temperature gradient in three different types of experiment: The voltage induced across a NS interface, the spatially decaying charge imbalance induced near the end of a superconducting film, and the charge imbalance induced by a uniform supercurrent. While all of the topics above are concerned with steady state charge imbalance, it is also possible to consider dynamic effects, such as the response to an impulse or fluctuations. Section 9 briefly describes such effects. Finally, Sec. 10 contains some

concluding remarks.

I should emphasize that this chapter is not an exhaustive account of charge imbalance phenomena, nor is the list of references by any means complete. However, I have attempted to list enough references to enable interested readers to find their way into the literature. Parts of this work have been published in an earlier review (Clarke 1981).

2. THEORY OF CHARGE IMBALANCE

In this section we outline the concepts of quasiparticle charge and charge imbalance, the generation and detection of charge imbalance by tunneling, and the relaxation of charge imbalance via electron-phonon scattering. The discussion follows the work of Tinkham and Clarke (1972), Tinkham (1972), Waldram (1975), Pethick and Smith (1979a), and Kadin et al. (1980).

2.1 Quasiparticle Charge and Charge Imbalance

We begin by considering the total electronic charge, Q_{tot} , in a superconductor, the overall charge at frequencies far below the plasma frequency being maintained at zero by the equal and opposite charge of the ion cores. From the BCS theory (Bardeen et al. 1957) we have

$$Q_{\text{tot}} = \frac{2}{\Omega} \sum_{\mathbf{k}} [u_{\mathbf{k}}^2 f_{\mathbf{k}} + v_{\mathbf{k}}^2 (1 - f_{-\mathbf{k}})], \quad (2.1)$$

where the sum is over \mathbf{k} states above and below k_F , and the factor of 2 arises from the sum over spin. In Eq. (2.1), Ω is the volume of the superconductor, and $f_{\mathbf{k}}$ is the occupancy of the state \mathbf{k} , which, in thermal equilibrium, is the Fermi function. The $u_{\mathbf{k}}$ and $v_{\mathbf{k}}$ are the usual BCS factors given by

$$u_{\mathbf{k}}^2 = \frac{1}{2}(1 + \xi_{\mathbf{k}}/E_{\mathbf{k}}) \quad (2.2)$$

and

$$v_{\mathbf{k}}^2 = \frac{1}{2}(1 - \xi_{\mathbf{k}}/E_{\mathbf{k}}), \quad (2.3)$$

where

$$\xi_k = \frac{\hbar^2 k^2}{2m} - \mu_s \quad (2.4)$$

is the kinetic energy of the electron of mass m in the state k referred to the chemical potential of the superfluid, μ_s , and

$$E_k = (\Delta^2 + \xi_k^2)^{1/2} \quad (2.5)$$

is the quasiparticle excitation energy. The energy E_k is positive for all values of k , while ξ_k is positive for $k > k_F$ and negative for $k < k_F$. The quantity v_k^2 is the probability that the state k is occupied by a Cooper pair, while $u_k^2 = 1 - v_k^2$ is the probability that the state k is unoccupied by a Cooper pair.

We can regard Eq. (2.1) as the sum of a superfluid contribution

$$Q_s = \frac{2}{\Omega} \sum_k v_k^2 \quad (2.6)$$

and a quasiparticle contribution

$$Q^* = \frac{2}{\Omega} \sum_k (u_k^2 - v_k^2) f_k = \frac{2}{\Omega} \sum_k q_k f_k, \quad (2.7)$$

where we have set $f_{-k} = f_k$. In Eq. (2.7) we have introduced the very important concept of the effective quasiparticle charge

$$q_k = u_k^2 - v_k^2 = \xi_k / E_k, \quad (2.8)$$

and defined the charge imbalance per unit volume, Q^* , which is the central subject of this chapter. We note that $q_k \rightarrow +1$ for $\xi_k \gg \Delta$ ($k > k_F$), and $q_k \rightarrow -1$ for $\xi_k \ll -\Delta$ ($k < k_F$). It is evident in Eq. (2.7) that if $f_k(\xi_k)$ is the Fermi function, which is even in ξ_k about μ_S , the quasiparticle charge, Q^* , is zero since q_k is odd in ξ_k . Thus, the total electronic charge is $(2/\Omega)\sum_k v_k^2$ at all temperatures, as we expect.

We now turn to a non-equilibrium situation in which f_k is no longer the Fermi function. In this case, Q^* may be non-zero and μ_S shifted from its equilibrium value, the Fermi energy, by an amount $\delta\mu_S$. As we shall see, Q^* and $\delta\mu_S$ are intimately related. As an example, suppose that we add excitations to the $k > k_F$ quasiparticle branch in a particular region of the superconductor. Overall charge neutrality will ensure that pairs with an equivalent charge are removed from the region. Thus, the chemical potential of the pairs must decrease by an amount $\delta\mu_S$, as indicated in Fig. 1(a). At the same time, the excitation spectrum shifts because its minimum still occurs at the pair chemical potential, as shown in Fig. 1(b). The effective quasiparticle charge is still $q_k = \xi_k/E_k$, but ξ_k is now referred to the shifted chemical potential, $\mu_S - \delta\mu_S$. Thus, the addition of a single electron-like excitation induces some quasiparticles near the bottom of the excitation spectrum to cross branches, producing a small increase in the charge of all the electron-like quasiparticles, and a small decrease in the charge of all the hole-like quasiparticles.

The quantities Q^* and $\delta\mu_S$ are related as follows. By charge neutrality

$$Q^* + Q_S|_{\delta\mu_S \neq 0} = \frac{2}{\Omega} \sum_k v_k^2 |_{\delta\mu_S = 0}, \quad (2.9)$$

or

$$Q^* = \frac{2}{-} \sum_k (v_k^2 |_{\delta\mu_S=0} - v_k^2 |_{\delta\mu_S \neq 0}). \quad (2.10)$$

Now the reduction in the number of pairs represented by the right hand side of Eq. (2.10) is just $2N(0)\delta\mu_S$, where $N(0)$ is the single-spin density of states per unit volume at the Fermi energy. Thus

$$Q^* = - 2N(0)\delta\mu_S. \quad (2.11)$$

We see that Eq. (2.1) is really a self-consistent equation for μ_S : Given any distribution, f_k , the constancy of Q_{tot} determines μ_S .

In the steady state with Q^* continuously injected at a rate \dot{Q}_i^* , the excess distribution relaxes at a rate $\tau_{Q^*}^{-1}$ to produce a steady state charge imbalance Q^* . Thus

$$\tau_{Q^*}^{-1} = \dot{Q}_i^*/Q^*. \quad (2.12)$$

The relaxation of Q^* may occur through both inelastic and elastic processes, as we discuss in Secs. (2.3) and (4).

2.2 Tunneling Generation and Detection of Charge Imbalance

We follow closely the approach developed by Tinkham (1972) and Pethick and Smith (1979a) to calculate the charge imbalance generated in a superconductor (S) by quasiparticle tunnel injection from a normal metal (N), and the voltage induced by this charge imbalance across a second NIS tunnel junction at zero bias current.

When a NIS junction is biased at a voltage V , the rate at which qua-

particles are injected into the state k of the superconductor is

$$\begin{aligned} \dot{f}_k|_i &= \frac{2\pi}{\hbar} |T|^2 \mathcal{N}_n(0) [u_k^2 f^0(E_k - eV) + v_k^2 f^0(E_k + eV) - f_k] \\ &= \frac{2\pi}{\hbar} |T|^2 \mathcal{N}_n(0) \left\{ \frac{1}{2} [f^0(E_k + eV) + f^0(E_k - eV)] - f_k \right. \\ &\quad \left. + \frac{1}{2} q_k [f^0(E_k - eV) - f^0(E_k + eV)] \right\}. \end{aligned} \quad (2.13)$$

Here, $|T|^2$ is the square of the tunneling matrix element, assumed to be independent of energy, and $\mathcal{N}_n(0)$ is the single-spin density of states in the volume of the metal. The Fermi functions $f^0(E_k \pm eV)$ refer to the normal metal, while f_k is the actual distribution in the superconductor, which is not, in general, the Fermi distribution.

We convert Eq. (2.13) into an expression for the rate of quasiparticle charge injection by multiplying by q_k and summing over k . Noting that only even terms contribute, we find

$$\dot{Q}_i^* = \frac{2\pi}{\hbar\Omega} |T|^2 \mathcal{N}_n(0) \sum_k q_k^2 [f^0(E_k - eV) - f^0(E_k + eV)]. \quad (2.14)$$

We have neglected the small contribution of the even part of $q_k f_k$ since the voltages generated by the nonequilibrium distribution are very small compared with the injection voltage. It is convenient to write Eq. (2.14) in the integral form:

$$\begin{aligned} \dot{Q}_i^* &= \frac{4\pi}{\hbar\Omega} |T|^2 \mathcal{N}_n(0) \mathcal{N}_s(0) \int_0^\infty \frac{\xi^2}{E^2} [f^0(E - eV) - f^0(E + eV)] d\xi \\ &= \frac{G_{NN}}{e^2 \Delta} \int_{-\infty}^\infty \rho^{-1}(E) [f^0(E - eV) - f^0(E + eV)] dE, \end{aligned} \quad (2.15)$$

where we have used $d\xi = (E/\xi)dE$. In Eq. (2.15), $\mathcal{N}(0)$ is the single-spin density of states in the volume of the superconductor when it is in the normal state, $\rho(E) = E/(E^2 - \Delta^2)^{1/2} = E/|\xi| = |q_k^{-1}|$ ($E > \Delta$) is the normalized BCS density of states in the superconductor, and $G_{NN} = 4\pi e^2 |T|^2 \times \mathcal{N}_n(0)\mathcal{M}(0)/\mathcal{N}$ is the conductance of the tunnel junction when the superconductor is in the normal state.

We can obtain an expression for the net current injected into a superconductor from a normal metal from Eq. (2.13). Summing over k and simplifying, we find

$$I = \frac{2\pi e}{\hbar} |T|^2 \mathcal{N}_n(0) \sum_k [f^0(E_k - eV) - f^0(E_k + eV) - 2q_k \delta f_k]. \quad (2.16)$$

where $\delta f_k = f_k - f^0$. We note that the E_k in f^0 are referred to the modified chemical potential. [Pethick and Smith (1979a) denote this f^0 by $f^0(1.e)$, where "1.e." means local equilibrium; our δf_k is precisely the same as their $\delta f_k^{1.e.}$.] For any injection voltage of practical interest the last term in Eq. (2.16) is negligible, and we can write I in the integral form:

$$\begin{aligned} I &= \frac{4\pi e}{\hbar} |T|^2 \mathcal{N}_n(0)\mathcal{M}(0) \int_0^\infty [f^0(E-eV) - f^0(E+eV)] d\xi \\ &= \frac{G_{NN}}{e} \int_\Delta^\infty \rho(E) [f^0(E-eV) - f^0(E+eV)] dE. \end{aligned} \quad (2.17)$$

We will find it useful to obtain an expression for Eq. (2.17) in the limit $eV \ll k_B T$ in which we can expand the Fermi functions to give $f^0(E \pm eV) = f^0(E) \pm [\partial f^0(E)/\partial E]eV$. This approximation leads to

$$I = G_{NN} \int_{\Delta}^{\infty} 2\rho(E) \left(- \frac{\partial f^{\circ}(E)}{\partial E} \right) V dE. \quad (eV \ll k_B T) \quad (2.18)$$

Since the conductance, G_{NS} , is just I/V , we obtain the reduced tunneling conductance for $eV/k_B T \rightarrow 0$, $g_{NS}(0) = G_{NS}(0)/G_{NN}$:

$$g_{NS}(0) \equiv Y(T) = 2 \int_{\Delta}^{\infty} \rho(E) \left(- \frac{\partial f^{\circ}(E)}{\partial E} \right) dE, \quad (2.19)$$

where $Y(T)$ is the Yoshida function.

We are now in a position to calculate the voltage generated by the steady state charge imbalance as measured by a second tunneling contact to a normal metal. This voltage, V_d , referred to the equilibrium chemical potential of the superconductor far away from the injected region is measured with zero current flowing through the detector junction. Since Eq. (2.16) is equally true for the injection and detection junctions, we can set $I = 0$, and use the low voltage expansion of the Fermi functions to obtain

$$V_d = \frac{2 \sum q_k f_k}{2e \sum [-\partial f^{\circ}(E)/\partial E]} = \frac{Q^*}{2N(0) e g_{NS}(0)}. \quad (2.20)$$

We have thus found a simple relation between Q^* or, equivalently, $-2N(0)\delta\mu_s$, and the voltage measured by the detector junction. If the detector junction does not show the ideal BCS behavior, one should use the measured normalized conductance in Eq. (2.20), rather than the BCS value.

To complete our description of tunneling generation and detection of

charge imbalance we combine Eqs. (2.12), (2.15), (2.17), and (2.20) so that we can deduce $\tau_{Q^*}^{-1}$ in terms of measureable or precisely calculable quantities. To do this, it is convenient to introduce the parameter F^* that enables us to express \dot{Q}_i^* in terms of the injection current I_i :

$$F^* = e \Omega \frac{\dot{Q}_i^*}{I_i} = \frac{\int_{\Delta}^{\infty} \rho^{-1}(E) [f^0(E - eV_i) - f^0(E + eV_i)] dE}{\int_{\Delta}^{\infty} \rho(E) [f^0(E - eV_i) - f^0(E + eV_i)] dE}. \quad (2.21)$$

We have used V_i to denote the injection voltage. From Eqs. (2.12), (2.20) and (2.21) we find

$$\tau_{Q^*}^{-1} = \frac{\dot{Q}_i^*}{Q^*} = \frac{F^* I_i}{2N(0) e^2 \Omega g_{NS}(0) V_d}. \quad (2.22)$$

The quantity F^* is readily calculable, while the quantities, I_i , Ω , $g_{NS}(0)$, and V_d are the quantities measured in the experiment.

In the limit of low injection voltages, $eV_i \ll k_B T$, the Fermi functions in Eq. (2.21) may be expanded to yield

$$F^* = Z(T)/Y(T), \quad (eV_i \ll k_B T) \quad (2.23)$$

where

$$Z(T) \equiv 2 \int_{\Delta}^{\infty} \rho^{-1}(E) \left(- \frac{\partial f^0(E)}{\partial E} \right) dE. \quad (2.24)$$

However, this limit is not very useful for most practical experiments with tunneling injection, where the voltage is large compared with both $\Delta(T)/e$ and $k_B T/e$. In these limits, one obtains

$$F^* = 1 - \pi\Delta/2|eV_i|. \quad [eV_i \gg k_B T, eV_i \gg \Delta(T)] \quad (2.25)$$

For a typical injection voltage, $eV_i/\Delta = 30$, we find $F^* = 0.95$.

2.3 Charge Imbalance Relaxation via Electron-Phonon Scattering

When an electron-like excitation (for example) is injected into a superconductor, in general it not only creates a charge imbalance but also increases the energy of the quasiparticle distribution above the equilibrium value. Thus, the processes that restore thermal equilibrium involve both cooling and charge relaxation, but these are not necessarily distinct processes. For example, if the quasiparticle is injected at any energy well above both $k_B T$ and $\Delta(T)$, it may scatter with the emission of a phonon to a lower energy on the same quasiparticle branch. In this process, the quasiparticle has not only cooled, but also given up some of its charge because q_k has been reduced from its initial value near unity to a lower value. This kind of inelastic process is governed by the coherence factor (Tinkham 1975)

$$(uu' - vv')^2 = \frac{1}{2} \left(1 + \frac{\xi\xi' - \Delta^2}{EE'} \right). \quad (2.26)$$

A second means of phonon-mediated charge relaxation is by recombination, a process that is governed by the coherence factor (Tinkham 1975)

$$(vu' + uv')^2 = \frac{1}{2} \left(1 + \frac{\Delta^2 - \xi\xi'}{EE'} \right). \quad (2.27)$$

In addition to inelastic processes, elastic scattering from non-mag-

netic or magnetic impurities can also relax Q^* provided the quasiparticle changes branches. For the case of non-magnetic impurities in an isotropic superconductor, this process is strictly forbidden by the coherence factor in Eq. (2.26), as can be seen immediately by realizing that if E and E' refer to different branches, $u' = v$ and $v' = u$. On the other hand, the coherence factor does not vanish for scattering from non-magnetic impurities in the case of anisotropic superconductors, or from magnetic impurities even in the isotropic case. We defer a discussion of elastic processes until Secs. 4 and 5.

It is evident that the calculation of the charge imbalance rate is, in general, a very complicated undertaking. In the limit $\Delta(T) \ll k_B T$, and in the absence of elastic processes, the situation simplifies, and one finds (Tinkham 1972, Schmid and Schön 1975, Pethick and Smith 1979a)

$$(F^* \tau_{Q^*})^{-1} = (\pi \Delta / 4 k_B T) \tau_E^{-1} \quad [\Delta(T) \ll k_B T]. \quad (2.28)$$

In Eq. (2.28), τ_E^{-1} is the inelastic scattering rate at T_c for a quasiparticle at the Fermi energy; the rate actually increases with the energy of the quasiparticle, but we shall neglect this dependence. For the more general case when $\Delta(T)$ is not small, one must resort to numerical calculations. Chi and Clarke (1979, 1980) solved the Boltzmann equation on a computer to find both the steady state quasiparticle distribution and the charge imbalance relaxation rate for a wide range of temperature and several values of the injection voltage. We briefly summarize the results of these calculations.

The Boltzmann equation can be written in the form

$$\dot{f}_\xi = G_\xi - G_{in\xi} - G_{el\xi} . \quad (2.29)$$

The first term G_ξ is the rate of injection into ξ_k , while $G_{in\xi}$ and $G_{el\xi}$ are the inelastic and elastic rates at which quasiparticles scatter out of ξ_k ; for the moment we set $G_{el\xi} = 0$. In a steady state situation $\dot{f}_\xi = 0$. For tunneling from a normal metal into a superconductor the injection rate is given by the first line of Eq. (2.13) with the terms labeled with ξ rather than k :

$$G_\xi = [G_{NN}/2N(0)e^{2\Omega}] \left\{ \frac{1}{2} (1 + \xi/E) [f^0(E - eV_i) - f^0(E)] - \frac{1}{2} (1 - \xi/E) \right. \\ \left. \times [f^0(E) - f^0(E + eV_i)] \right\}. \quad (2.30)$$

We have used the Fermi distribution for the distribution functions, thereby assuming that departure from equilibrium is small. The inelastic scattering rate is proportional to $\alpha^2 F(\Omega)$, the average of the product of the square of the matrix elements for the electron-phonon interaction and the phonon density of states. We assume that $F(\Omega)$ is quadratic in Ω , and can be written in the form $F(k_B T_c / \hbar) (\Omega / k_B T_c)^2$. With this assumption, $G_{in\xi}$ can be written down using the Golden Rule (Kaplan et al. 1976, Chang and Scalapino 1977, Chang 1979, CC):

$$G_{in\xi} = \frac{2\pi}{\hbar} \frac{\alpha^2 F(k_B T_c / \hbar)}{Z_1(0) (k_B T_c)^2} \int_{-\infty}^{\infty} d\xi' \times \\ \left[\left(1 - \frac{\xi\xi'}{EE'} + \frac{\Delta^2}{EE'} \right) (E+E')^2 \{ [1+n^0(E+E')] f_\xi f_{\xi'} - n^0(E+E') (1-f_\xi) (1-f_{\xi'}) \} \right]$$

$$\begin{aligned}
& +\frac{1}{2}\left(1+\frac{\xi\xi'}{EE'}-\frac{\Delta^2}{EE'}\right)(E-E')^2\Theta(E-E')\{[1+n^0(E-E')]f_{\xi}(1-f_{\xi'})-n^0(E-E')f_{\xi'}(1-f_{\xi})\} \\
& +\frac{1}{2}\left(1+\frac{\xi\xi'}{EE'}-\frac{\Delta^2}{EE'}\right)(E-E')^2\Theta(E'-E)\{n^0(E'-E)f_{\xi}(1-f_{\xi'})-[1+n^0(E'-E)]f_{\xi'}(1-f_{\xi})\}. \quad (2.31)
\end{aligned}$$

In Eq. (2.31), $Z_1(0)$ is the electron-phonon renormalization factor, typically about 2 for most metals, Θ is the Heaviside function, which is zero for negative arguments and unity for positive arguments, and $n^0(\Omega)$ is the Bose-Einstein distribution function for the phonons.

In solving the Boltzmann equation, it is convenient to write $f_{\xi} = f^0 + \delta f_{\xi}$, where f^0 is the Fermi function at energy $(\xi^2 + \Delta^2)^{1/2}$ and ξ is referred to the shifted chemical potential. We rewrite the equation in terms of even and odd components of δf_{ξ} , $(\delta f_{\xi} + \delta f_{-\xi})/2$ and $(\delta f_{\xi} - \delta f_{-\xi})/2$, make initial guesses for these components and iterate the Boltzmann equation until the solution is self-consistent. We calculate Q^* from $2N(0)\Sigma_{\xi}(\delta f_{\xi} - \delta f_{-\xi})$ and $\tau_{Q^*}^{-1}$ from \dot{Q}_I^*/Q^* , using Eq. (2.15).

Figure 2 shows the computed value of $[4k_B T \tau_E / \pi \Delta(T)] \tau_{Q^*}^{-1}$ vs. $\Delta(T)/k_B T$ for three injection voltages. At T_c , the computed value is precisely unity, but as the temperature is lowered, the function first increases and then decreases. At all temperatures below T_c , $\tau_{Q^*}^{-1}$ increases with injection voltage, reflecting the increase in the inelastic scattering rate with increasing energy. Figure 3 shows the computed temperature dependence of $\tau_{Q^*}^{-1}$ down to $0.3 T_c$ for two values of injection voltage. The relaxation rate goes through a peak and then decreases steadily as the temperature is lowered. It should be emphasized first, that the

time τ_E is itself strongly temperature dependent, and second, that in real superconductors elastic scattering in the presence of gap anisotropy is likely to increase the value of τ_Q^{-1} substantially at low temperatures. Finally, we note that according to Eq. (2.22) the measured voltage V_d is proportional to $F^* \tau_{Q^*} I_i$. In Fig. 4 we plot both τ_Q^{-1} and $(F^* \tau_{Q^*})^{-1}$ vs. $eV_i/\Delta(T)$. For $eV_i \gtrsim 6\Delta(T)$, we observe that $F^* \tau_{Q^*}$ becomes independent of V_i , and the V_d becomes linear in I_i .

This concludes our theoretical survey. We now move on to discuss experimental results.

3. EXPERIMENTS ON TIN

Historically, the first measurements of charge imbalance using tunneling injection were on Sn films, and it is convenient to begin with a discussion of these results because it is possible to obtain a temperature range in which the charge relaxation due to elastic scattering is negligible compared with that due to inelastic scattering (Clarke 1972, Clarke and Paterson 1974, Moody and Paterson 1979).

The configuration used in all tunneling injection experiments is shown in Fig. 5. After oxidizing the Al base electrode (XX'), typically 150 nm thick, one deposits a Sn electrode (YY'), 200 to 400 nm thick. An insulating layer of varnish or (in the later experiments) SiO₂ is used to mask off a window near the center of the injector junction. The Sn film is oxidized slightly, and a diagonal strip (ZZ') of CuAl (3wt.%Al) about 2 μm thick is evaporated to form the detector junction. To reduce the series resistance of the CuAl strip, it is covered with a Pb film; the Cu film is made sufficiently thick and dirty to eliminate Josephson tunneling between the Al and Pb films.

Typically, four samples were fabricated simultaneously on a single substrate, and the detector junctions were connected in series. The voltage across the junctions was measured with a null-balancing SQUID voltmeter (see, for example, Clarke 1976) that ensured that the detector voltage was measured at zero current. Each junction could be investigated independently by applying a current to the appropriate injector junction. The samples and SQUID were immersed in liquid helium, and carefully shielded against external magnetic field fluctuations. The current-voltage characteristics of both the injector and detector junc-

tions were determined: Typically, the injector junctions had a resistance of about 1Ω ($V_i > 2\Delta/e$), while the detector junctions were about $10^{-5} \Omega$. The conductance of the detector junctions was often in excess of the BCS prediction, but it was found that if one used the measured values of $g_{NS}(0)$ in Eqs. (2.22), different samples produced values of τ_{Q*}^{-1} in good agreement with each other.

In Fig. 6 we have plotted $g_{NS}(0)\Omega V_d/I_i = F^*\tau_{Q*}/2N(0)e^2$ vs. T/T_c for three Sn samples of different thicknesses, and one sample in which the Sn has been alloyed with 3wt.%In (Clarke and Paterson 1974). The mean free path in the pure Sn samples was boundary limited, while that in the alloy was estimated to be 42 nm. The fact that the data for the pure Sn samples lie on a smooth curve demonstrates that $F^*\tau_{Q*}$ scales with Ω . Near T_c , V_d/I_i , which is proportional to $F^*\tau_{Q*}$ increases rapidly with increasing temperature. The solid line in Fig. 6 is a fit of the curve $g_{NS}(0)\Omega V_d/I_i = 4.0 \times 10^{-14} k_B T_c / \Delta(T) \Omega \text{ cm}^3$ to the data at high temperatures. Using the value $N(0) = 1.39 \times 10^{22} \text{ eV}^{-1} \text{ cm}^{-3}$ [computed from $N(0) = 3\gamma/2\pi^2 k_B^2$, where γ is the coefficient of the electronic heat capacity taken from Kittel (1976)] in Eq. (2.22) we find $(F^*\tau_{Q*})^{-1} = 5.6 \times 10^9 (\Delta/k_B T_c) \text{ s}^{-1}$. Equating this value with the prediction of Eq. (2.28), we find $\tau_E = 1.4 \times 10^{-10} \text{ s}$.

Below $T/T_c = 0.95$, $F^*\tau_{Q*}$ is larger for the SnIn sample than for the Sn samples. This difference arises from the contribution of elastic charge relaxation in the clean samples, a topic that we consider in the following section.

4. EXPERIMENTS ON ALUMINUM

4.1 Charge Relaxation via Elastic Scattering from Non-Magnetic Impurities

The coherence factor $(uu' - vv')^2$ forbids charge relaxation via elastic scattering when the energy gap is isotropic. However, in the presence of gap anisotropy a quasiparticle may be scattered between two regions of the Fermi surface at which the energy gap is different, so that the coherence factor is no longer zero. This situation was first discussed by Tinkham (1972), and subsequently by Chi and Clarke (1979) using a computer solution of the Boltzmann equation. We briefly outline the latter treatment.

The elastic scattering rate $G_{el\xi}$ that appears in the Boltzmann equation [Eq. (2.29)] is given by

$$G_{el\xi} = \frac{\tau_1^{-1}}{2} \left\langle \rho_{\Delta'}(E) \left[1 - \frac{\Delta\Delta'}{E^2} - \left(1 - \frac{\Delta^2}{E^2} \right)^{1/2} \left(1 - \frac{\Delta'^2}{E^2} \right)^{1/2} \right] \right\rangle_{\Delta, \Delta'} [f_{\xi}(1 - f_{\xi'}) - f_{\xi'}(1 - f_{\xi})]. \quad (4.1)$$

Here, τ_1^{-1} is the elastic scattering rate of an electron when the metal is in the normal state, $\rho_{\Delta'}(E)$ is the final density of states, one-half times the first square bracket is the coherence factor, and the two terms in the second square bracket are the occupation factors for elastic scattering from ξ to ξ' and the reverse process, respectively. The symbol $\langle \rangle_{\Delta, \Delta'}$ indicates an angular average over the gap-anisotropy distribution. To first order, we can replace $\rho_{\Delta'}(E)$ with $\rho_{\bar{\Delta}}(E)$, where $\bar{\Delta}$ is the average energy gap. To average the coherence factor we express it in terms of the mean square gap anisotropy $\langle \delta^2 \rangle = \langle (\Delta - \bar{\Delta})^2 \rangle$. Neglecting terms of order $\langle \delta^2 \rangle^{1/2}/\bar{\Delta}$, one can write $\langle (uu' - vv')^2 \rangle = \langle \delta^2 \rangle / 2(E^2 - \bar{\Delta}^2)$ for $E > \bar{\Delta}$;

for $E \leq \bar{\Delta}$, one takes the value at $E = \bar{\Delta} + \langle \delta^2 \rangle^{1/2}/2$.

For clean superconductors the normalized mean square gap anisotropy (Markowitz and Kadanoff 1963) $\langle a^2 \rangle = \langle \delta^2 \rangle / \bar{\Delta}^2$ is constant, independent of temperature. However, for dirty superconductors (Anderson 1959) $\langle a^2 \rangle$ is reduced from its clean limit value $\langle a^2 \rangle_0$ to a value given approximately by $\langle a^2 \rangle = \langle a^2 \rangle_0 / [1 + (\hbar/2\tau_1\bar{\Delta})^2]$. Combining these expressions, we find

$$G_{el\xi} = \tau_1^{-1} \frac{\langle a^2 \rangle_0}{1 + (\hbar/2\tau_1\bar{\Delta})^2} \frac{\bar{\Delta}^2 E}{2(E^2 - \bar{\Delta}^2)^{3/2}} (f_\xi - f_{-\xi}) \quad (E \geq \bar{\Delta} + \langle \delta^2 \rangle^{1/2}/2), \quad (4.2)$$

where we have set $\xi' = -\xi$; this is an excellent approximation for the values of anisotropy encountered in real metals.

We can use Eq. (4.2) to interpret the results obtained for Sn and SnIn in Fig. 6. For the clean films we expect the mean free path, l , to be typically 300 nm, while for the SnIn film it was estimated to be 42 nm. Using $v_F = 0.65 \times 10^6 \text{ ms}^{-1}$ [calculated from $v_F = (\pi^2 k_B^2 / e^2 \gamma) \sigma / l$ (Pippard 1965), where σ is the conductivity, and $\sigma / l = 9.5 \times 10^{10} \text{ } \Omega^{-1} \text{ cm}^{-1}$ (Chambers 1952)], we estimate τ_1 to be 2.2 ps and 15.5 ps for the clean and SnIn films, respectively. Thus, the factor $1/\tau_1 [1 + (\hbar/2\tau_1\bar{\Delta})^2]$ is about 0.85 for the Sn films and 0.19 for the SnIn film. Now below about $0.8 T_C$, the total measured rate (including both elastic and inelastic processes) is roughly two times higher in Sn than in SnIn, leading us to conclude that the elastic contribution is small for SnIn, but comparable with the inelastic rate in Sn. As we increase the temperature towards T_C , $\hbar/2\tau_1\bar{\Delta}$ becomes large compared with unity, and $G_{el\xi}$ scales roughly as $\bar{\Delta}^4$. Thus, in the limit $T \rightarrow T_C$, the elastic contribution becomes negligible with the inelastic process, and the data for the Sn and SnIn

samples become indistinguishable.

Chi and Clarke (1979) measured τ_{Q*}^{-1} in Al films in which the mean free path was reduced by evaporating them in an oxygen atmosphere. The experimental configuration was similar to that shown in Fig. 5, except that it was not necessary to deposit a Pb film over the Cu film. They compared their results with computer solutions of the Boltzmann equation in which Eq. (4.2) was included in the limit $(\hbar/2\Delta\tau_1) \gg 1$ appropriate to the experiments. Figure 7 shows $(F^*\tau_{Q*})^{-1}$ vs. $\Delta(T)/k_B T_C$ for five representative samples with parameters listed in Table I. The values $v_F = 1.36 \times 10^6 \text{ ms}^{-1}$ [calculated from the free electron value divided by the thermal effective electron mass (Kittel 1976)], $\rho l = 9 \times 10^{16} \text{ } \Omega\text{m}^2$ (Fickett 1971), and $N(0) = 1.74 \times 10^{28} \text{ eV}^{-1} \text{ m}^{-3}$ (Gschneider 1964) were used. The solid lines are the best fit to the theory using τ_E^{-1} and the characteristic elastic charge relaxation rate $\tau_{Q*el}^{-1}(0) = 2\tau_1(k_B T_C)^2 \langle a^2 \rangle_0 / \hbar^2$ as fitting parameters. For each sample, the value of τ_E^{-1} was obtained from the data in the limit $\Delta(T)/k_B T_C \rightarrow 0$, while $\tau_{Q*el}^{-1}(0)$ was determined from the upward curvature required to fit the data at lower temperatures. It should be realized that the actual gap anisotropy in these films is very small. Thus, for the cleanest film listed in the table, $\langle a^2 \rangle = 2 \times 10^{-4} \langle a^2 \rangle_0$ at $0.9 T_C$. The high sensitivity of τ_{Q*}^{-1} to very small gap anisotropies reflects the relatively slow inelastic scattering rate in Al. For the cleanest films studied (not listed in Table I) the average value of τ_E was about 12 ns.

4.2 Inelastic Scattering in Aluminum

CC also extracted values of τ_E from their data over a wide range of mean free paths, ranging from about 400 nm to 1 nm. The transition temperatures of these films increased from about 1.2K for the cleanest films

to about 2.1K for the dirtiest film. They found that the apparent value of τ_E decreased much more rapidly than T_c^{-3} (which would be expected from an electron-phonon interaction), from about 12 ns for $T_c = 1.2K$ to about 1 ns for $T_c = 2.1K$. This rapid increase in the inelastic scattering rate with T_c remained a puzzle for several years, but recent work on the enhancement of electron-electron scattering due to localization effects provides a rather convincing explanation (Gordon et al. 1983), Santhanam and Prober 1983). We briefly describe this work.

The theory of Abrahams et al. (1981) predicts that for dirty ($l < \hbar v_F / k_B T$) 2D ($\hbar v_F l / 3 k_B T > d^2$) samples the electron-electron scattering rate is given by

$$\tau_{ee}^{-1} = \frac{e^2 R_{\square}}{2\pi \hbar^2} k_B T \ln(T_1/T), \quad (4.3)$$

where d is the film thickness, R_{\square} is the resistance of a square film and T_1 is roughly 10^{12} K. Gordon et al. and Santhanam and Prober extracted values of τ_{ee}^{-1} from measurements of the magnetoconductance of dirty Al films, and found good agreement with Eq. (4.3). Near T_c , Entin-Wohlman and Orbach (1981) showed that the charge relaxation rate due to electron-electron scattering is given by

$$(F^* \tau_{Q*})_{ee}^{-1} = (\pi \Delta / 4 k_B T) \tau_{ee}^{-1}, \quad (4.4)$$

so that one can immediately apply Eq. (4.3) to the inelastic scattering rates measured near T_c by CC. Setting $T = 1K$ in the logarithmic term in Eq. (4.3) (and neglecting the temperature dependence of this term) we find

$\tau_{ee}^{-1} = 1.5 \times 10^8 R_{\square} T_c \text{ sec}^{-1}$. For the dirtiest samples studied by CC ($T_c \approx 2\text{K}$, $R_{\square} \approx 6\Omega$), one predicts $\tau_{ee} \approx 0.5 \text{ ns}$ from Eq. (4.3), a value within a factor of 2 of the experimental results. Both Gordon et al. and Santhanam and Prober show that the CC data for dirty Al are quite well fitted by Eq. (4.3).

For the cleanest samples studied by CC, the electron-electron scattering rate should be negligible compared with the electron-phonon scattering rate. The measured value of τ_E , about 12 ns, is a factor of 3 or more below the value of about 40 ns calculated by Kaplan et al. (1976) and Lawrence and Meador (1978). The magnetoconductance data of Gordon et al., however, lead to $\tau_E \approx 12 \text{ ns}$ in the clean limit, a value that is very compatible with the CC value. This discrepancy between measured and theoretical values of τ_E in Al thus appears to be well substantiated, and is worthy of further study.

We note in passing that the values of $\langle a^2 \rangle_0$ obtained by CC assume, of course, that the inelastic scattering consists of electron-phonon processes only. If, as now seems highly probable, electron-electron scattering was significant or even dominant in the dirtier samples, since the distribution in the presence of electron-electron scattering differs from that in the presence of electron-phonon scattering, the values of $\langle a^2 \rangle_0$ quoted for these samples will be somewhat in error.

It is also possible to determine the inelastic and elastic scattering rates as a function of energy by measuring the nonequilibrium distribution injected via a tunnel junction by means of a second tunnel junction (Kaplan et al. 1977, Chang 1977, Kirtley et al. 1978, Gray 1981). In measurements on clean Al films, Gray found $\tau_E \approx 12 \text{ ns}$, in excellent agreement

with the CC result, while Kirtley et al. found $\tau_E = 0.25$ ns in Al films with $T_c = 2.4$ K. More surprisingly, an analysis of both experiments produced an elastic scattering time that was essentially independent of the quasiparticle energy. This result is clearly in disagreement with the prediction of Eq. (4.2), and not understood in the present theoretical framework.

5. CHARGE RELAXATION IN THE PRESENCE OF MAGNETIC IMPURITIES OR A SUPER-CURRENT

5.1 Elastic Scattering from Magnetic Impurities

The addition of magnetic impurities to a superconductor destroys the degeneracy between time-reversed electron states through the exchange interaction between the conduction electrons and the impurities, giving the Cooper pairs a finite lifetime. The inverse of this lifetime, the pair breaking rate, is the elastic spin-flip scattering rate for electrons in the normal metal, τ_S^{-1} (Abrikosov and Gor'kov 1960). The presence of impurities can have a dramatic effect on the charge relaxation rate, as was first pointed out by Schmid and Schön (SS, 1975) and later studied by Pethick and Smith (1981a,b), Entin-Wohlman and Orbach (1979), and Lemberger and Clarke (LC, 1981a). This effect occurs because the coherence factor for elastic spin-flip scattering from one quasiparticle branch to the other in an isotropic superconductor is not zero, but of the form

$$(uu' + vv')^2 = 4u^2v^2 = \Delta^2/E^2. \quad (5.1)$$

Since this factor approaches unity as $E \rightarrow \Delta$, we expect the spin-flip scattering to have an appreciable effect on $\tau_{Q^*}^{-1}$ when $\tau_S^{-1} \gtrsim \tau_E^{-1}$.

SS found

$$(\Gamma^* \tau_{Q^*})^{-1} = \frac{\pi \Delta}{4k_B T_C \tau_E} \left(1 + \frac{2\tau_E}{\tau_S} \right)^{1/2} \cdot (\tau_{Q^*}^{-1} \ll \tau_E^{-1}) \quad (5.2)$$

A factor $(1 + \kappa^2 \Gamma / \Delta^2 \tau_E)^{1/2}$ has been omitted in Eq. (5.2), where $\Gamma =$

$(2\tau_E)^{-1} + \tau_S^{-1}$, since it is very close to unity for all values of τ_E , τ_S , and Δ used in the experiments to be described later.

LC included a term

$$G_{sf\xi} = \frac{1}{\tau_S} \frac{\Delta^2}{E^2} \frac{E}{|\xi|} (f_{\xi} - f_{-\xi}) \quad (5.3)$$

in the Boltzmann equation to account for spin-flip scattering, and computed solutions with $G_{el\xi} = 0$ (since this term is negligible compared with $G_{sf\xi}$ for concentrations of magnetic impurities of experimental interest). Figure 8 shows $(F^*\tau_{Q*})^{-1}$, normalized to the SS factor $(\pi/4\tau_E)(1 + 2\tau_E/\tau_S)^{1/2}$ vs. $\Delta/k_B T_C$ for several values of τ_E/τ_S . For values of $\Delta/k_B T_C < 1$, the computed values of $(F^*\tau_{Q*})^{-1}$ lie above the SS result, and, furthermore, increase monotonically compared with the SS prediction as τ_E/τ_S increases.

Using a configuration similar to that in Fig. 5, LC measured τ_{Q*}^{-1} in Al films doped with Er. Figure 9 shows $(F^*\tau_{Q*})^{-1}$ vs. $\Delta/k_B T_C$ for 3 samples with the parameters listed in Table II; the values of $N(0)$ and ρl were the same as those used by CC. It was assumed that $\tau_E = 12(1.2/T_C)^3$ ns; the estimated spin-flip time was taken from Craven et al. (1971), $\tau_S^{-1} = 1.9 \times 10^{13} n_{Er} s^{-1}$, where n_{Er} is the concentration of Er atoms. The rate $(F^*\tau_{Q*})^{-1}$ is linear in $\Delta/k_B T_C$ for $\Delta/k_B T_C \lesssim 0.8$, which is consistent with the SS result [Eq. (5.2)] provided that one assumes that this expression can be extrapolated to much higher values of $\Delta/k_B T_C$ than one can justify theoretically. The data in this range were used to calculate the values of $\tau_S(\text{meas.})$ listed in Table II. The slope S of the linear region for all the samples studied is plotted vs. the SS expression

$(\pi/4\tau_E)(1 + 2\tau_E/\tau_S)^{1/2}$ in Fig. 10. One sees that the data generally fall on a straight line through the origin, indicating that Eq. (5.2) predicts the data remarkably well for $\Delta/k_B T_C \lesssim 0.8$.

Figure 9 also shows curves computed from the Boltzmann equation. It is immediately apparent that the fit to the data is much worse than that of the SS prediction. The discrepancy between the computed and experimental curves is further emphasized in Fig. 11, where $(SF^*\tau_{Q*})^{-1}$ is plotted vs. $\Delta/k_B T_C$ for one sample of each Er concentration. It is apparent that the data, normalized in this way, lie on a universal curve, in complete contrast to the computed curves shown in Fig. 8, in which the same quantity increases markedly with τ_E/τ_S at a given temperature.

More recently, Beyer Nielsen et al. (1982) have examined this problem using a quasiclassical Green's function approach, taking into account the broadening of the states due to the presence of the magnetic impurities. Their results lie very much closer to the solutions to the Boltzmann equation obtained by Lemberger and Clarke than to the SS results.

This marked discrepancy between the data and the solutions to the kinetic equation is extremely puzzling. It cannot be explained by invoking an additional charge relaxation mechanism in the experiments because the experimental rate $(F^*\tau_{Q*})^{-1}$ lies substantially below, rather than above the computed rate. One can rule out the possibility of impurity-impurity interactions, and of Kondo anomalies. However, it is noteworthy that the mean free path of most of the samples was sufficiently short that electron-electron scattering played at least some role in the charge relaxation. Thus, it is just possible that the discrepancy arises from the different quasiparticle distributions that occur in the presence of electron-phonon

and electron-electron scattering. Since electron-electron scattering does not reduce the energy of the quasiparticles, there will be a smaller quasiparticle population at low energies compared with that in the presence of an equal electron-phonon scattering rate. As a result, the charge relaxation rate due to magnetic impurity scattering will be reduced, since $G_{sf\xi}$ is proportional to Δ^2/E^2 [Eq. (5.3)]. Thus, the presence of electron-electron scattering is expected to lower the overall charge relaxation rate compared with the value one would compute assuming that the measured inelastic relaxation rate was due solely to electron-phonon processes. Obviously, only a solution of the Boltzmann equation with the inclusion of an appropriate electron-electron relaxation term (Entin-Wohlman and Orbach 1981) will resolve this issue.

5.2 Elastic Scattering in the Presence of a Supercurrent

In the presence of a supercurrent, the quasiparticle energies are raised by an amount $\mathbf{p}_k \cdot \mathbf{v}_s$, where \mathbf{p}_k is the momentum of a quasiparticle in state k , and \mathbf{v}_s is the superfluid velocity (Aronov 1974, Galperin et al. 1974). Thus, quasiparticles at the Fermi energy where \mathbf{v}_s and \mathbf{p}_k are in the same direction are raised by $p_F v_s$, while those where \mathbf{v}_s and \mathbf{p}_k are in opposite directions are lowered by $p_F v_s$. This current-induced anisotropy allows elastic scattering to relax charge imbalance in much the same way as gap anisotropy. Maki (1969) has shown that an appropriate electron relaxation rate for thin films [$d \ll (\ell \xi_0)^{1/2}$] in the dirty limit ($\ell \ll \xi_0$) is

$$\frac{1}{\tau_S} = \frac{\ell v_F}{6} \left(\frac{p_S}{\hbar} \right)^2, \quad (5.4)$$

where $\xi_0 = \hbar v_F / \pi \Delta(0)$, and p_S is the momentum of a Cooper pair. We can use Eq. (5.4) in Eq. (5.2) or (5.3) to predict the charge relaxation rate as a function of p_S . For the case of magnetic impurities LC found that at a given temperature $(F^* \tau_{Q^*})^{-1}$ was proportional to $(1 + 2\tau_E/\tau_S)^{1/2}$, as predicted by SS. Thus, we can immediately write down an expression for the detector voltage at a given temperature and injection current in the presence of a supercurrent, I_S :

$$V_d(I_S) = \frac{V_d(0)}{(1 + 2\tau_E/\tau_S)^{1/2}} = \frac{V_d(0)}{(1 + b_{SS} I_S^2)^{1/2}} \quad (5.5)$$

where from Eq. (5.4)

$$b^{SS} = 2\tau_E/\tau_S I_S^2 = \tau_E \ell v_F p_S^2 / 3\hbar^2 I_S^2. \quad (5.6)$$

For uniform currents much less than the critical current we can use the relations (Tinkham 1975) $p_S = 2mv_S$, $j_S = n_S e v_S$, $n_S = mc^2/4\pi e^2 \lambda^2$ and, in the dirty limit, $\lambda(0) = \lambda_L(0)(\xi_0/\ell)^{1/2}$ to find

$$b^{SS} = \left(\frac{8\pi e}{\hbar c^2}\right)^2 \frac{\tau_E v_F \xi_0^2 \lambda_L^4(0) \lambda^4(T/T_C)}{3\ell d^2 w^2 \lambda^4(0)}. \quad (5.7)$$

Here, w is the film width, $\lambda_L(0)$ is the London penetration depth, and $\lambda(T/T_C)/\lambda(0)$ is a well-known function (Tinkham 1975).

Lemberger and Clarke (1981b) solved the Boltzmann equation in the presence of a supercurrent by replacing $1/\tau_S$ in Eq. (5.3) with Eq. (5.4) to obtain

$$G_{S\xi} = \frac{\ell v_F}{6} \left(\frac{p_S}{\hbar}\right)^2 \frac{\Delta^2}{E|\xi|} (f_\xi - f_{-\xi}). \quad (5.8)$$

With this substitution, the results computed in Sec. 5.1 can be carried over to the present case. Thus, for fixed temperature and injection voltage,

$$V_d(I_S) = \frac{V_d(0)}{(1 + b^{\text{num}} I_S^2)^{1/2}}, \quad (5.9)$$

where $b^{\text{num}}(T)$ is the numerical value produced by the computer. In general, $b^{\text{num}}(T)$ will differ from $b^{SS}(T)$, as evident in Sec. 5.1, and we can compare both values with the measured value, $b^{\text{meas}}(T)$.

Lemberger and Clarke (1981b) performed experiments using the usual geometry with a supercurrent introduced along the Al film in which the charge imbalance is generated. To increase the uniformity of the current distribution, a Nb groundplane was sputtered onto the substrate and covered with an insulating layer before the sample was deposited. A representative plot of $V_d(I_S)$ vs. I_S is shown in Fig. 12. As predicted by Eqs. (5.5) and (5.9), the value of $|V_d|$ decreased quadratically with increasing $|I_S|$ at low supercurrents, becoming linear in I_S at higher supercurrents. The slight asymmetry in the curves about $I_S = 0$ was due to the non-negligible value of I_1 . After shifting the origin appropriately, curves of the form $(1 + bI_S^2)^{1/2}$ were fitted; the quality of the fit is excellent. Experimentally determined values of b are shown in Fig. 13 for two samples, together with the fitted curves b^{SS} and b^{num} . The temperature dependence of b^{SS} is in excellent agreement with the data, while b^{num} is in substantial disagreement. Furthermore, the ratio $\langle b^{SS}(T) / b^{meas}(T) \rangle$ varies between $1/3$ and $1/2$, an agreement which, given the uncertainties in the values of v_F , ℓ , $\lambda_L(0)$, and τ_E , is considered quite acceptable.

We therefore draw the same conclusions as for the case of magnetic impurities: The Schmid-Schön theory fits the measured data very accurately, even at values of $\Delta/k_B T_C$ much larger than one could reasonably expect, while the computed solution to the Boltzmann equation does not fit the data. However, it is again just possible that this discrepancy could be resolved by the inclusion of electron-electron scattering in the Boltzmann equation.

6. RESISTANCE OF THE NORMAL METAL-SUPERCONDUCTOR INTERFACE

We now begin a discussion of a series of situations other than tunnel injection in which charge imbalance plays a role. The first of these concerns the electrical resistance of the normal metal-superconductor (NS) interface, a subject about which there exists a substantial literature. The first important experimental work was that of Pippard et al. (1971) who measured the electrical resistance of superconductor-normal-metal-superconductor (SNS) sandwiches in which the normal metal was too thick and/or too dirty to sustain a Josephson supercurrent. They observed that, near the transition temperature of the superconductor, T_c , the resistance increased rapidly with increasing temperature. Yu and Mercereau (1972) showed that the excess resistance was associated with a potential that decayed exponentially into the superconductor. Subsequently, Harding et al. (1974) studied the resistance of SNS sandwiches in which the mean free path of the superconductor was shortened by alloying, and found an additional boundary resistance at low temperatures as well as a greatly enhanced rise in resistance near T_c . More recently, Hsiang and Clarke (1980) made measurements on a series of samples in the clean limit, and used their results to obtain values of τ_E in Pb, Sn, and In.

The theory of the NS interface resistance has been widely investigated. The work of Rieger et al. (1971), who used a time-dependent Ginzburg-Landau theory, contained some essentially correct ideas, but did not produce the correct quasiparticle propagation length in the superconductor. Pippard et al. (1971) and Harding et al. (1974) used a Boltzmann equation approach that was later extended by Waldram (1975),

and reviewed by Pippard (1981). The microscopic theory was developed by Schmid and Schön (1975), and has been extended by Ovchinnikov (1977, 1978), Artemenko and co-workers (1977, 1978) and Krähenbühl and Watts-Tobin (1978, 1979). Hsiang and Clarke (1980) gave a simple description valid in the limit $\Delta/k_B T \ll 1$ by adapting the tunnel injection theory that accounted quantitatively for their experimental data, and that was verified by Pethick and Smith (1981a) using their two-fluid model. Most recently, Blonder et al. (1982) have used the Bogoliubov equations to treat the transmission and reflection of particles at the NS interface that includes a barrier of arbitrary strength.

In the clean limit $\ell \gg \xi(T)$ the essential picture that emerges from this work is as follows. When a charge imbalance is created in one region of a superconductor, it relaxes over a length

$$\lambda_{Q^*} = (\ell v_F \tau_{Q^*} / 3)^{1/2} = (D \tau_{Q^*})^{1/2}, \quad (6.1)$$

where we assume $\ell \ll v_F \tau_{Q^*}$. Very close to T_c almost all of the excitations incident from N propagate into S, so that, in the presence of an external current, a quasiparticle current flows in the superconductor. In the usual situation where the transverse dimensions of the interface are much larger than the London penetration depth, there is no net current in the interior of the superconductor. The internal quasiparticle current is cancelled by a pair current, with a corresponding flow of supercurrent on the surface. The electric field is continuous at the interface, and the electric field, the electric potential, Q^* , and the quasiparticle current all decay exponentially into S with a characteristic

length λ_{Q^*} (see Fig. 14). When the temperature is lowered somewhat, a substantial fraction of quasiparticles have energies $\lesssim \Delta_{\infty}(T)$, and are Andréev (1964) reflected at or near the NS interface. In this process, a $k_{>}$ ($k_{<}$) quasiparticle incident from N is scattered onto the $k_{<}$ ($k_{>}$) branch, and the current carried by these two excitations continues in the superconductor as a supercurrent. Thus, there is no boundary resistance associated with these quasiparticles, and there is a discontinuity in the electric field at the interface (Fig. 14). The potential is continuous at the interface, but its spatial derivative is not. In the presence of a current, the boundary scattering processes introduce disequilibrium in the quasiparticle distributions within an inelastic scattering length on either side of the interface.

As the temperature is lowered still further ($\Delta_{\infty} \gg k_B T$), essentially all of the quasiparticles are Andréev reflected at the interface, and there is no quasiparticle current in S. Correspondingly, the electric field and potential are zero in S (Fig. 14) and there is no boundary resistance. (In fact, the Andréev scattering process occurs over a distance $\sim \xi_0$, so that the discontinuities in the electric field and the derivative of the potential extend over this region. Furthermore, there will be a small boundary resistance of order $\xi \rho_s / A$ that is negligible in most practical situations.)

We now outline the simple model of Hsiang and Clarke (HC) that is valid in the limit $\Delta_{\infty}(T)/k_B T \ll 1$. We assume that the transition temperature of the normal metal is much less than T, so that we can set $\Delta = 0$ for $x < 0$ (Fig. 14). In the superconductor, Δ rises from its value at the boundary, $\Delta_0(T)$, to its full value, $\Delta_{\infty}(T)$, over a distance of roughly

the Ginzburg-Landau (1950) coherence length, $\xi(T)$, that is always much less than λ_{Q^*} in the temperature range investigated experimentally. However, we note that quasiparticles with energies greater than $\Delta_\infty(T)$ may undergo some charge relaxation in the region where Δ varies spatially. At least in the limit $\Delta \ll k_B T$, this contribution to the overall relaxation rate is likely to be small, and we shall neglect it. We assume that the current densities are sufficiently low that they do not perturb Δ . We further assume that quasiparticles with energies greater than $\Delta_\infty(T)$ are transmitted into S with probability unity; this is the most serious approximation because some of the quasiparticles in this energy range will undergo Andreev reflection. Quasiparticles with energies $< \Delta_\infty(T)$ are Andreev reflected at a plane taken as $x = 0$ [since $\xi(T) \ll \lambda_{Q^*}$]. Finally, we assume that the quasiparticles are close to thermal equilibrium even in the vicinity of the interface; we emphasize that this is a reasonable approximation only for $\Delta_\infty \ll k_B T$.

The charge imbalance generated by the uniform injection of a current I_1 into volume Ω of a superconductor in the limit $eV_1 \ll k_B T$ is given from Eqs. (2.21) to (2.23) by

$$Q^* = \frac{Z(T)}{Y(T)} \frac{I_1 \tau_{Q^*}}{e\Omega} . \quad (eV_1 \ll k_B T) \quad (6.2)$$

In the case of the NS interface, I_1 is just the quasiparticle current injected into S, and is related to the total current, I by

$$Y(T) = I_1 / I. \quad (6.3)$$

Equation (6.3) follows from the realization that in a SIN tunnel junction at low voltages a fraction $[1 - Y(T)]$ of the current that flows at T_c cannot flow at a temperature $T < T_c$ because there are no states available in S at energies $< \Delta(T)$, whereas at the NS interface, in our approximation, this same fraction $[1 - Y(T)]$ of the total current is transmitted into S as a pair current. Combining Eqs. (6.1) to (6.3), and replacing the exponentially decaying Q^* with a value that is constant at the value $Q^*(0)$ for $x \leq \lambda_{Q^*}$ and 0 for $x > \lambda_{Q^*}$, we find

$$Q^*(0) = \frac{Z(T)I\tau_{Q^*}}{eA\lambda_{Q^*}}. \quad (6.4)$$

The excess voltage, V_b , at each interface of the SNS sandwich adds to the voltage developed across the normal metal, and the total potential across the sandwich is measured with superconducting leads making metallic contact with the superconducting films. This is in contrast to the usual tunneling measurement of Q^* , where the potential is measured by a tunneling contact to a normal metal. Thus, we set $g_{NS}(0) = 1$ in Eq. (2.20), and combine the result with Eq. (6.4) to obtain the boundary resistance

$$R_b = \frac{V_b}{I} = \frac{Z(T)\lambda_{Q^*}\rho_S}{A}. \quad (\Delta \ll k_B T) \quad (6.5)$$

In Eq. (6.5) we have set $\tau_{Q^*} = 3\lambda_{Q^*}^2/lv_F$ and used the free electron model (Kittel 1976) to calculate $\rho_S = 3/2e^2N(0)lv_F$. As $T \rightarrow T_c$, $Z(T) \rightarrow 1$, and the boundary resistance is just the resistance of a length λ_{Q^*} of the superconductor in the normal state. As the temperature is lowered,

$Z(T)$ decreases, reflecting the fact that fewer quasiparticles are able to propagate into the superconductor. At low temperatures (Clarke et al. 1979) $Z(T) = (k_B T / \Delta)^{1/2} \exp(-\Delta / k_B T)$, so that R_D vanishes exponentially as $T \rightarrow 0$, as we expect. However, we repeat our warning that the model is not expected to be quantitatively correct at intermediate temperatures.

If one measures R_D near T_C one can deduce values of τ_{Q^*} . As was discussed in Secs. 2.3 and 4, in general, both inelastic and elastic scattering contribute to $\tau_{Q^*}^{-1}$. We can make a crude estimate of the elastic relaxation rate in the presence of gap anisotropy for the materials used in the experiments to be described by assuming $E = k_B T_C$ in Eq. (4.2). This leads us to the conclusion that electron-phonon scattering should dominate at temperatures above $0.9 T_C$. Since $\Delta / k_B T = 1$ at $T / T_C = 0.9$, it appears that in the range of validity of Eq. (6.5), $\Delta / k_B T \ll 1$, the charge relaxation should be dominated by inelastic scattering, and we assume that $\tau_{Q^*} = 4k_B T \tau_E / \pi \Delta_\infty(T)$.

HC measured the resistances of the SNS junctions listed in Table III. The PbBi-CuAl samples were made by evaporating the materials onto glass substrates; the CuAl was $\sim 2 \mu\text{m}$ thick, while the PbBi was $\sim 20 \mu\text{m}$ thick, considerably greater than λ_{Q^*} over the experimental temperature range. In the remaining samples, the superconductor (up to $80 \mu\text{m}$ thick) was evaporated onto the two sides of Ir foils about $70 \mu\text{m}$ thick. The foils were cleaned by sputter etching in argon, the argon was pumped out of the system, and the superconducting material was evaporated onto each side of the foil. Two or three samples were connected in series and their resistances measured with a SQUID voltmeter. The variation of re-

sistance with temperature is shown in Fig. 15 for one representative sample of each type. Near T_c , the resistance rises rapidly with increasing temperature, while at low temperatures the resistance is nearly independent of temperature. To within the experimental accuracy, the low temperature resistance was equal to the estimated resistance of the normal metal.

To compare the data with Eq. (6.5), in Fig. 16 we plot the measured resistance vs. $Z(T)(k_B T/\Delta)^{1/2}$. The solid lines are a least squares fit to the data for $T > 0.9 T_c$ ($0.96 T_c$ for Sn). The fit is good -- in fact, for (a), (c) and (d) it is surprising that such good agreement extends down to temperatures as low as $0.9 T_c$ where $\Delta \sim k_B T$. The slope of the lines in Fig. 16 is $4(2v_F \tau_E/3\pi)^{1/2} \rho_g/A$, and yields the average values of τ_E listed in Table III. The values of τ_E calculated by Kaplan et al. (1976) from $\alpha^2 F$ are also listed for comparison. The agreement is generally quite good. Using the fitted values of τ_E , we have plotted the resistance predicted by Eq. (6.5) in Fig. 15. Except for Sn, the extrapolated low-temperature resistance is in good agreement with the measured resistance, thus providing a good check on the consistency of our results. Particularly in the cases of PbBi and In, the fit is remarkably good even at intermediate temperatures, a result that is probably coincidental, particularly since the expression used for τ_{Q^*} is quite inappropriate in this range. However, it may be that the increase in the elastic charge relaxation rate as the temperature is lowered tends to compensate for the decrease in the inelastic rate, thus keeping τ_{Q^*} roughly constant at temperatures below about $0.9 T_c$.

As pointed out in the description of the tunneling model, the effect

of Andreev reflection on the quasiparticle distribution is neglected. The detailed theory of Waldram (1975) takes into account the nonequilibrium quasiparticle distribution, but the fact that one would have to use several parameters to fit the experimental data makes a meaningful test of the theory somewhat difficult. More recently, Blonder et al. (1982) have developed a theory in which they interpose a tunneling barrier of arbitrary strength between the normal metal and the superconductor, and calculate the probabilities of reflection and transmission as a function of this strength. They have used this model to account for the current-voltage characteristics of Cu-Nb point contacts that could be varied from tunneling to metallic contacts (Blonder and Tinkham 1983) and for the subharmonic gap structure observed in various types of weak links (Klapwijk et al. 1982, Octavio et al. 1983). The model is strictly applicable only to the case of a hole with a radius much less than λ in an insulating screen between two metals, so that the resistance is due to the constriction impeding the ballistic propagation of electrons. This leads to the assumption that the incoming electrons from the S side are described by a Fermi function, $f^0(E)$, while those coming in from the N side are described by $f^0(E - eV)$. Within this approximation, Blonder et al. compute the Andreev reflection of quasiparticles at the interface for varying strengths of the tunneling barrier. For the case of a clean metallic contact, their result agrees with Eq. (6.5) at T_c but has a somewhat different temperature dependence at lower temperatures, the exact form depending on the degree of disorder at the interface and the ratio of the Fermi velocities in the two metals. However, this picture of a small-area constriction impeding

the ballistic propagation of electrons, while highly appropriate for point contacts or microbridges, is unlikely to be an appropriate description of the large area SNS sandwiches studied here.

To conclude this section on the NS interface, we note briefly that Hsiang (1980) studied the effect of a magnetic field applied parallel to the plane of SNS sandwiches in which the superconductor was $\text{Pb}_{0.98}\text{Bi}_{0.02}$, and the normal metal was Cd. The PbBi films are bulk, type-II superconductors in which the spin relaxation rate is given by (Maki 1969, de Gennes 1966, Tinkham 1975)

$$\frac{1}{\tau_s} = \frac{2v_{Fe}H}{3c} . \quad (6.6)$$

Hsiang measured the boundary resistance as a function of applied magnetic field and temperature, and extracted values of $\tau_{Q*}^{-1}(T,H)$. Using Eq. (6.6) in Eq. (5.2) he was able to estimate τ_s^{-1} as a function of H. Although there was a good deal of spread in the results, he was able to establish reasonable agreement between the measured value of τ_s^{-1} and the value predicted by Eq. (6.6).

7. PHASE SLIP CENTERS

A subject of major importance that has received widespread attention is the phase-slip center (PSC) in one-dimensional superconducting filaments or films. Reviews of this subject have been written by Tinkham (1979) and Skocpol (1981). Webb and Warburton (1968) first reported the appearance of discrete voltage steps in the current-voltage characteristics of Sn whiskers very close to T_c . Similar effects were observed by Meyer and van Minnigerode (1972) and Meyer (1973). However, the first understanding of the origin of the effect was put forward in the classic paper by Skocpol, Beasley and Tinkham (SBT) (1974), and we will begin with a brief outline of this work.

Figure 17 shows a typical I-V characteristic obtained by SBT for the whole length of a Sn strip, 140 μm long, 4 μm wide, and 0.1 μm thick, shown inset. As the current is increased from zero, there is an initial zero voltage region followed by a series of voltage steps to resistive regions, the dynamic resistance of which increase by approximately equal increments. As the current is reduced, there is a corresponding series of voltage steps to lower voltages, but with considerable hysteresis. The SBT explanation of these phenomena is as follows (see Fig. 18).

As the current, I , is increased eventually it exceeds the critical current, I_c , at the weakest point in the microbridge. The order parameter in this region collapses to zero and the current is forced to flow as a normal current, thereby allowing the superfluid to build up again and to resume carrying the current. This cycle repeats at a frequency $2eV/h$, where V is the average voltage across the region. Each time the order parameter falls to zero, the phase difference between the two ends

of the bridge slips by 2π : Hence the name "phase-slip center." The width of the region over which the superfluid oscillates is roughly $2\xi(T)$. Now since the superfluid current oscillates between zero and its critical value, on the average approximately one-half of the current in this region flows as a supercurrent, and the other half as a normal current. Since the temperature is very close to T_c , virtually all of the normal current will propagate into the superconducting regions on either side of the phase-slip region, where it will be converted into a supercurrent over a characteristic length λ_{Q*} . The time average of the pair electrochemical potential, $\bar{\mu}_s$, is constant on either side of the phase-slip region, with a difference eV between the two sides. The time averaged quasiparticle potential, $\bar{\mu}_{qp}$, changes smoothly with distance as indicated in Fig. 18. Thus, the voltage across the PSC (at distances large compared with λ_{Q*}) is given by

$$V = 2(I - \beta I_c)\rho_s\lambda_{Q*}/A, \quad (7.1)$$

where $\beta = 1/2$, and we have used Eq. (6.5) with $Z(T) = 1$. The dynamic resistance is

$$\partial V/\partial I = 2\rho_s\lambda_{Q*}/A. \quad (7.2)$$

This picture explains the essential features of Fig. 17. Each step in voltage corresponds to the creation of a PSC, each of which contributes $2\rho_s\lambda_{Q*}/A$ to the dynamic resistance. SBT were able to set outer limits on the location of each PSC by measuring the voltages across dif-

ferent probes on their bridge (inset, Fig. 17). In the example shown in Fig. 17, they found that the first four steps were produced by one PSC forming successively in each of the regions II, I, IV and III, while the fifth step was produced by a second PSC appearing in region IV. However, one very puzzling feature was the fact that the measured characteristic length for the charge imbalance relaxation was essentially independent of temperature, with a magnitude of approximately $(2v_F\tau_E/3)^{1/2}$. This fact prevented the SBT explanation from being a completely satisfying picture of the PSC. However, Dolan and Jackel (1977) resolved this difficulty in an elegant experiment in which they prepared a microbridge with a series of superconducting voltage leads along one side of the bridge and a series of normal voltage leads along the other. The probes were typically 2 μm apart, and formed tunnel junctions with the microbridge. In this way, they were able to measure the average superfluid and normal potentials, $V_S = \mu_S/e$ and $V_N = \mu_{qp}/e$ across a PSC, the position of which was defined by a small notch in the microbridge. Figure 19 shows their measured values of V_S and V_N . As expected, V_S changes abruptly, since $\xi(T)$ is less than the probe spacing, while V_N changes over a much greater length. Values of τ_{Q*} deduced from the spatial variation of V_N showed the predicted $(T_c - T)^{-1/4}$ temperature dependence, and produced the value $\tau_{Q*}^{-1} = 6.3 \times 10^9 (\Delta/k_B T_c) \text{s}^{-1}$, in excellent agreement with the results of Clarke and Paterson (1974) discussed in Sec. 3. Since this work on PSC was performed at $T \geq 0.98 T_c$, inelastic scattering should completely dominate the charge relaxation.

It was subsequently shown (Kadin et al. 1978) that heating effects can modify the I-V characteristics so as to mask the temperature dependence

of λ_{Q^*} . Very near T_c , the step becomes rounded, and, as the current is increased, the step due to the entrance of the next PSC may appear before the asymptotic value of the dynamic resistance is reached. Further below T_c , local heating distorts the I-V characteristic by adding curvature and creating hysteresis. Kadin et al. were able to show that when heating effects were taken into account, the temperature dependence of λ_{Q^*} was as expected. Very recently, Stuivinga et al. (1983b) have presented a detailed model of heating effects in PSCs.

Kadin et al. (1978) also studied the effect of a magnetic field, H , applied parallel to the plane of tin PSCs, and found that the inferred value of τ_{Q^*} was reduced by the field. The magnetic field dependence of $\tau_{Q^*}^{-1}$ was consistent with the prediction of Schmid and Schön [Eq. (5.2)], with (Maki 1969, de Gennes 1966, Tinkham 1975)

$$\tau_{Q^*}^{-1} = \frac{\Delta(0,0)H^2}{\mu H_c^2(0)}. \quad (7.3)$$

Here, $\Delta(0,0)$ is the energy gap at zero temperature in zero magnetic field, and $H_c(0)$ is the parallel critical field at zero temperature. This work was the first experimental demonstration of the essential correctness of the SS theory of charge imbalance relaxation in a magnetic field.

More recently, Aponte and Tinkham (1983) made careful measurements on Sn microbridges with a series of probes, and found values of λ_{Q^*} with the expected temperature dependence. Their plot of λ_{Q^*} vs. $1 - T/T_c$ is reproduced in Fig. 20, and we see that the best fit to the slope is -0.28 . However, given the size of the error bars, this slope is not significantly different from $-1/4$. From the measured values of λ_{Q^*} they deduce $\tau_{Q^*} =$

$(1.0 \pm 0.2) \times 10^{-10} \Delta(0)/\Delta(T)$ sec. [$\tau_{Q*}^{-1} = (5.7 \pm 1.1) \times 10^9 \Delta(T)/k_B T_c$ s⁻¹, in excellent agreement with the results of Clarke and Paterson (1974) and Dolan and Jackel (1977).]

Klapwijk and Mooij (1976) studied PSCs in Al films, and also found that the characteristic length obtained from I-V characteristics was independent of temperature. However, very recently Stuivinga et al. (1981, 1983a) measured the charge relaxation length directly using a series of probes, and found that λ_{Q*} scaled rather accurately as $(1 - T/T_c)^{-1/4}$. They deduced a value for τ_E of 4 ns (using $\rho l = 4 \times 10^{-16} \Omega m^2$). This value is about a factor of 3 smaller than that obtained by Chi and Clarke (Sec. 4). Stuivinga et al. point out that the low value of τ_E rules out the possibility that elastic scattering in the presence of the supercurrent could have enhanced τ_{Q*}^{-1} significantly, as they had suggested earlier (Stuivinga et al. 1982). Furthermore, their films were clean enough (the maximum value of R_{\square} was about 0.4Ω) that electron-electron collisions should not have contributed in a major way to the measured inelastic relaxation rate. Thus, the very low measured value of τ_E remains a puzzle, although, as we shall see in Sec. 8.2, other measurements of λ_{Q*} in Al produce comparable values.

Very little experimental work has been carried out on the region of the core, for the obvious reason that its dimensions are so small. However, Skocpol and Jackel (1981) were able to make probes sufficiently small to measure the variation of Δ across a PSC in Sn and found that Δ was greatly suppressed in the core, as one would expect.

The interaction between neighboring PSCs or, in general, any type of weak link, is a complicated subject. Lindelof and Bindslev Hansen

(1981) have given an extensive review. The effect of one PSC on the critical current of another arises from a spatially decaying charge imbalance. Such effects were first observed by Jillie et al. (1977), but the only quantitative results appear to be those of Aponte and Tinkham (1983), whose work we now briefly describe. Two neighboring PSCs were fabricated on the same strip of Sn, each PSC being nucleated at a narrowed portion of the strip so that its position was accurately known. The I-V characteristics of the PSC between probes C and L (inset, Fig. 21) were measured as a function of the current flowing through the PSC between probes L and D. For values of $I(LD)$ less than the critical current of the PSC in segment LD, there is no effect on the PSC in segment CL. For larger values of $I(LD)$, there is a change in the apparent critical current of CL, which is increased (decreased) when the applied currents in the two segments are flowing in the same (opposite) direction. However, the magnitude of the change in $I_c(CL)$ is not the same for the two directions of current in LD: The decrease when the currents are opposed is larger than the increase when the currents are in the same direction. This asymmetry reflects the two contributions to the interaction: A heating term, which depresses $I_c(CL)$ irrespective of the direction of $I(LD)$, and a term due to the diffusion of a quasiparticle current from the source PSC to the detector PSC. The diffusive quasiparticle current produced by LD will be in the same direction as the applied current $I(LD)$, so that in the regions outside the probes L and D, there will be an exponentially decaying supercurrent in the opposite direction to $I(LD)$ that cancels the quasiparticle current at each point. When the applied currents are in the same direction, the supercurrent induced in the

detector CL by the source LD will be in the opposite direction to $I(\text{CL})$, thus reducing the supercurrent that flows (below the critical current of CL) and enhancing the critical current. On the other hand, when the applied currents are opposed, the critical current of CL will be depressed. By decomposing the change in $I_c(\text{CL})$ into symmetric and antisymmetric components, Aponte and Tinkham were able to separate out the heating and quasiparticle contributions. The normal current in the center ($x = 0$) of the PSC, $I_N(0) = I - \beta I_c$, was obtained by dividing Eq. (7.1) by Eq. (7.2); β was found to be 0.6. The quasiparticle current in a uniform strip would be $I_N(0)\exp(-x/\lambda_{Q*})$; however, it was necessary to correct for the diffusion of the quasiparticles into the probes. With this correction, the value of λ_{Q*} yielded $\tau_{Q*} = (1.2 \pm 0.4) \times 10^{-10} \Delta(0)/\Delta(T)$ s, in excellent agreement with the value obtained from the direct measurement of λ_{Q*} described earlier. Given the fact that the heating effects were also in accord with a simple model, this picture of the effect of one PSC on the critical current of another appears to describe the experimental facts very well.

The interaction of two PSCs when both are at non-zero voltage is more complicated. Under appropriate conditions, the voltages and hence the frequencies of two nearby PSCs can become locked together (Palmer and Mercereau 1977, Jillie et al. 1977, 1980, Lindelof and Bindslev Hansen 1977, 1981). It appears most likely that the interaction arises from charge imbalance waves, a subject that we will discuss briefly in Sec. 9.

In concluding this section, we remark that it is rather satisfying that the simple model for the PSC proposed by SBT gives such a good account of most of the experimental observations. One needs only to con-

sider the time-averaged electrochemical potentials, without delving into the details of the time dependent processes, to explain all the observed phenomena with the exception of the voltage locking effect.

8. CHARGE IMBALANCE INDUCED BY A TEMPERATURE GRADIENT

Although the usual thermoelectric effects observed in normal metals, namely the Seebeck and Peltier effects and the Thompson heat, vanish in superconductors, there are observable effects due to temperature gradients in superconductors. Schön (1981a) and Van Harlingen (1982) have recently reviewed the various effects that can occur. In this section, we describe three experiments in which a temperature gradient induces a charge imbalance.

8.1 Thermoelectric Generation of Charge Imbalance at a NS Interface

Artemenko and Volkov (1976) were the first to point out that charge imbalance could be induced by a temperature gradient across an NS interface. The quasiparticle current in a superconductor, J_N , contains a contribution $(\sigma/e)(eE - \nabla\mu_0)$, where σ is the electrical conductivity of the quasiparticles, E is the electric field, and μ_0 is the quasiparticle chemical potential (which depends only on the number of electrons and the temperature). Now since the pairs in a superconductor do not accelerate in the steady state, we have $eE - \nabla\mu_S = 0$, so that the transport equation can be written in the form

$$\begin{aligned} J_N &= (\sigma/e)\nabla(\mu_S - \mu_0) + L_T(-\nabla T) \\ &= [\sigma/2N(0)e^2](-\nabla Q^*) + L_T(-\nabla T), \end{aligned} \quad (8.1)$$

where $L_T(T)$ is the thermoelectric coefficient, and we have made use of Eq. (2.11). In the relaxation time approximation, the steady-state charge imbalance is determined from the Boltzmann equation (Pethick and

Smith 1979):

$$\frac{dQ^*}{dt} = -\nabla \cdot j_N - Q^*/\tau_{Q^*} = 0. \quad (8.2)$$

We now consider the one dimensional case of a NS interface, where the normal metal occupies the region $x < 0$ and the superconductor occupies the region $x \geq 0$, in the presence of a temperature gradient dT/dx . In addition to the constraint $j_S(x) + j_N(x) = 0$ that holds throughout the superconductor, the requirement that each current be continuous across the boundary $x = 0$ imposes the condition $j_S(0) = j_N(0) = 0$. As a result, $\nabla \cdot j_N \neq 0$ near the interface, and there will be a corresponding charge imbalance. Combining Eqs. (8.1) and (8.2), in one dimension we find

$$j_N - \lambda_{Q^*}^2 d^2 j_N / dx^2 = L_T (-dT/dx) \quad (8.3)$$

and

$$Q^* - \lambda_{Q^*}^2 d^2 Q^* / dx^2 = \tau_{Q^*} L_T d^2 T / dx^2. \quad (8.4)$$

For the case $d^2 T / dx^2 = 0$ and subject to the constraint $j_N(0) = 0$, we can solve Eqs. (8.3) and (8.4) to find

$$Q^*(x) = 2N(0)e^2 \lambda_{Q^*} S(dT/dx) \exp(-x/\lambda_{Q^*}) \quad (8.5)$$

and

$$j_N(x) = L_T(-dT/dx)[1 - \exp(-x/\lambda_{Q^*})], \quad (8.6)$$

where $S \equiv L_T/\sigma$ is the thermopower in the superconducting state. Figure 22 sketches j_N , j_S and Q^* vs. x . From Eq. (8.5), we see that the voltage at the NS interface due to charge imbalance is $Q^*(0)/2N(0)e^2 = \lambda_{Q^*}SdT/dx$.

These effects may be investigated experimentally by measuring the potential difference across a SNS' sandwich in the presence of a heat current (we assume that the normal layer is thick enough to exclude Josephson tunneling). The excess voltages due to the charge imbalance at the NS interface are $-\lambda_{Q^*}SP/A\kappa$ and $-\lambda'_{Q^*}S'P/A\kappa'$, where $P = A\kappa(-dT/dx) = A\kappa'(-dT/dx)'$ is the heat current, κ and κ' are the thermal conductivities of S and S', and A is the cross sectional area. Thus, the total voltage drop across a SNS' sandwich is

$$V = - \left(\frac{d_N S_N}{A\kappa_N} + \frac{\lambda_{Q^*} S}{A\kappa} + \frac{\lambda'_{Q^*} S'}{A\kappa'} \right) P, \quad (8.7)$$

where the first term is just the contribution of the normal layer of thickness d_N and thermal conductivity κ_N .

Van Harlingen (1981) measured these effects in Pb-Cu-PbBi and In-Al-Sn sandwiches. The sample was mounted in a vacuum can and the voltage generated across the two superconductors (at regions far from the interfaces) in the presence of a known heat current was measured with a null-balancing SQUID voltmeter. Figure 23(a) shows V/P vs. T for a Pb-Cu-PbBi sample. Near the transition temperature, T_c , of the Pb there is a divergence in

V/P that arises from the rapid increase in λ_{Q^*} in Pb: $\lambda_{Q^*}(T) = \lambda_{Q^*}(0)(1 - t)^{-1/4}$. The transition temperature of the PbBi was considerably higher than that of the Pb, so that the voltage produced by the charge imbalance in the PbBi varied relatively slowly with temperature below 7.2K. The dip in Fig. 23(a) is characteristic of the thermopower of Cu, and arises from the Kondo effect in the presence of magnetic impurities. The solid line is a fit to the data well below T_c , extrapolated to T_c . The difference between this line and the data near T_c represents the voltage, V_S , due to the charge imbalance in the Pb, and is plotted vs. $(1 - t)^{-1/4}$ in Fig. 23(b). We see that near T_c V_S/P is proportional to $(1 - t)^{-1/4}$, as expected. Van Harlingen estimated S from the slope of this line, $-\lambda_{Q^*}(0)S/\kappa$, using a value for κ obtained from the measured electrical conductivity and the Wiedemann-Franz law, and the value $\lambda_{Q^*}(0) = 2.7 \mu\text{m}$ obtained from the measured electrical resistance of the SNS' junction. His value of $S = -7.8 \times 10^{-7} \text{VK}^{-1}$ near T_c compares with the value of $-2.2 \times 10^{-7} \text{VK}^{-1}$ obtained by Christian et al. (1958) on Pb in the normal state. Given the strong dependence of S on the impurity content of the material, this discrepancy is by no means unreasonable; unfortunately, it was not possible to measure S independently in the material used in the experiment.

Van Harlingen found comparable results on In-Al-Sn sandwiches near the In transition temperature. Subsequently, Battersby and Waldram (1983) studied similar effects in Pb-Cu-Pb and Pb-Cu-PbBi sandwiches, and obtained excellent agreement between the value of the thermopower in Pb and that measured directly on a bulk sample prepared in a similar way.

8.2 Spatial Dependence of Charge Imbalance Induced by a Temperature Gradient near a Superconducting Boundary

Mamin et al. (1983, 1984) performed experiments designed to measure the spatial decay of the charge imbalance [Eq. (8.5)] near the end of an Al film in the presence of a temperature gradient. Their sample configuration is shown in Fig. 24. The Al film, deposited on a glass substrate, was 500 μm wide and typically 300 nm thick. A series of probes was fabricated on top of the Al film with a photolithographic lift-off procedure. Each probe consisted of 800 nm of Cu (3wt%Al) followed by about 5 nm of Fe and 200 nm of Pb (5wt%In). The Fe layer prevented Josephson tunneling between the Al and the PbIn. Near the end of the Al film, the probes were 2 μm wide with a 6 μm separation between centers. The voltage developed across each junction was measured with a null-balancing SQUID voltmeter relative to a wide probe far from the end of the film; the voltmeter was connected to each probe in turn by means of a mechanical superconducting switch operated from outside the cryostat. The normal state thermopower was measured in another part of the Al film, again by means of the SQUID voltmeter. The substrate was mounted in a vacuum can, and a heater and thermometers were attached to allow a known temperature gradient to be established.

The value of $\lambda_{Q^*}(T)$ was determined by injecting current through one probe and measuring the voltage at nearby probes. In all cases, the observed voltage was accurately exponential over as much as five decades: A representative example is shown in Fig. 25. The measured value of $\lambda_{Q^*}(T)$ is plotted vs. $(1 - T/T_c)$ in Fig. 26: The slope is -0.22 ± 0.03 . The value of $\tau_{Q^*} = 2N(0)e^2\lambda_{Q^*}^2/\sigma$ estimated from the measured values of

λ_{Q^*} and σ and with $N(0) = 1.74 \times 10^{28} \text{ eV}^{-1} \text{ m}^{-1}$ (Gschneidner 1964) yields $\tau_E = 1.6 \pm 0.2 \text{ ns}$, assuming that only electron-phonon scattering contributes to the charge relaxation near T_c as is implied by the fact that $\lambda_{Q^*} \propto (1 - T/T_c)^{-1/4}$. Two other samples yielded $\tau_E = 2.7 \pm 0.5 \text{ ns}$ and $2.3 \pm 0.4 \text{ ns}$. The average value of τ_E , about 2 ns, is about a factor of 6 smaller than that obtained by CC (Sec. 4). All three samples were sufficiently clean that charge relaxation due to electron-electron scattering should have been quite negligible. To eliminate the possibility that the Al films in the decay measurements differed in some way from those used in the CC experiments, Mamin et al. fabricated two samples in which the Al was deposited simultaneously, one in the configuration of Fig. 24 and one in the configuration of Fig. 5. The inferred values of τ_E were about 2 and 11 ns, respectively, in agreement with previous results. We note that the value of τ_E obtained from the decay measurements is only about a factor of two smaller than that obtained by Stuiyinga et al. (1981, 1983) from measurements on phase-slip centers in Al (Sec. 7). At the time of writing, there is no explanation for the discrepancy in the values of τ_E observed in the tunnel injection and spatial decay measurements. However, we emphasize that this discrepancy concerning τ_E does not enter into the discussion of thermoelectric effects, for which only the measured value of $\lambda_{Q^*}(T)$ is required.

We now turn to a discussion of the charge imbalance generated by a temperature gradient. Figure 27 shows $V(x)$ vs. distance for a sample at four different temperatures. In contrast to the behavior observed for the current injection experiments, the data show significant downward curvature near the end of the Al film. A straight-line fit to the data points farthest from the end of the Al film yields a decay length of $24 \pm 4 \text{ } \mu\text{m}$ that is independent of temperature, and always longer than the

temperature-dependent length measured in the current injection case. Thus, one concludes that the charge imbalance decay length measured in the thermoelectric experiment is not equal to λ_{Q^*} , presumably because the temperature gradient is non-uniform over a region near the end of the Al film where the heat flow enters the film from the substrate. In a quasi-one-dimensional model, it is easy to show that the gradient is given by

$$\frac{dT}{dx} = \frac{dT}{dx}\Big|_{\infty} [1 - \exp(-x/\lambda_T)], \quad (8.8)$$

where $dT/dx|_{\infty}$ is the gradient far from the end of the film and $\lambda_T = (gd/y_K)^{1/2}$. Here, g and d are the thermal conductivity and thickness of the Al film, and y_K is the Kapitza resistance of a unit area between the film and substrate. If we assume $d = 300$ nm, $g = 6$ Wm⁻¹ K⁻¹, and $y_K = 5 \times 10^3$ Wm⁻² K⁻¹ at T_c (Kaplan 1979), we find $\lambda_T = 20$ μ m. When Eq. (8.8) is inserted in Eqs. (8.3) and (8.4), one finds

$$V(x) = \frac{\lambda_{Q^*}^2}{\lambda_{Q^*}^2 - \lambda_T^2} (\lambda_{Q^*} e^{-x/\lambda_{Q^*}} - \lambda_T e^{-x/\lambda_T}) S \frac{dT}{dx}\Big|_{\infty}. \quad (8.9)$$

Figure 27 shows the fit of the data to Eq. (8.9) using values of $\lambda_{Q^*}(T)$ from the current injection experiments, and regarding S and λ_T as adjustable parameters. The fits are generally satisfactory. The inferred value of S near T_c was $(-2.7 \pm 0.6) \times 10^{-8}$ VK⁻¹, compared with a value measured in the normal state of $(-1.05 \pm 0.06) \times 10^{-8}$ VK⁻¹. Two other samples yielded values of $(-1.4 \pm 0.3) \times 10^{-8}$ VK⁻¹ and $(-1.0 \pm 0.3) \times 10^{-8}$ VK⁻¹ compared with normal state values of $(-0.94 \pm 0.06) \times$

10^{-8} VK^{-1} and $(-1.12 \pm 0.06) \times 10^{-8} \text{ VK}^{-1}$, respectively. Overall, the experiments provide a strong experimental verification of the theory of thermoelectric effects in superconductors, and, in particular, demonstrate that there is no discontinuity in the value of L_T at T_c .

8.3 Supercurrent-Induced Charge Imbalance in the Presence of a Temperature Gradient

A quite different kind of effect due to a temperature gradient was first pointed out by Pethick and Smith (1979b) who predicted that a charge imbalance proportional to $I \cdot VT$ should exist in the presence of a supercurrent I . Clarke et al. (1979a) observed this effect in Sn films, and established that the measured voltage was proportional to $I \cdot VT$, as predicted, but was two to three orders of magnitude smaller than the predicted value. This discrepancy arose because the theory assumed that the elastic scattering rate was negligible compared with the inelastic rate, whereas the reverse was true in the experiment. Three further theories then appeared (Schmid and Schön 1979, Clarke and Tinkham 1980, and Beyer Nielsen et al. 1980) in attempts to account quantitatively for the temperature dependence and magnitude of the data. More recently, Heidel and Garland (1981) observed similar effects in Al films, while Fjordbøge et al. (1981) have given a more detailed account of their work on Sn.

The experimental configuration used by Fjordbøge et al. is shown in Fig. 28. The Sn (or Sn + 3wt.%In) film was typically 300 nm thick and 0.1 mm wide in the narrow region. After the Sn was oxidized, three Cu (+3%Al) disks - 1 μm thick were deposited, followed by three Pb strips. In a given experiment, one of the three Sn-SnOx-Cu tunnel junctions was

used to measure the quasiparticle potential relative to the pair potential with a SQUID voltmeter. The substrate was mounted in a vacuum can, with a heater at each end, and thermometers were attached to the reverse side. In Figs. 29 and 30 we plot measured values of V vs. I for five values of ∇T and V vs. ∇T for 10 values of I for a representative sample. The voltage is clearly proportional to $I \cdot \nabla T$. Figure 31 shows $V_{\text{NS}}(0)/IVT$ vs. t for the same sample: To within the experimental resolution, all 8 samples showed the same behavior. In Fig. 32, we plot $V_{\text{NS}}(0)T/IVT$ vs. $(1 - t)$ for the same sample; the divergence at temperatures above about $0.8 T_c$ is close to $(1 - t)^{-1}$. It was found that the magnitude of the quantity $V_{\text{NS}}(0)T(1 - t)A/IVT$, where A is the cross-sectional area of the films, was very nearly the same for relatively clean Sn films, in which the mean free path was limited by boundary scattering, as for SnIn films in which the mean free path was limited by boundary scattering to about 60 nm.

Figure 33 indicates the physical origin of the effect. In Fig. 33(a) there is a thermal gradient, but no applied supercurrent. Quasiparticles moving from the left are at an effective temperature $T - \delta T$, while those moving from the right are at $T + \delta T$, where T is the local temperature. Thus, there is an imbalance in the populations of the $k > k_F$ and $k < k_F$ branches on the righthand side of the Fermi surface, but an equal and opposite imbalance on the lefthand side: As a result, $Q^* = 0$. If we now impose a superfluid velocity v_S [Fig. 33(b)] the excitation energies are raised and lowered on opposite sides of the Fermi surface by an amount $p_k \cdot v_S$ [see Sec. 5.2]. The induced asymmetry ensures that the population imbalances on opposite sides of the Fermi surface no

longer cancel, and the resulting charge imbalance is the origin of the observed voltage. We now briefly review the theoretical situation.

The result of Schmid and Schön (1979) can be written in the form

$$V = \frac{p_F \ell}{6eg_{NS}(0)} \frac{v_S \cdot \nabla T}{T} \frac{\Delta}{k_B T (1 - Z) \text{ch}^2(\Delta/2k_B T)} \ln(8\Delta\tau_E/\hbar). \quad (8.10)$$

Here, p_F is the Fermi momentum, and Z is given by Eq. (2.24). Clarke and Tinkham (1980) used a simple kinetic approach to obtain

$$V = \frac{p_F \ell}{6eg_{NS}(0)} \frac{v_S \cdot \nabla T}{T} \frac{\Delta}{k_B T (1 - Z) \text{ch}^2(\Delta/2k_B T)}. \quad (8.11)$$

Equation (8.10) exceeds Eq. (8.11) by a factor of $\ln(8\Delta\tau_E/\hbar)$, which varies relatively slowly with temperature over the experimental range studied, with an average value of about 6. Apart from this factor, the Schmid-Schön and Clarke-Tinkham approaches yield the same result. One can convert v_S into a current density by writing $v_S = j_S/n_S e = \mu_0 j_S \lambda^2(T) e/m$, and using the result $\lambda^2(T) = \lambda_L^2(0)(1 + \xi_0/\ell)(1 - t^4)^{-1}$ (Tinkham 1975) to find

$$v_S = \frac{\mu_0 j_S e \lambda_L^2(0)(1 + \xi_0/\ell)}{m(1 - t^4)}. \quad (8.12)$$

Near T_C , $1 - Z \rightarrow \pi\Delta/4k_B T$, $\text{ch}^2(\Delta/2k_B T) \rightarrow 1$, and $1 - t^4 \rightarrow 4(1 - t)$, so that the temperature dependence of the voltage at fixed current is dominated by the temperature dependence of v_S , $(1 - t)^{-1}$, in good agreement with the experimental results. The curves calculated for the two theories

with $v_F = 6.5 \times 10^5 \text{ ms}^{-1}$, $\lambda_L(0) = 5 \times 10^{-8} \text{ m}$, and $\xi_0 = 2.3 \times 10^{-7} \text{ m}$ are plotted in Fig. 32. The curves were fitted at $T/T_c = 0.99$ by multiplying Eq. (8.11) by 2.4, and Eq. (8.10) by 0.4. A detailed critique of these two theories can be found in the paper by Pethick and Smith (1981b).

Beyer Nielson et al. (1980) and, subsequently, Pethick and Smith (1981a,b) have solved the Boltzmann equation in the clean limit for the case where $\tau_E^{-1} \rightarrow 0$ and for an isotropic energy gap to obtain

$$V = \frac{p_F \ell}{e g_{NS}(0)} \frac{v_s \cdot \nabla T}{T} \left[\frac{1.93 \Delta / k_B T}{ch^2(\Delta / 2k_B T)} + \frac{8/15}{\exp(\Delta / k_B T) + 1} \right]. \quad (8.13)$$

Equation (8.13) is also plotted in Fig. 32, and evidently has a different temperature dependence than the experimental data. In Eq. (8.13), the first term in square brackets dominates the second for $T/T_c \lesssim 0.998$, that is, throughout the experimentally realizable range. The first term arises from quasiparticles in the energy range $\Delta - p_F v_s$ to $\Delta + p_F v_s$ in which the available phase space for charge relaxation via elastic scattering is reduced. This effect is particularly pronounced for quasiparticles with energies near $\Delta - p_F v_s$. As a result, the charge imbalance in this "pocket" takes a relatively long time to relax compared with that at energies above $\Delta + p_F v_s$, which is accounted for by the second term in square brackets in Eq. (8.13). However, it appears that, in practice, the energy levels in the pocket are sufficiently smeared out that the calculated enhancement of the relaxation time is not very significant. There are at least three mechanisms by which this smearing may occur: Inelastic scattering, gap anisotropy, and impurity scattering (Schön 1981a, 1981b, Beyer Nielsen et al. 1982). When the contribution of the pocket is eliminated, the second term in square brackets

becomes dominant but, unfortunately, is valid only very close to T_c .

Beyer Nielsen et al. (1982) have used a Green's function approach to calculate the voltage in the dirty limit in the presence of electron-phonon scattering, and find

$$V = \frac{2p_F \ell}{3eg_{NS}(0)} \frac{v_s \cdot VT}{T} \frac{F(\Delta/k_B T)}{1 + \lambda}, \quad (8.14)$$

where λ is the electron-phonon interaction parameter, and F is a specified dimensionless function. Near T_c , Eq. (8.14) agrees with the Schmid-Schön result, Eq. (8.10). Figure 34 shows Eq. (8.14) plotted versus T/T_c together with the data obtained by Fjordbøge et al. for their dirtiest sample. The theoretical curve has been fitted at one temperature by scaling with a factor of 0.43. Given that effects of anisotropy are not included in the theory, the fit is satisfactory.

As noted earlier, Heidel and Garland (1981) measured similar effects in Al. The spread in their values of $Vg_{NST}/I \cdot VT$ from sample to sample was an order of magnitude, substantially greater than for the work on Sn. This variation perhaps reflects variations in the homogeneity of the Al films. The temperature dependence of the data fitted the SS and CT theories [Eqs. (8.10) and (8.11)], but not the prediction of Eq. (8.13), which, of course, is valid only in the clean limit, while the samples were definitely in the dirty limit. Heidel and Garland also examined two samples with 520 and 1660 ppm Er, respectively, and found no significant difference in the magnitude of the effect compared with the samples with no magnetic impurities. This result is consistent with the idea (Clarke and Tinkham 1980) that the charge imbalance generation is a

volume process in which the generation and relaxation processes cannot be independently varied. Thus, the value of Q^* is imposed by the temperature gradient, the magnitude depending only on the transport mean free path which limits the distance over which the gradient is effective in producing a nonequilibrium population. Thus, times such as τ_E and τ_{Q^*} play very little role in determining the magnitude of Q^* . This situation is in complete contrast to the other charge imbalance experiments described earlier, such as tunnel injection, the NS interface, phase slip centers or generation by a temperature gradient in the absence of an applied supercurrent, where the generation occurs at a well-defined spatial homogeneity, and the generation and relaxation of Q^* are quite distinct processes. Thus, as we have seen in Sec. 5.1, the effect of a small amount of Er in Al dramatically lowers Q^* in tunnel injection experiments.

9. DYNAMICAL CHARGE IMBALANCE

All of the experiments, and the associated theories, described above are concerned with a steady state situation, in which the charge imbalance is maintained at a constant value by a suitable generation process. However, it is appropriate to remark briefly on dynamical charge imbalance effects where, for example, one considers the time decay of a pulse of charge imbalance. Under such circumstances, Kadin et al. (1980) show that the appropriate decay rate is τ_E^{-1} , rather than $\tau_{Q^*}^{-1}$. The physical reason for the difference is as follows. In a steady state measurement, the charge imbalance relaxes by means of changes in the distribution function alone, the charge, q_k , associated with a given k -value remaining fixed. This leads to the well-established result $\tau_{Q^*}^{-1} = (\pi\Delta/4k_B T)\tau_E^{-1}$. On the other hand, when a pulse of charge imbalance decays with time, in addition to the relaxation of the distribution there is an accompanying change in q_k as the nonequilibrium value of μ_s decays towards its equilibrium value. Kadin et al. show that in the limit $\Delta(T)/k_B T \ll 1$, this additional process modifies the charge imbalance relaxation rate to τ_E^{-1} .

Kadin et al. show that, in general, Q^* should obey a charge imbalance relaxation equation

$$D\tau_{Q^*}\nabla^2 Q^* = \tau_0\tau_E\ddot{Q}^* + (\tau_0 + \tau_E)\dot{Q}^* + Q^*, \quad (9.1)$$

where $\tau_0 = \tau_1(n/n_s)$ is the response time of the supercurrent to a change in the total current (n and n_s are the densities of electrons and superfluid electrons in the normal and superconducting states). In the low frequency limit, Eq. (9.1) immediately yields the static decay length

$(D\tau_{Q^*})^{1/2}$ [Eq. (6.1)]. However, in general, Eq. (9.1) describes damped, dispersive charge imbalance waves with the dispersion relation

$$-\Lambda^2 k^2 = (1 + i\omega\tau_0)(1 + i\omega\tau_E), \quad (9.2)$$

where Λ is a characteristic length, for waves of the form $\exp[i(\omega t - k \cdot r)]$.

One might expect charge imbalance waves to be generated by PSCs, so that the Josephson oscillations of two neighboring PSCs could be locked together by this mechanism, resulting in voltage locking. As mentioned in Sec. 7, such effects have been observed, and although the evidence is perhaps not overwhelming, it seems very plausible that charge imbalance waves are responsible for this interaction.

The concept of dynamical charge imbalance also occurs in a quite different situation, namely charge imbalance fluctuations (Lemberger 1981). Whenever a charge imbalance is generated, there is an associated electrical resistance: It is, of course, this resistance that is measured directly in the measurements on the NS interface described in Sec. 6. Lemberger (1981) has pointed out that in thermal equilibrium there must be fluctuations in Q^* related to this resistance via Nyquist's theorem (Nyquist 1928). We briefly describe this analysis.

Lemberger calculates the mean square fluctuation $\langle(\delta\mu_S)^2\rangle$ in the limit $\Delta(T)/k_B T \ll 1$, neglecting gradients in $\delta\mu_S$. Thus, the result can be applied only to situations in which $\delta\mu_S$ is spatially uniform, for example, charge imbalance injected into a superconducting film of thickness $\ll \lambda_{Q^*}$ via a tunnel barrier of area $\gg \lambda_{Q^*}^2$. By combining the theory of

charge imbalance with equilibrium thermodynamics, he obtains the result that in thermal equilibrium (no applied current)

$$\langle(\delta\mu_S)^2\rangle = 2(k_B T)^2 / \pi N(0) \Omega \Delta(T) \quad [\Delta(T) \ll k_B T]. \quad (9.3)$$

For tunneling injection into a superconductor, the resistance $R_{Q^*} = V_d/I_i$ in the limit $\Delta(T)/k_B T \ll 1$ is easily obtained from Eq. (2.22) with $F^* = 1$, $g_{NS}(0) = 1$ and $\tau_{Q^*} = 4k_B T \tau_E / \pi \Delta(T)$:

$$R_{Q^*} = 4k_B T \tau_E / 2\pi N(0) e^2 \Omega \Delta(T). \quad (9.4)$$

This resistance is in series with the tunneling resistance of the barrier. It was observed by Clarke and Paterson (1974) and Lemberger and Clarke (1981) as a dip in the conductance of the detector junctions near T_C , and measured in detail by Lemberger (1981).

To apply the Nyquist result, one assumes that the RC time constant of the injection junction is much less than τ_E , that the resistance of the injection junction is large compared with R_{Q^*} , and that τ_0 is small compared with τ_E . Under these conditions, the Nyquist theorem yields

$$\langle(\delta\mu_S/e)^2\rangle = 4k_B T R_{Q^*} B, \quad (9.5)$$

where B is the bandwidth for the fluctuations. Substituting Eqs. (9.3) and (9.4) in Eq. (9.5), one finds $B = 1/4\tau_E$. Thus, the relaxation time for charge imbalance fluctuations, as for other dynamical charge imbalance relaxation processes, is τ_E .

Apart from the voltage locking of neighboring PSCs, there appears to be no experimental work on dynamical charge imbalance processes. This is obviously an area in which more research is needed.

10. CONCLUDING SUMMARY

In this chapter, I have reviewed the essential ideas of charge imbalance in superconductors, and discussed the various physical situations in which charge imbalance plays a role. We first considered the situation in which charge imbalance is injected via a tunnel junction at a rate $\dot{Q}_i^* = F^* I_i / e\Omega$ and then relaxes in one or more of several possible ways to produce a steady state voltage $V = Q^* / 2N(0)eg_{NS}(0)$ that is measured by a tunneling contact to a normal metal. Such measurements yield the charge imbalance relaxation rate, $\tau_{Q^*}^{-1}$. In the absence of gap anisotropy or magnetic scattering and in the limit $\Delta(T)/k_B T \rightarrow 0$, the charge relaxation is due solely to electron-phonon processes and occurs at a rate $(F^* \tau_{Q^*})^{-1} = (\pi\Delta(T)/4k_B T)\tau_E^{-1}$ (neglecting electron-electron scattering for the moment).

Under appropriate conditions, elastic scattering also relaxes charge imbalance. In the presence of non-zero gap anisotropy the coherence factor $(uu' - vv')^2$ for branch crossing is no longer zero, and elastic scattering produces charge relaxation at a rate that scales approximately as $\Delta^4(T)$ near T_c . This effect has been observed in both Sn and Al. The mean free path in the Al films was reduced by oxygen doping, a process that also enhanced T_c , in some cases substantially. The films with significantly enhanced transition temperatures exhibited much faster inelastic relaxation rates than could be explained in terms of electron-phonon scattering; recent work has explained these rates rather satisfactorily in terms of electron-electron scattering. The presence of magnetic impurities can greatly enhance $\tau_{Q^*}^{-1}$ because the coherence factor for branch crossing $(uu' + vv')^2$, approaches unity at low energies. Experimental data

obtained on Al doped with Er is in excellent agreement with the Schmid-Schön prediction $(F^* \tau_{Q^*}^{-1}) = [\pi \Delta(T) / 4k_B T_c \tau_E] (1 + 2\tau_E / \tau_S)^{1/2}$ over a wide range of values of τ_E / τ_S for $\Delta / k_B T_c \lesssim 0.8$. Charge relaxation can also be induced by a supercurrent: The current induces an asymmetry across the Fermi surface that allows branch relaxation via elastic scattering. The results from experiments on dirty Al are again in excellent agreement with the Schmid-Schön result. However, computer solutions of the Boltzmann equation in the last two cases produced results that were strikingly different from the experimental data. It now seems probable that electron-electron scattering was non-negligible in all of these samples, and it is possible that the inclusion of this process in the Boltzmann equation would remove the discrepancy.

The next three sections were concerned with various experiments in which charge imbalance plays a central role. The resistance of the NS interface near T_c can be explained in terms of charge imbalance injected into the superconductor where it decays with a characteristic length λ_{Q^*} . A simple modification of the tunneling theory for the injection of Q^* yields a result that is in excellent agreement with experiments on Pb, Sn, and In, and that produces very reasonable values of τ_E . The voltage steps and dynamic resistance of the I-V characteristics of microstrips containing phase slip centers is nicely explained in terms of the charge imbalance injected from the normal core of each PSC into the neighboring superconducting regions. The interaction of nearby PSCs at zero voltage can also be explained in terms of this static model, but the frequency locking that occurs at non-zero voltages probably involves an interaction via charge imbalance waves.

Three experiments were described in which a temperature gradient was involved. The first involved the measurement of the charge imbalance induced in a superconductor near a normal contact in the presence of a temperature gradient across the NS interface. The second was concerned with measurements of the spatial decay of the charge imbalance near the end of an Al film along which a temperature gradient was maintained. Both of these experiments involve the thermopower S of the superconductor. In each case, the agreement of theory and experiment was very satisfactory, and the measured values of S were in reasonable accord with measured normal state values. The third experiment involved the charge imbalance generated by a temperature gradient in the presence of an applied supercurrent. The agreement between the results and theoretical predictions is now in a very satisfactory state.

The last section briefly described dynamical charge imbalance effects, in particular charge imbalance waves and charge imbalance fluctuations. This is an area where there seems to be considerable scope for further experimental work.

Values of the electron-phonon scattering rate, τ_E^{-1} , have been extracted from experiments on tunnel injection, the NS interface and PSCs, in which one measures the steady state value of Q^* induced by a known injection rate into a known volume, and also from measurements of λ_{Q^*} , in which one measures the spatial decay of Q^* along a superconducting strip. The values of τ_E obtained for each of the metals Pb, Sn, and In are generally consistent and in good agreement with predictions based on α^2F , with an overall spread of perhaps a factor of two in each case. On the other hand, the values of τ_E obtained for relatively clean Al films

are very puzzling. Measurements from tunneling injection and detection yield about 12 ns, a value that is in good agreement with values obtained from magnetoconductance data. This value is 3 or 4 times lower than the predicted value. Furthermore, estimates of τ_E obtained from λ_{Q^*} measured near PSCs or near a tunnel injection junction yield values of τ_E of 4 and 2 ns, respectively. Although it is now clear that electron-electron scattering can play an important or even dominant role in relatively dirty Al, it is most improbable that it plays a significant role in clean films. Thus, at present, there seems to be no explanation of these very large discrepancies in the values of τ_E .

It is noteworthy that Al was the material used in the measurements of $\tau_{Q^*}^{-1}$ in the presence of magnetic impurities or of a supercurrent, which are in disagreement with the predictions of the Boltzmann equation. In this case it is possible, but by no means certain, that electron-electron scattering may explain the discrepancy. Thus, although Al has been a widely used material in experiments on charge imbalance, it is clearly a "bad actor", at least partly because the electron-phonon scattering rate is so slow that other charge relaxation mechanisms are of much greater relative importance than they are in Pb, Sn, and In. Obviously, much remains to be done to resolve these issues.

Despite the problems associated with Al, however, experiments on charge imbalance are generally in remarkably good agreement with theoretical predictions, illustrating in a rather striking way some of the fundamental subtleties of superconductivity, such as quasiparticle charge, coherence factors, and a variety of pair breaking mechanisms.

ACKNOWLEDGEMENTS

Much of the work described here was carried out in collaboration with others, namely C. C. Chi, U. Eckern, B. R. Fjordbøge, T-Y. Hsiang, T. R. Lemberger, P. E. Lindelof, H. J. Mamin, J. L. Paterson, A. Schmid, G. Schön, M. Tinkham, and D. J. Van Harlingen, to all of whom I express my grateful thanks. In addition I should like to thank J-J. Chang, O. Entin-Wohlman, J. M. Gordon, R. Orbach, A. B. Pippard, C. C. Pethick, D. E. Prober, D. J. Scalapino, H. Smith, and J. R. Waldram for helpful discussions.

This work was supported by the Director, Office of Energy Research, Office of Basic Energy Sciences, Materials Sciences Division of the U.S. Department of Energy under Contract Number DE-AC03-76SF00098.

REFERENCES

- Abrahams, E., Anderson, P. W., Lee, P. A., and Ramakrishnan, T. V., 1981, Phys. Rev. B 24, 6783.
- Abrikosov, A. A. and Gor'kov, L. P., 1960, Zh. Eksp. Teor. Fiz. 39, 1781 [Sov. Phys. JETP 12:1243].
- Anderson, P. W., 1959, J. Phys. Chem. Solid 11, 26.
- Andréev, A. F., 1964, Zh. Eksp. Teor. Fiz. 46, 182 [Sov. Phys. JETP 19, 1228].
- Aponte, J. M. and Tinkham, M., 1983, J. Low Temp. Phys. 51, 189.
- Aronov, A. G., 1974, Zh. Eksp. Teor. Fiz. 67, 178 [Sov. Phys. JETP 40, 90].
- Artemenko, N. and Volkov, A. F., 1976, Zh. Eksp. Teor. Fiz. 70, 1051 [Sov. Phys. JETP 43, 548].
- Artemenko, N. and Volkov, A. F., 1977, Zh. Eksp. Teor. Fiz. 72, 1018 [Sov. Phys. JETP 45, 533].
- Artemenko, N., Volkov, A. F., and Zaitsev, A. V., 1978, J. Low Temp. Phys. 30, 487.
- Bardeen, J., Cooper, L. N., and Schrieffer, J. R., 1957, Phys. Rev. 108, 1175.
- Battersby, S. J. and Waldram, J. R., 1983, unpublished.
- Beyer Nielsen, J., Ono, Y. A., Pethick, C. J., and Smith, H., 1980, Solid State Comm. 33, 925.
- Beyer Nielsen, J., Pethick, C. J., Rammer, J., and Smith, H., 1982, J. Low Temp. Phys. 46, 565.
- Blonder, G. E., Tinkham, M., and Klapwijk, T. M., 1982, Phys. Rev. B 25, 4515.
- Blonder, G. E. and Tinkham, M., 1983, Phys. Rev. B 27, 112.

- Chambers, R. G., 1952, Proc. Roy. Soc. Lond. 215, 481.
- Chang, J.-J., 1977, Phys. Rev. Lett. 39, 1352.
- Chang, J.-J., 1979, Phys. Rev. B 19, 1420.
- Chang, J.-J. and Scalapino, D. J., 1977, Phys. Rev. B 15, 2651.
- Chi, C. C. and Clarke, J., 1979, Phys. Rev. B 19, 4495.
- Chi, C. C. and Clarke, J., 1980, Phys. Rev. B 21, 333.
- Christian, J. W., Jan, J. P., Pearson, W. P., and Templeton, I. M., 1958, Proc. Roy. Soc. Lond. A245, 213.
- Clarke, J., 1972, Phys. Rev. Lett. 28, 1363.
- Clarke, J., 1976, in: Superconductor Applications: SQUIDS and Machines, eds. B. B. Schwartz and S. Foner (Plenum, New York).
- Clarke, J., 1981, in: Nonequilibrium Superconductivity, Phonons, and Kapitza Boundaries, ed. Gray, K. E. (Plenum, New York)ch.5.
- Clarke, J., Eckern, U., Schmid, A., Schön, G., and Tinkham, M., 1979, Phys. Rev. B 20, 3933.
- Clarke, J., Fjordbøge, B. R., and Lindelof, P. E., 1979a, Phys. Rev. Lett. 43, 642.
- Clarke, J. and Paterson, J. L., 1974, J. Low Temp. Phys. 15, 491.
- Clarke, J. and Tinkham, M., 1980, Phys. Rev. Lett. 44, 106.
- Craven, R. A., Thomas, G. A., and Parks, R. D., 1971, Phys. Rev. B 4, 2185.
- de Gennes, P. G., 1966, Superconductivity of Metals and Alloys (Benjamin, New York).
- Dolan, G. J. and Jackel, L. D., 1977, Phys. Rev. Lett. 39, 1628.
- Entin-Wohlman, O. and Orbach, R., 1979, Phys. Rev. B 19, 4510.
- Entin-Wohlman, O. and Orbach, R., 1981, Phys. Rev. B 24, 1177.
- Fickett, F. R., 1971, Cryogenics 11, 349.

- Fjordbøge, B. R., Lindelof, P. E., and Clarke, J., 1981, *J. Low Temp. Phys.* 44, 535.
- Galperin, Yu. M., Gurevich, V. L., and Kozub, V. I., 1974, *Zh. Eksp. Teor. Fiz.* 66, 1387 [*Sov. Phys. JETP* 39, 680].
- Ginzburg, V. L. and Landau, L. D., 1950, *Zh. Eksp. Teor. Fiz.* 20, 1064.
- Gordon, J. M., Lobb, C. J., and Tinkham, M., 1983, *Phys. Rev. B* 28, 4046.
- Gray, K. E., 1981, in: *Nonequilibrium Superconductivity, Phonons, and Kapitza Boundaries*, ed. Gray, K. E. (Plenum, New York)ch. 5.
- Gschneidner, K. A., 1964, *Solid State Phys.* 16, 275.
- Harding, G. L., Pippard, A. B., and Tomlinson, J. R., 1974, *Proc. Roy. Soc. Lond.* A340, 1.
- Heidel, D. F. and Garland, J. C., 1981, *J. Low Temp. Phys.* 44, 295.
- Hsiang, T. Y., 1980, *Phys. Rev. B* 21, 956.
- Hsiang, T. Y. and Clarke, J., 1980, *Phys. Rev. B* 21, 945.
- Jillie, D. W., Lukens, J. E., and Kao, Y. H., 1977, *Phys. Rev. Lett.* 38, 915.
- Jillie, D. W., Nerenberg, M. A. H., and Blackburn, J. A., 1980, *Phys. Rev.* 21B, 125.
- Kadin, A. M., Skocpol, W. J., and Tinkham, M., 1978, *J. Low Temp. Phys.* 33, 481.
- Kadin, A. M., Smith, L. N., and Skocpol, W. J., 1980, *J. Low Temp. Phys.* 33, 497.
- Kaplan, S., 1979, *J. Low Temp. Phys.* 37, 343.
- Kaplan, S. B., Chi, C. C., Langenberg, D. N., Chang, J. J., Jafarey, S., and Scalapino, D. J., 1976, *Phys. Rev. B* 14, 4854.
- Kaplan, S. B., Kirtley, J. R., and Langenberg, D. N., 1977, *Phys. Rev. Lett.* 39, 291.

Kirtley, J. R., Kent, D. S., Kaplan, S. B., and Langenberg, D. N., 1978, J. Physique Supplement 39, C6-511.

Kittel, C., 1976, Introduction to Solid State Physics, 5th edition (Wiley, New York).

Klapwijk, T. M. and Mooij, J. E., 1976, Phys. Lett. 57A, 97.

Klapwijk, T. M., Blonder, G. E., and Tinkham, M., 1982, Physica 109B, 1657.

Krähenbühl, Y. and Watts-Tobin, R. J., 1979, J. Low Temp. Phys. 35, 569.

Lawrence, W. E. and Meador, A. B., 1978, Phys. Rev. B 18, 1154.

Lemberger, T. R., 1981, Phys. Rev. B 24, 4105.

Lemberger, T. R. and Clarke, J., 1981a, Phys. Rev. B 23, 1088.

Lemberger, T. R. and Clarke, J., 1981b, Phys. Rev. B 23, 1100.

Lindelof, P. E. and Bindslev Hansen, J., 1977, J. Low Temp. Phys. 29, 369.

Lindelof, P. E. and Bindslev Hansen, J., 1981, in: Nonequilibrium Superconductivity, Phonons, and Kapitza Boundaries, ed. Gray, K. E. (Plenum, New York)ch. 19.

Maki, K., 1969, in: Superconductivity, ed. Parks, R. D. (Marcel Dekker, New York).

Mamin, H. J., Clarke, J., and Van Harlingen, D. J., 1983, Phys. Rev. Lett. 51, 1480.

Mamin, H. J., Clarke, J., and Van Harlingen, D. J., 1984, Phys. Rev. B (to appear).

Markowitz, D. and Kadanoff, L. P., 1963, Phys. Rev. 131, 563.

Meservey, R. and Schwartz, B. B., 1969, in: Superconductivity, ed. Parks, R. D. (Marcel Dekker, New York).

Meyer, J. D., 1973, Appl. Phys. 2, 303.

Meyer, J. and von Minnigerode, G., 1972, Phys. Lett. 38A, 529.

Moody, M. V. and Paterson, J. L., 1979, J. Low Temp. Phys. 34, 83.

- Nyquist, H., 1928, Phys. Rev. 32, 110.
- Octavio, M., Tinkham, M., Blonder, G. E., and Klapwijk, T. M., 1983, Phys. Rev. B 27, 6739.
- Ovchinnikov, Yu. N., 1977, J. Low Temp. Phys. 28, 43.
- Palmer, D. W. and Mercereau, J. E., 1977, Phys. Lett. 61A, 135.
- Pethick, C. J. and Smith, H., 1979a, Annals of Physics 119, 133.
- Pethick, C. J. and Smith, H., 1979b, Phys. Rev. Lett. 43, 640.
- Pethick, C. J. and Smith, H., 1981a, in: Nonequilibrium Superconductivity, Phonons, and Kapitza Boundaries, ed. Gray, K. E. (Plenum, New York) ch. 15.
- Pethick, C. J. and Smith, H., 1981b, J. Phys. C13, 6313.
- Pippard, A. B., 1965, The Dynamics of Conduction Electrons (Gordon and Breach, New York).
- Pippard, A. B., 1981, in: Nonequilibrium Superconductivity, Phonons, and Kapitza Boundaries, ed. Gray, K. E. (Plenum, New York)ch. 12.
- Pippard, A. B., Shepherd, J. G., and Tindall, D. A., 1971, Proc. Roy. Soc. Lond. A324, 17.
- Rieger, T. J., Scalapino, D. J., and Mercereau, J. E., 1971, Phys. Rev. Lett. 27, 1787.
- Santhanam, P. and Prober, D. E., 1983, unpublished.
- Schmid, A. and Schön, G., 1975, J. Low Temp. Phys. 20, 207.
- Schmid, A. and Schön, G., 1979, Phys. Rev. Lett. 43, 793.
- Schön, G., 1981a, in: Festkörperprobleme (Advances in Solid State Physics), Vol. 21, ed. Trensck, J. (Vieweg, Braunschweig)p.341.
- Schön, G., 1981b, Physica 107B, 171.
- Skocpol, W. J., 1981, in: Nonequilibrium Superconductivity, Phonons, and Kapitza Boundaries, ed. Gray, K. E. (Plenum, New York)ch. 18.

- Skocpol, W. J., Beasley, M. R., and Tinkham, M., 1974, J. Low Temp. Phys. 16, 145.
- Skocpol, W. J. and Jackel, L. D., 1981, Physica 108B, 1021.
- Stuivinga, M., Mooij, J. E., and Klapwijk, T. M., 1981, Physica 108B, 1023.
- Stuivinga, M., Mooij, J. E., and Klapwijk, T. M., 1982, J. Low Temp. Phys. 46, 555.
- Stuivinga, M., Ham, C. L. G., Klapwijk, T. M., and Mooij, J. E., 1983a, J. Low Temp. Phys. 53, 633.
- Stuivinga, M., Klapwijk, T. M., Mooij, J. E., and Bezuijen, A., 1983b, J. Low Temp. Phys. 53, 673.
- Tinkham, M., 1972, Phys. Rev. B 6, 1747.
- Tinkham, M., 1975, Introduction to Superconductivity (McGraw-Hill, New York).
- Tinkham, M., 1979, Festorperprobleme (Advances in Solid State Physics), ed. Trensck, J., Vol.19, p.363.
- Tinkham, M. and Clarke, J., 1972, Phys. Rev. Lett. 28, 1366.
- Van Harlingen, D. J., 1981, J. Low Temp. Phys. 44, 163.
- Van Harlingen, D. J., 1982, Physica 109 and 110 B + C, 1710.
- Waldram, J. R., 1975, Proc. Roy. Soc. Lond. A345, 231.
- Webb, W. W. and Warburton, R. J., 1968, Phys. Rev. Lett. 20, 461.
- Yu, M. L. and Mercereau, J. E., 1972, Phys. Rev. Lett. 28, 1117.

Table I. Measured and Calculated Quantities for Five Al Samples

Sample	T_c (K)	ℓ (nm)	τ_E (ns)	$\tau_{Q*el}^{-1}(0)\tau_E$	$\langle a^2 \rangle_o$
8	1.267	78	13	0.62	0.022
11	1.306	23	8	0.093	0.017
12	1.411	12.5	5.8	0.062	0.025
13	1.573	6.0	1.5	0.031	0.076
15	2.113	1.0	1.0	a	a

- a. the upward curvature was too small to enable an estimate of $\tau_{Q*el}^{-1}(0)$ to be made.

Table II. Measured and Calculated Parameters for AlEr Films

Sample	Er conc (ppm)	T_c (K)	l (nm)	τ_E (ns)	τ_S (est.) (ps)	τ_S (meas.) (ps)
1	21	1.338	38	8.6	2500	1100
6	81	1.350	32	8.3	650	860
7	220	1.410	22	7.4	240	210

Table III. Properties of SNS Junctions. The Measured Values of τ_E are Averaged over 2 or 3 Samples of Each Type.

Superconductor/ normal metal	Type	Measured τ_E (10^{-10} s)	Calculated ^a τ_E (10^{-10} s)
Pb _{0.99} Bi _{0.01} ⁻ Cu _{0.97} Al _{0.03}	film	0.25	0.23(Pb)
Sn-Ir	foil	2.6	2.7
Sn _{0.99} In _{0.01} ⁻ -Ir	foil	1.1	2.7(Sn)
In-Ir	foil	1.1	1.0

a. Kaplan et al. (1976)

FIGURE CAPTIONS

- Fig. 1. The effect on (a) condensate density, and (b) the quasiparticle excitation spectrum when electron-like excitations are added to the superconductor. The solid and dashed lines represent equilibrium and displacement from equilibrium, respectively.
- Fig. 2. $(4k_B T \tau_E / \pi \Delta) \tau_{Q^*}^{-1}$ vs. $\Delta(T)/k_B T$ and T/T_C : Computed values for $eV_i = 0.01 \Delta(T)$ ($-\square-$), $10 \Delta(T)$ ($-o-$), and $10k_B T_C$ ($-\Delta-$) (Chi and Clarke 1980).
- Fig. 3. Computed values of $(4/\pi) \tau_{Q^*}^{-1}$ vs. $\Delta(T)/k_B T$ and T/T_C for $eV_i = 0.01 \Delta(T)$ ($-\square-$), and $10 \Delta(T)$ ($-o-$) (Chi and Clarke 1980).
- Fig. 4. $[4k_B T \tau_E / \pi \Delta(T)] \tau_{Q^*}^{-1}$ and $[4k_B T \tau_E / \pi \Delta(T)] (F^* \tau_{Q^*})^{-1}$ vs. $eV_i / \Delta(T)$ for $T = 0.9 T_C$ (Chi and Clarke 1980).
- Fig. 5. Configuration of tunneling experiment to generate and detect charge imbalance in a Sn film. A SQUID voltmeter is used to measure the voltage between the Sn and Cu films generated by the current passed between the Al and Sn films (Clarke 1972).
- Fig. 6. $\delta_{NS}(0) 2V_d / I_1$ vs. T/T_C for pure Sn and SnIn. The solid line is a fit of $k_B T_C / \Delta(T)$ to the data for SnIn for $T/T_C \gtrsim 0.7$ (Clarke and Paterson 1974).
- Fig. 7. Measured values of $(F^* \tau_{Q^*})^{-1}$ vs. $\Delta/k_B T_C$ for 5 samples listed in Table I (sample numbers shown in parenthesis). The solid lines are a best fit to the solution of the Boltzmann equation (Chi and Clarke 1979).
- Fig. 8. $(F^* \tau_{Q^*})^{-1}$ normalized to $(\pi/4\tau_E)(1 + 2\tau_E/\tau_S)^{1/2}$ vs. $\Delta/k_B T_C$. The curves approach the origin with unity slope. The dashed line is an extrapolation of the SS theory to low temperatures. The

inset shows the region near the origin (Lemberger and Clarke 1980a).

Fig. 9. Experimental values of $(F^* \tau_{Q*})^{-1}$ vs. $\Delta/k_B T_C$ for samples with Er concentrations of 21 (#1), 81 (#6), and 220 (#7) at.ppm, with straight lines drawn through the data by eye. The other curves, which represent computer solutions to the Boltzmann equation, have the same slope as the data in the limit $\Delta/k_B T_C \rightarrow 0$ (Lemberger and Clarke 1980a).

Fig. 10. S (slope of $(F^* \tau_{Q*})^{-1}$ vs. $\Delta/k_B T_C$ for small $\Delta/k_B T_C$) vs. $(\pi/4\tau_E)(1 + 2\tau_E/\tau_S)^{1/2}$ for all samples. The solid line through the origin has unity slope (Lemberger and Clarke 1980a).

Fig. 11. $(SF^* \tau_{Q*})^{-1}$ vs. $\Delta/k_B T_C$ for one representative sample of each impurity concentration (Lemberger and Clarke 1980a).

Fig. 12. Typical experimental plot of V_d vs. I_S for fixed I_i . The points are a fit to a function of the form $V_d(I_S) = V_d(0)/(1 + bI_S^2)^{1/2}$, with b as the fitting parameter (Clarke and Lemberger 1980b).

Fig. 13. Data points are measured values of b , solid and dashed lines are fits of b^{SS} and b^{num} to the data. The values of T_C , λ , and τ_E are 1.370 K, 25 nm and 5.3 ns for sample 1 and 1.514 K, 11 nm, and 2.7 ns for sample 2. The average values of b^{SS}/b^{meas} over the temperature range studied are 0.36 and 0.51 for samples 1 and 2; the value $\lambda_L(0) = 160$ nm (Meservey and Schwartz 1969) was used (Lemberger and Clarke 1980b).

Fig. 14. Variation of energy gap, Δ , electric field, E , electric potential, V , normal current, j_N , and supercurrent, j_S , across an NS interface for $k_B T/\Delta \rightarrow 0$, $k_B T \sim \Delta$, and $\Delta/k_B T \rightarrow 0$. The gap is

taken to be zero in N , and the normal state properties are assumed to be the same in the two metals (Hsiang and Clarke 1980).

Fig. 15. Circles are measured total resistance vs. T/T_c for SNS junctions listed in Table III. The solid lines above $0.9 T_c$ [$0.96 T_c$ in (b)] are the fit to Eq. (6.5), while the dashed lines show the extrapolation of the theory to lower temperatures (Hsiang and Clarke 1980).

Fig. 16. Total measured resistance vs. $Z(T)(k_B T/\Delta)^{1/2}$ for the samples shown in Fig. 15. The solid lines are a least-squares fit to the data for $T > 0.9 T_c$ [$0.96 T_c$ for (b)] (Hsiang and Clarke 1980).

Fig. 17. I vs. V for the whole length of the Sn bridge $140 \mu\text{m}$ long, $4 \mu\text{m}$ wide, and $0.1 \mu\text{m}$ thick shown inset (Skocpol et al. 1974).

Fig. 18. Schematic representation of phase-slip center.

Fig. 19. Spatial variation of V_S and V_N across a PSC in a SN microbridge at the position marked with an arrow (Dolan and Jackel 1977).

Fig. 20. Temperature dependence of the quasiparticle diffusion length in Sn PSC. The best fit (solid line) for $n = 0.28$ is compared to the expected $(1 - T/T_c)^{-1/4}$ divergence (dashed line) (Aponte and Tinkham 1983).

Fig. 21. I - V characteristics of segment CL taken for different fixed values of the current through the segment LD. Plus and minus signs correspond to the cases when the currents in the two segments flow in the same or opposite directions, respectively (Aponte and Tinkham 1983).

- Fig. 22. (a) Normal current (j_N) and supercurrent (j_S), and (b) Q^* vs. distance x near the end of a superconductor in the presence of a temperature gradient dT/dx (Mamin et al. 1984).
- Fig. 23. (a) Plot of the measured thermoelectric voltage per unit power V/P vs. T for a Pb-Cu-PbBi sample. The solid curve is characteristic of the normal thermopower of Cu. (b) Fit of the charge imbalance contribution V_S/P to the temperature dependence λ_{Q^*} , $(1 - t)^{-1/4}$ (Van Harlingen 1981).
- Fig. 24. Sample configuration for measurement of Q^* induced by temperature gradient. Note different length scales (Mamin et al. 1984).
- Fig. 25. Measured λ_{Q^*} from current injection: Voltage, V , normalized to injected current, I , for a series of probes (Mamin et al. 1984).
- Fig. 26. Temperature dependence of λ_{Q^*} from current injection: λ_{Q^*} vs. $(1 - T/T_c)$ (Mamin et al. 1984).
- Fig. 27. $V(x)$ vs. x for thermopower measurements at 4 different temperatures. Solid lines are fits to Eq. (8.9) (Mamin et al. 1984).
- Fig. 28. Sample configuration for $I \cdot \nabla T$ experiment (Fjordbøge et al. 1981).
- Fig. 29. V vs. I for 5 values of ∇T (Fjordbøge et al. 1981).
- Fig. 30. V vs. ∇T for 10 values of I . At each value of ∇T , the voltage is defined to be zero at $I = 0$ (Fjordbøge et al. 1981).
- Fig. 31. $V_{NS}(0)/IVT$ vs. reduced temperature, t (Fjordbøge et al. 1981).
- Fig. 32. $V_{NS}(0)/IVT$ vs. $(1 - t)$. The three theoretical formulas have been fitted to the experimental data by scaling them appropriately (Fjordbøge et al. 1981).

Fig. 33. Schematic representation of quasiparticle excitations in presence of (a) temperature gradient and (b) temperature gradient and applied supercurrent.

Fig. 34. Comparison of theory of Beyer Nielsen et al. (1982) with data from dirty tin sample of Fjordbøge et al. (1981) (Beyer Nielsen et al. 1982).

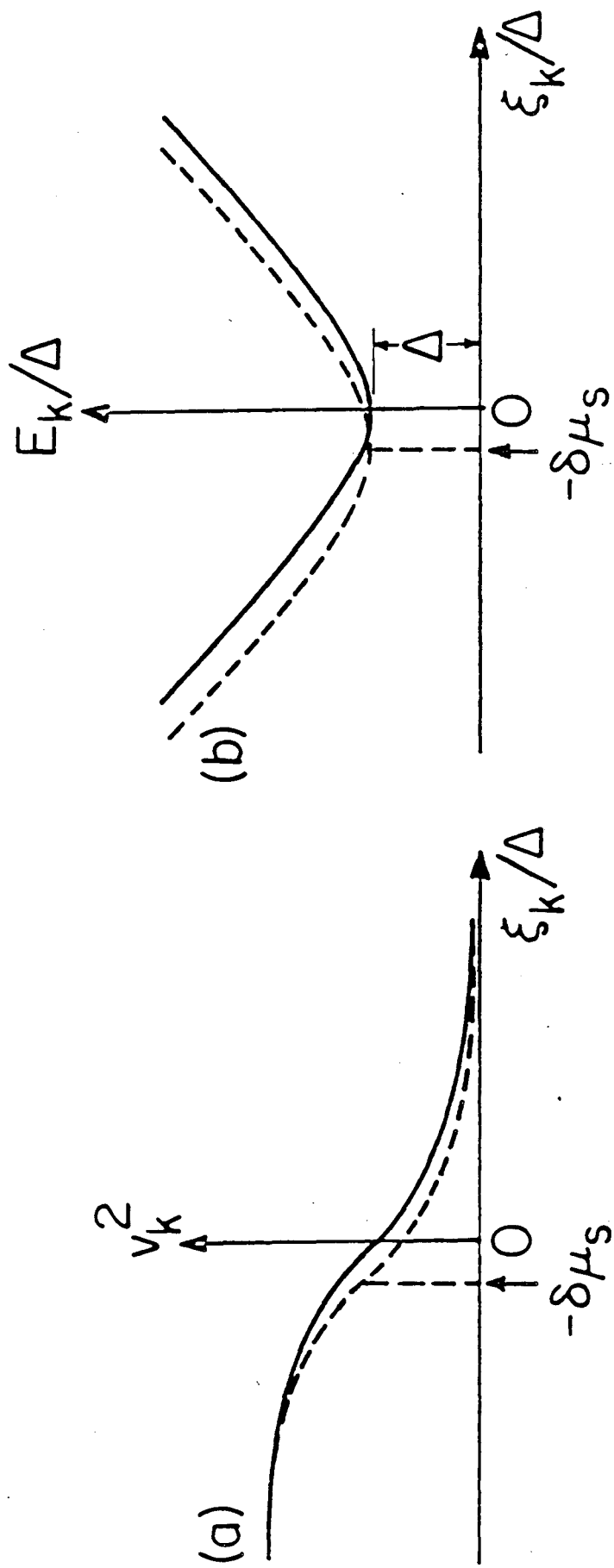


Fig. 1

XBL 808-5640

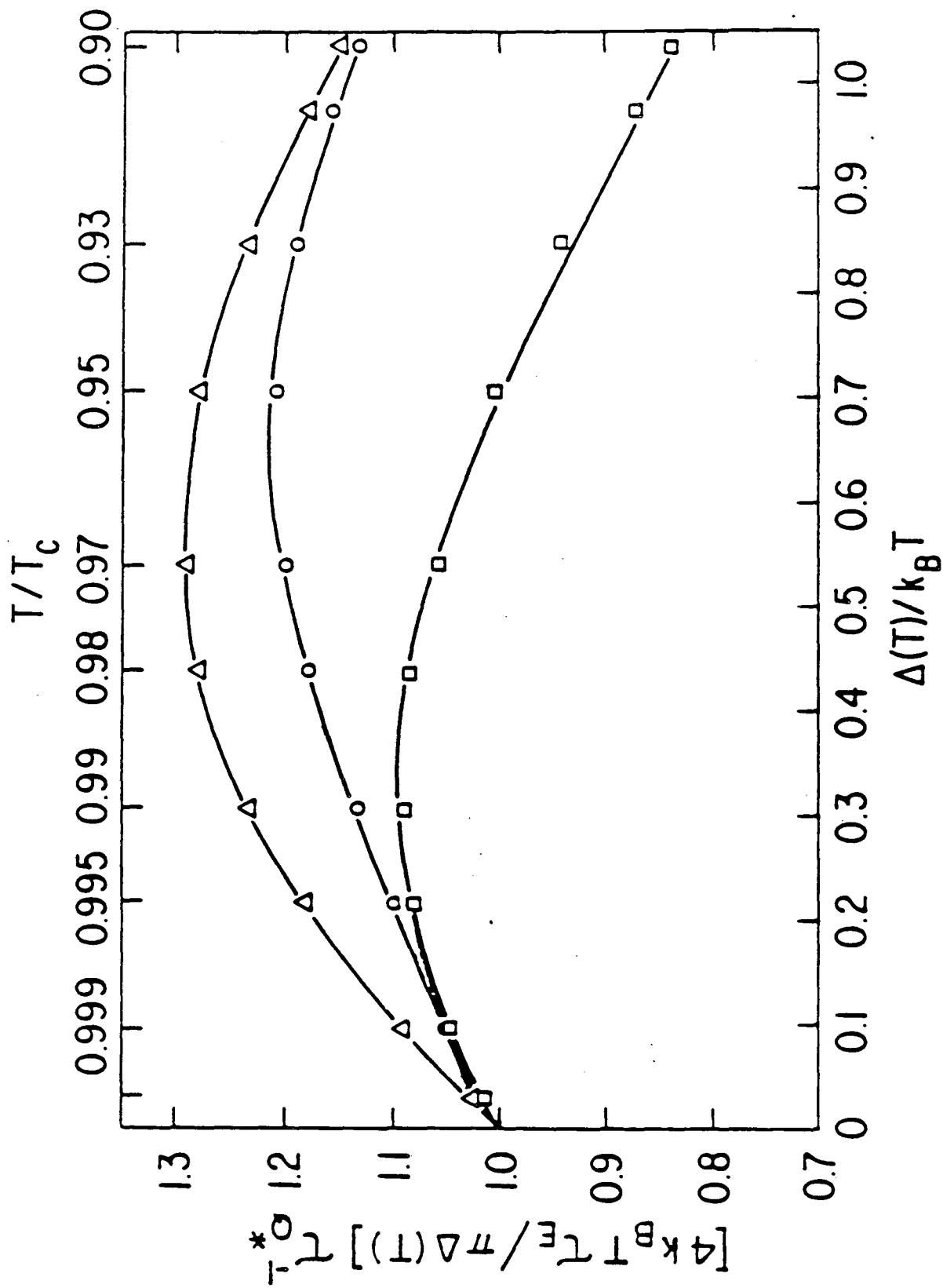


Fig. 2

XBL-808-5633A

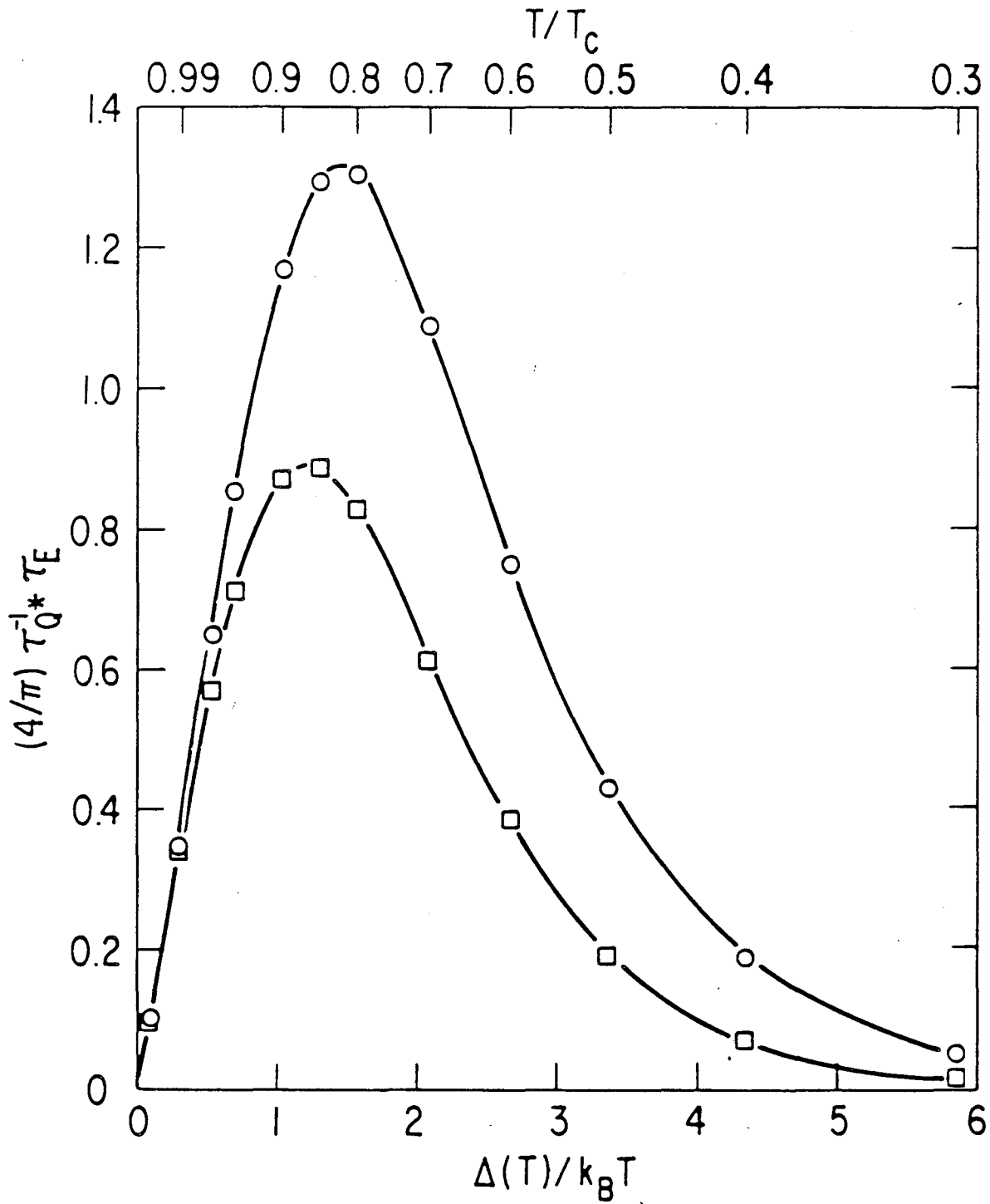


Fig. 3

XBL808-5632 A

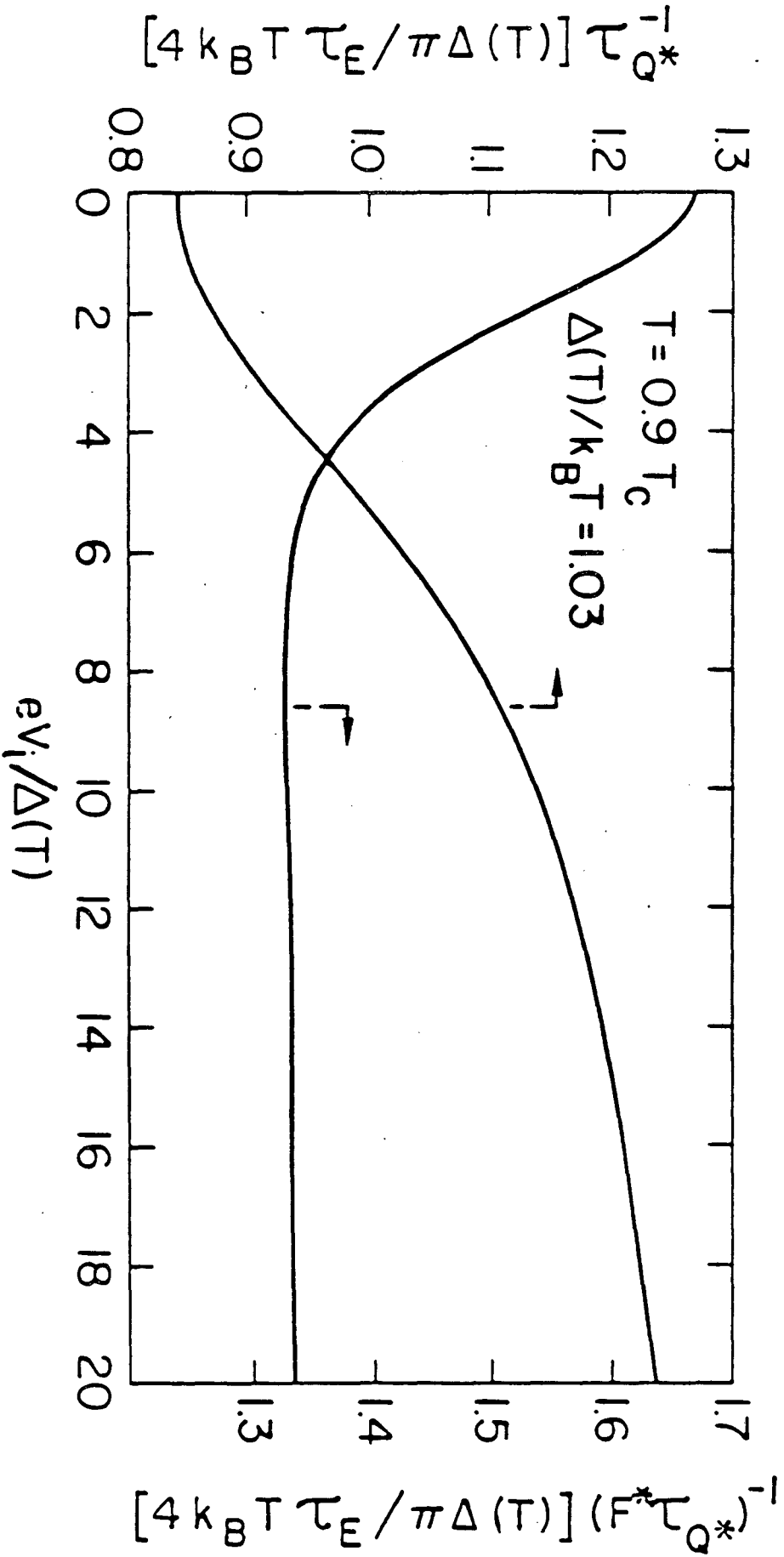
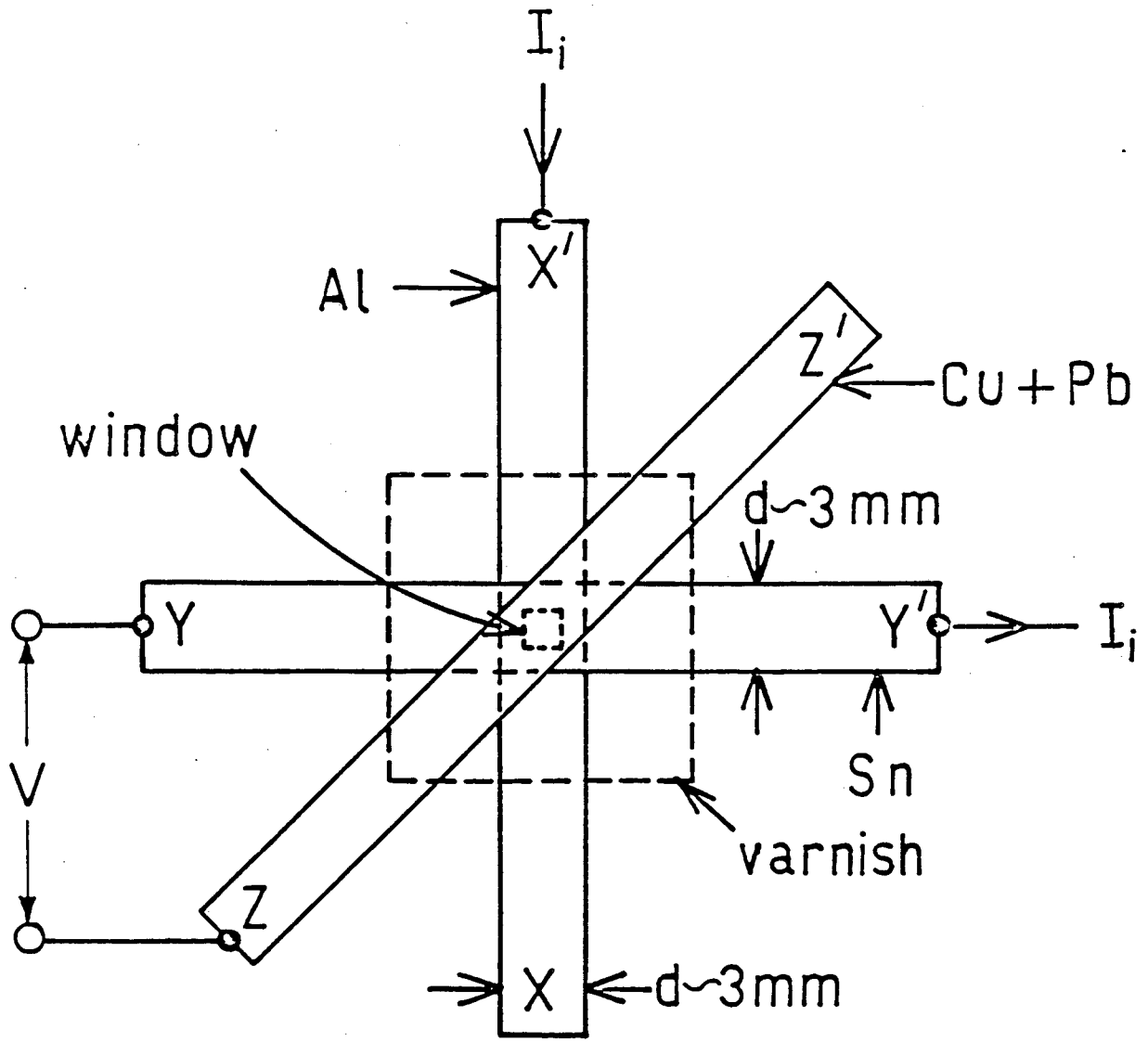


Fig. 4



XBL 841-6506

Fig. 5

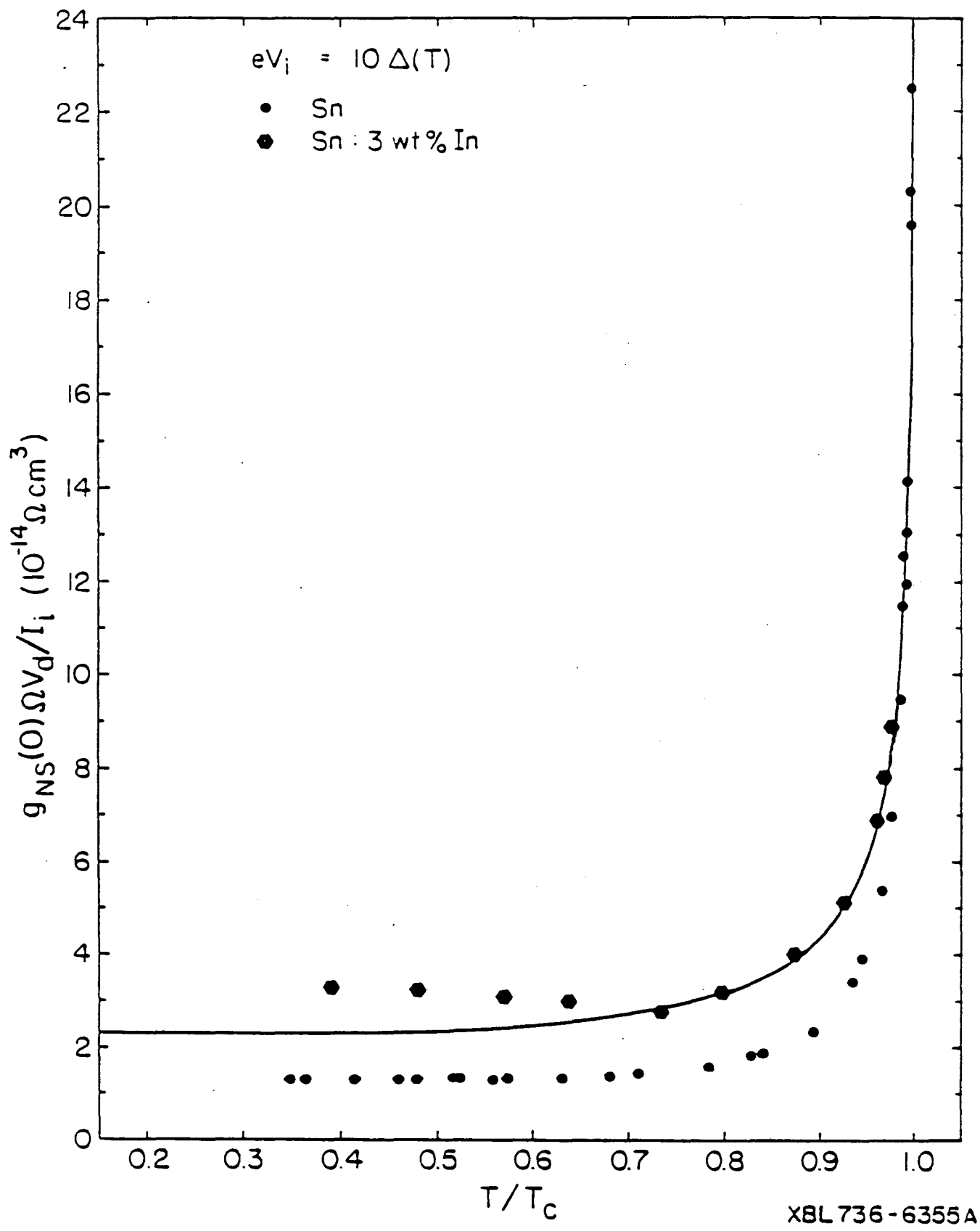


Fig. 6

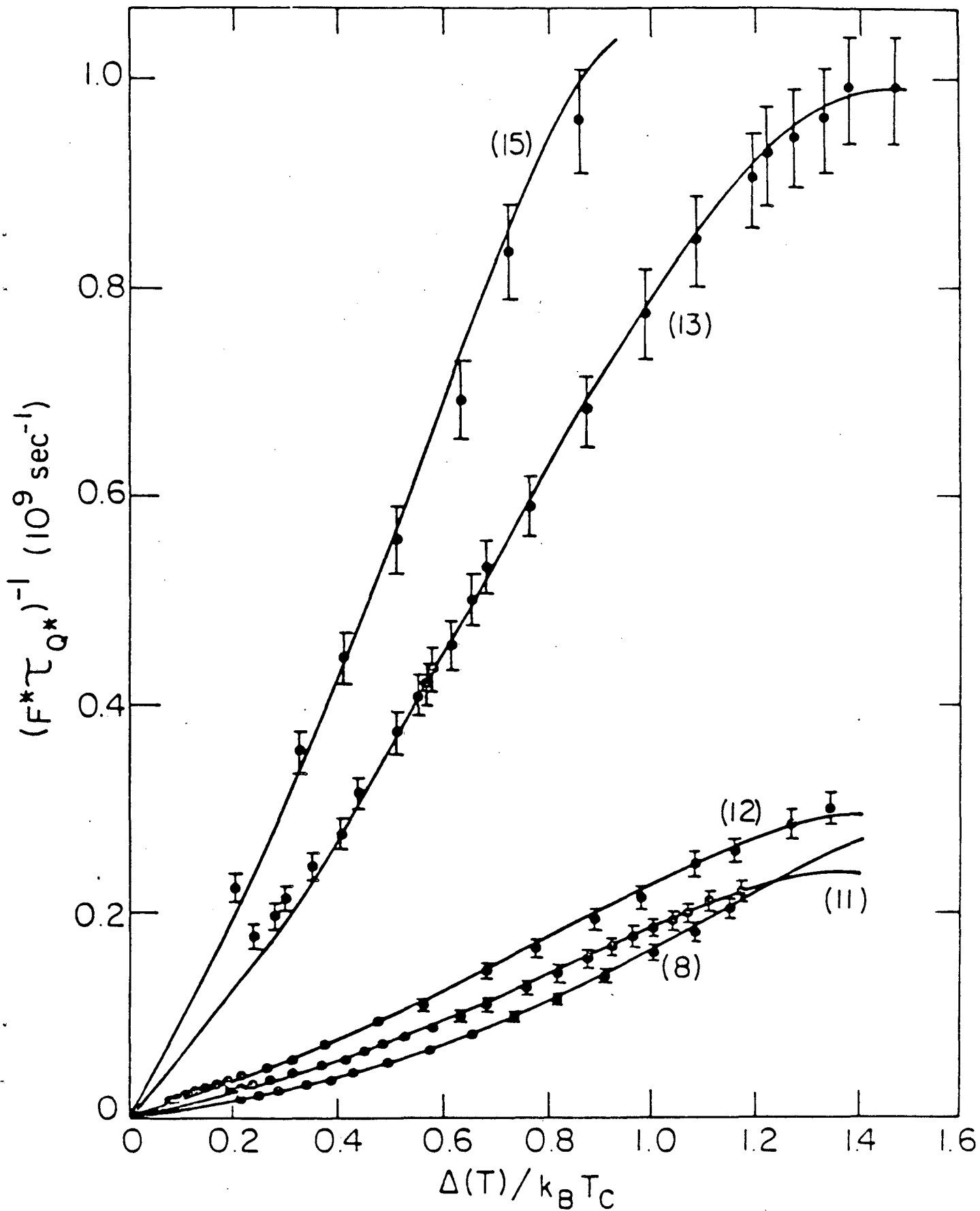
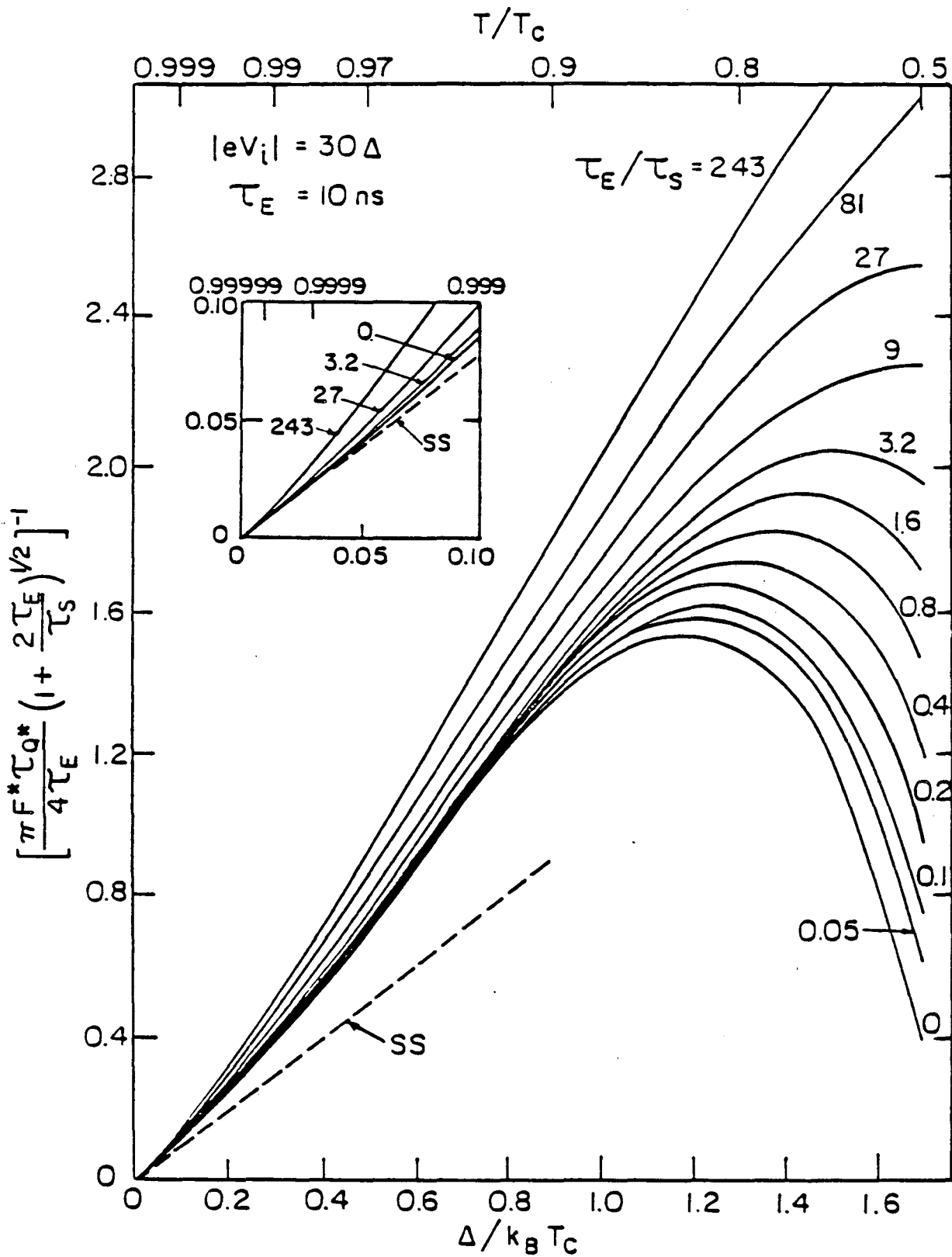


Fig. 7



XBL 804-5027

Fig. 8

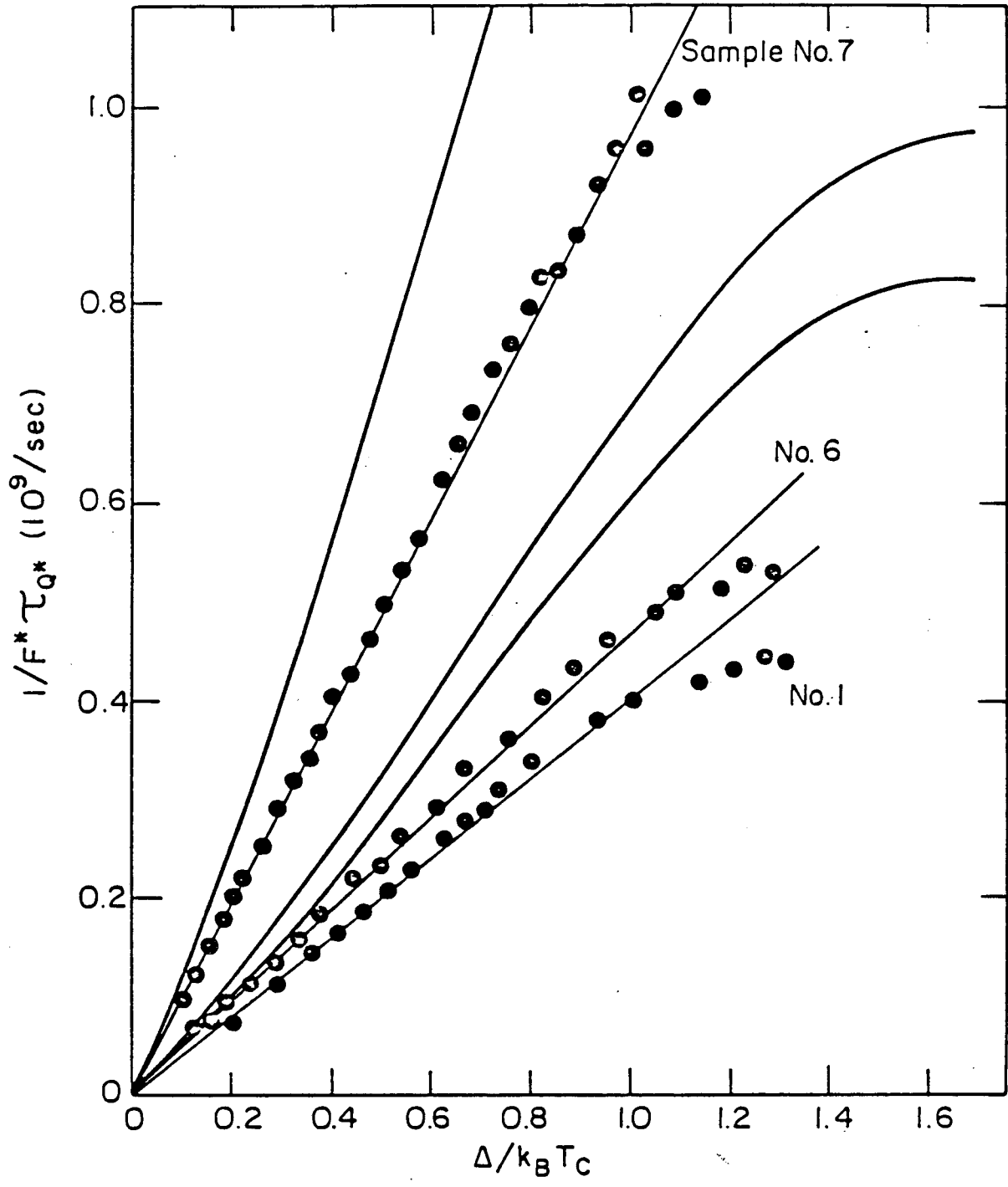
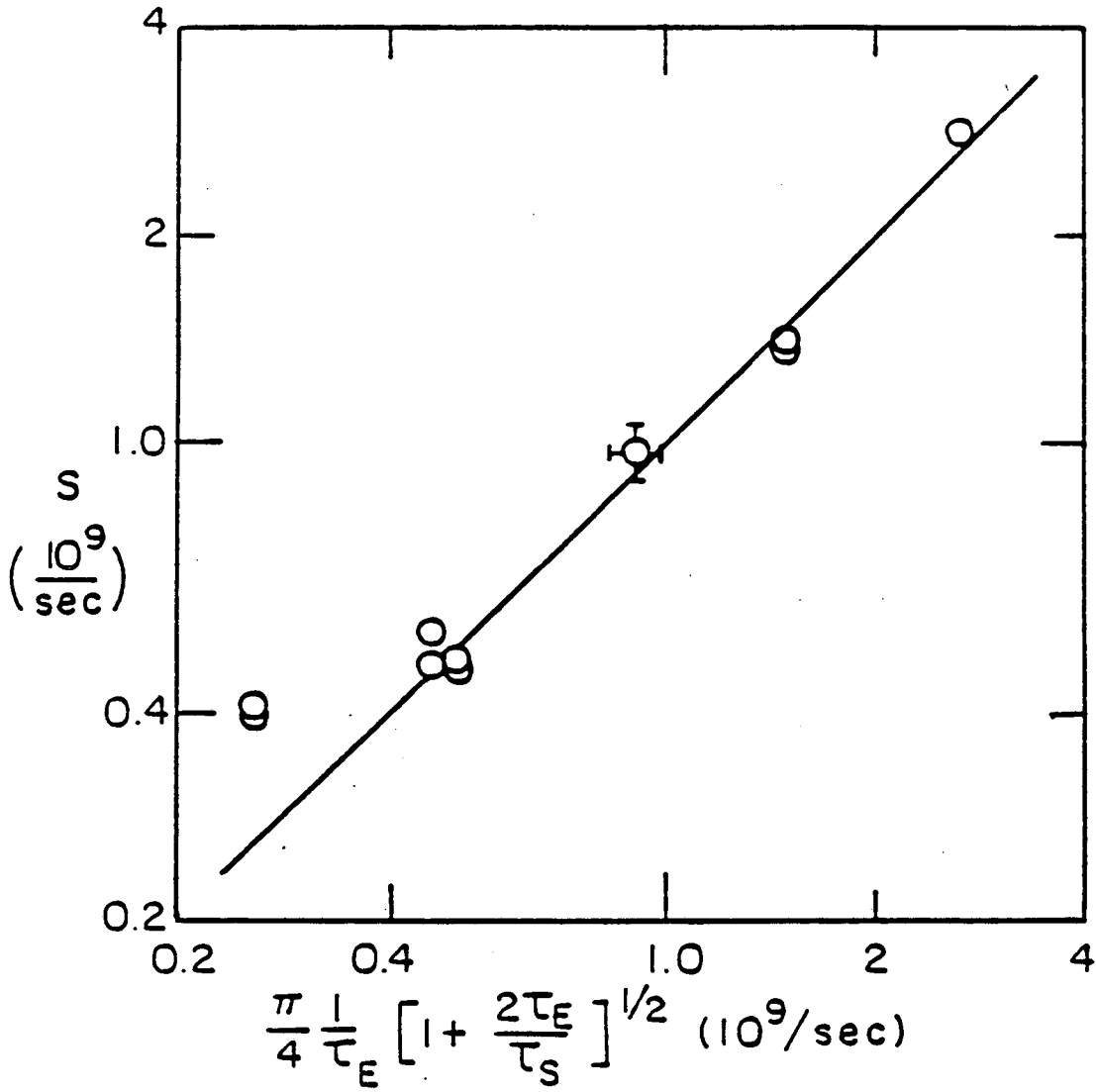


Fig. 9

XBL 804-5031



XBL 804-5026

Fig. 10

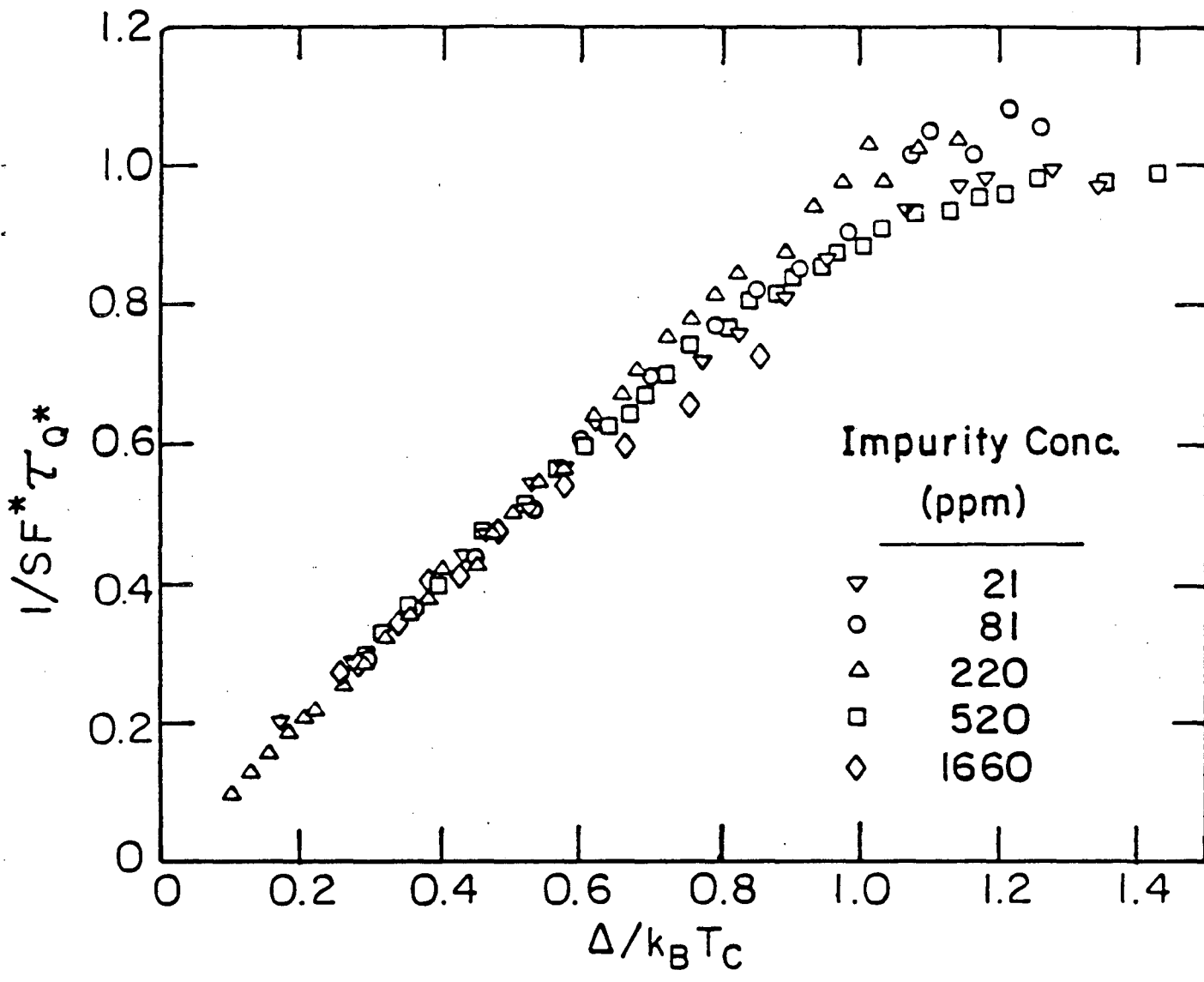


Fig. 11

XBL 807-5473A

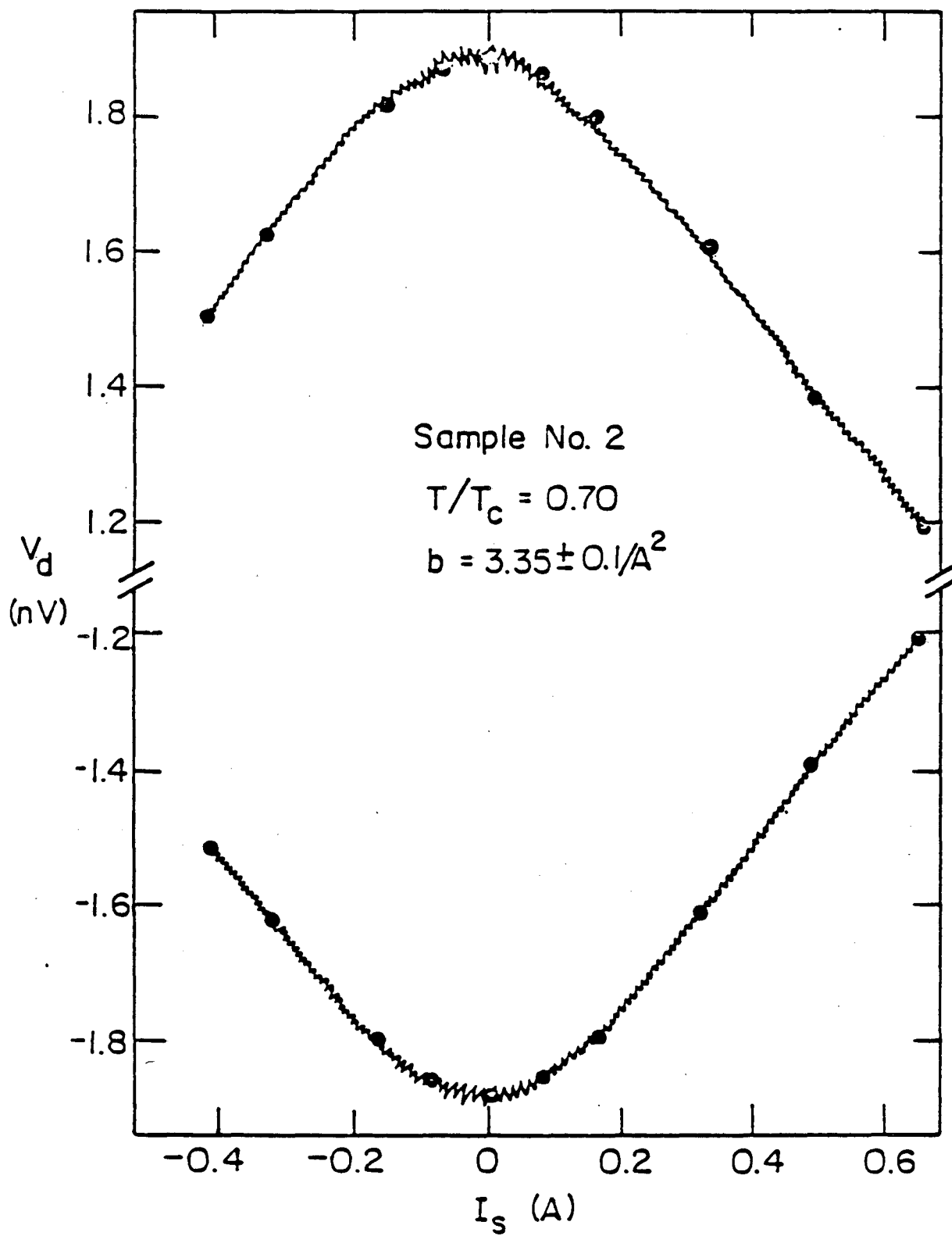


Fig. 12

XBL 808-5669

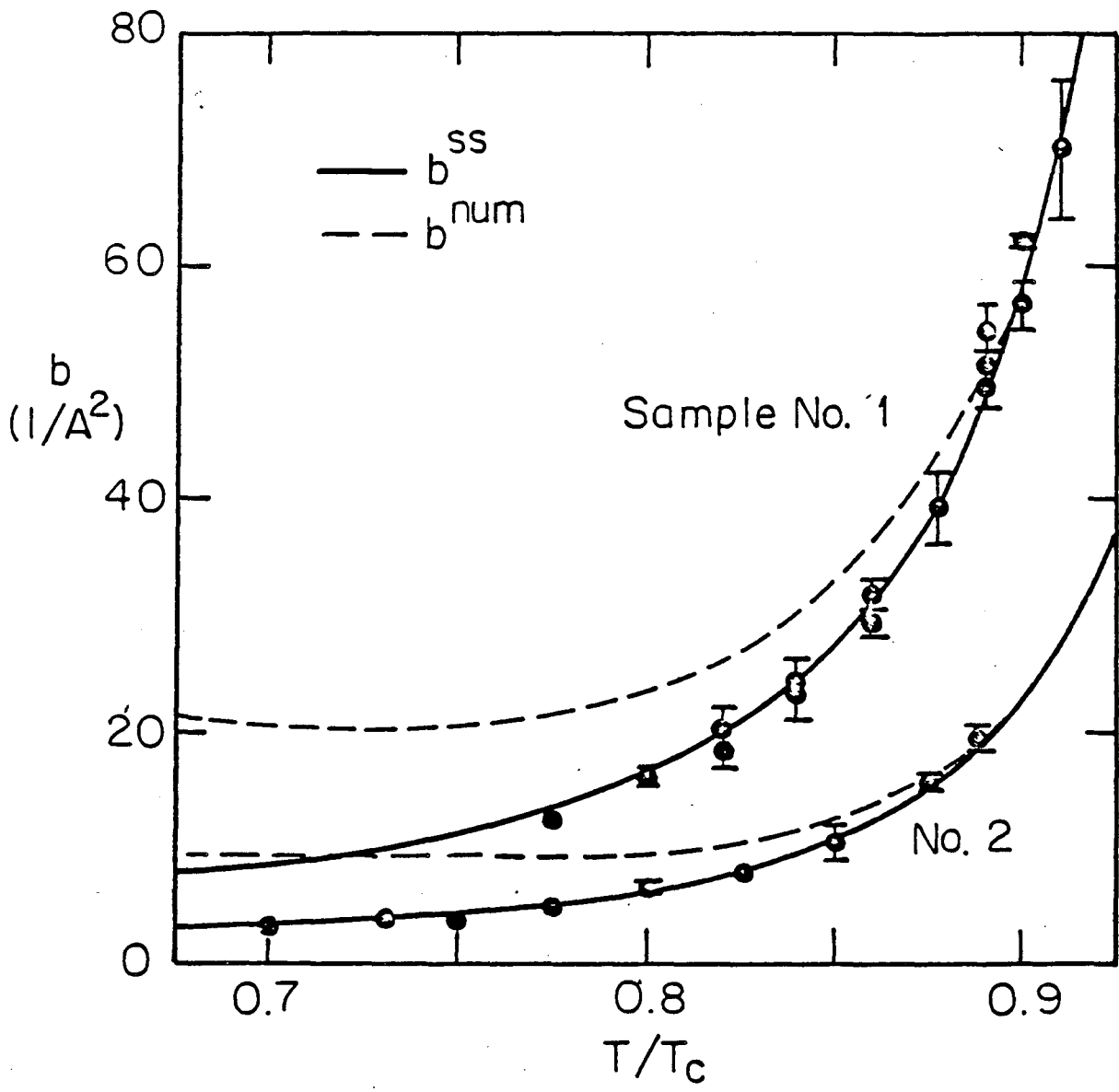
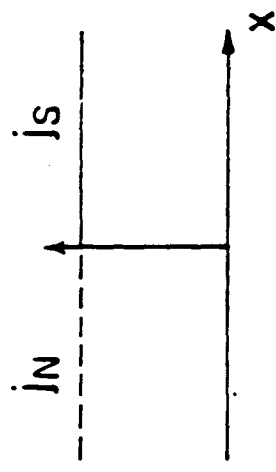
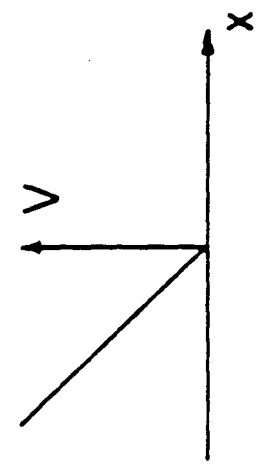
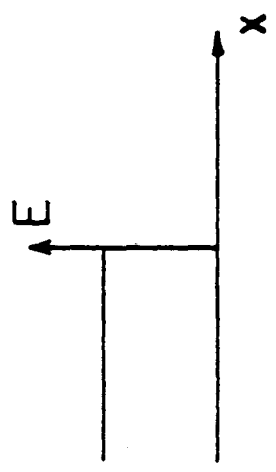
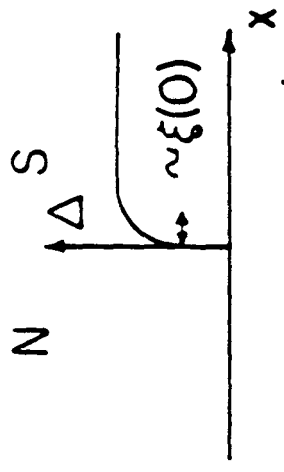


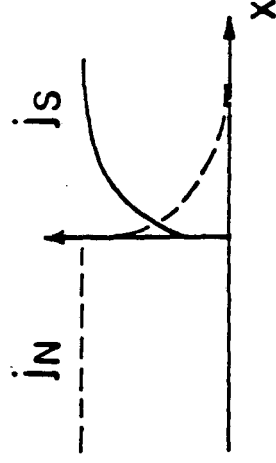
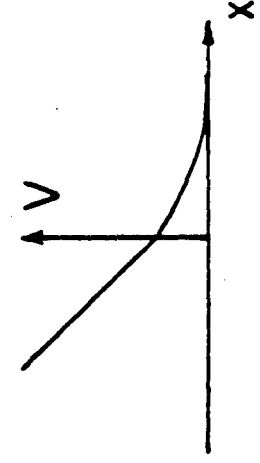
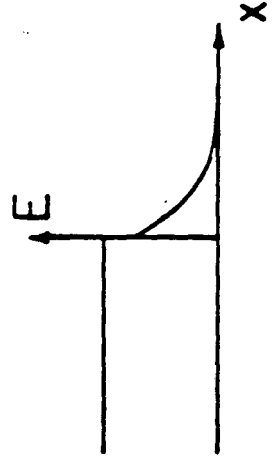
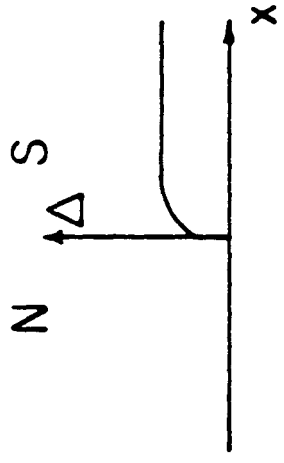
Fig. 13

XBL 808-5666

$$k_B T / \Delta \rightarrow 0$$



$$k_B T \sim \Delta$$



$$\Delta / k_B T \rightarrow 0$$

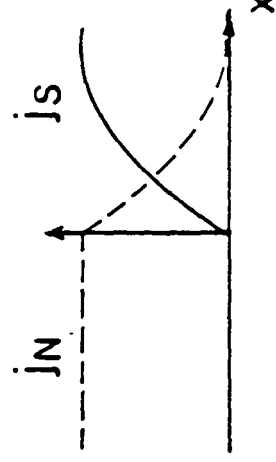
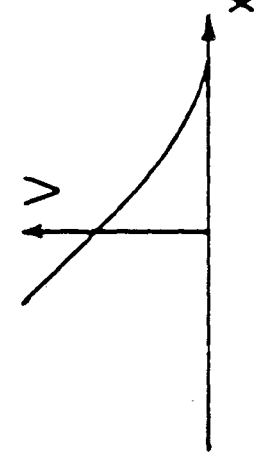
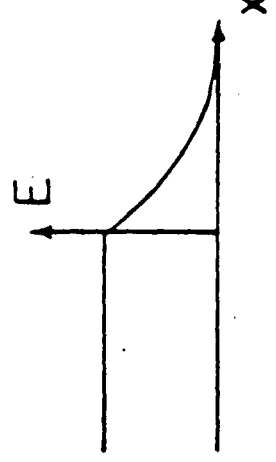
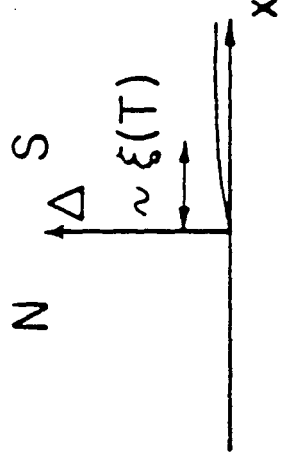
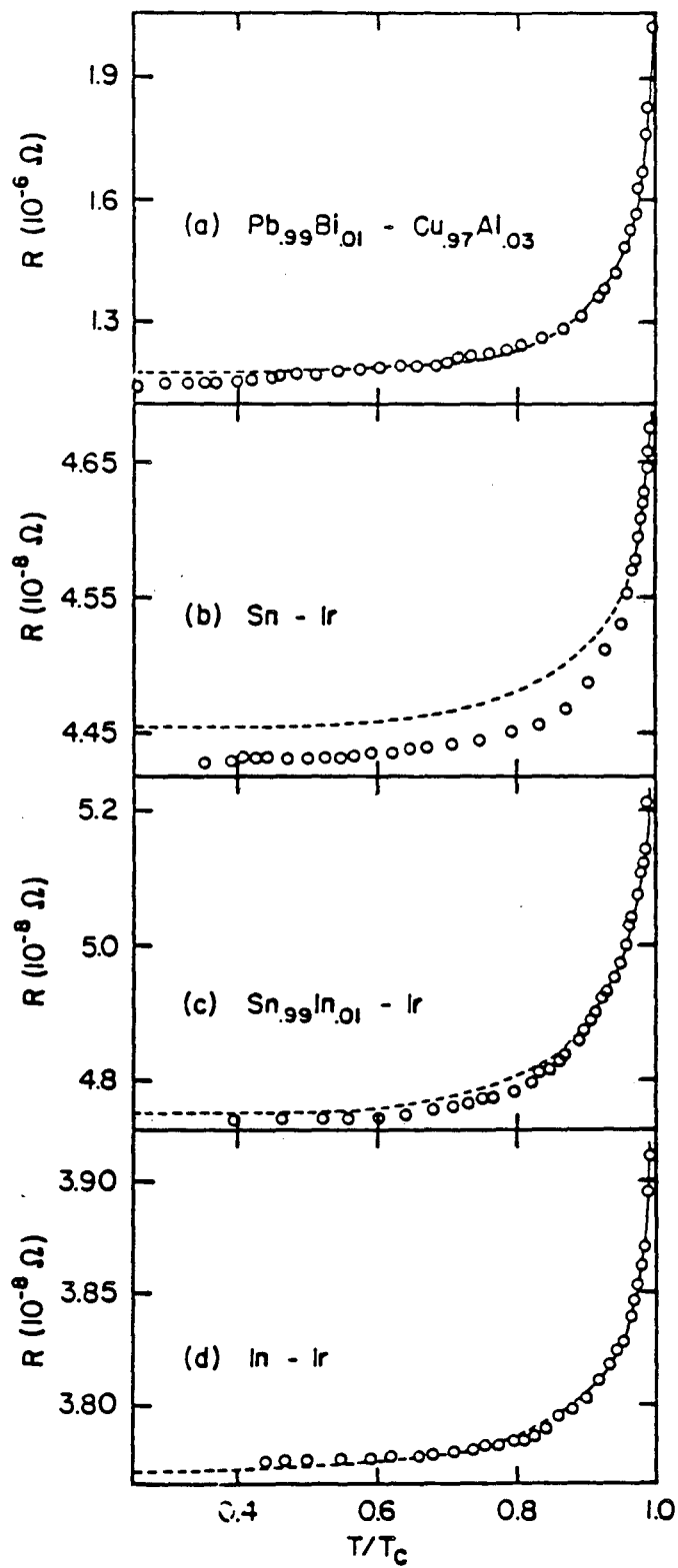


FIG. 14

XBL 808-5631



XBL 7911-12869

Fig. 15

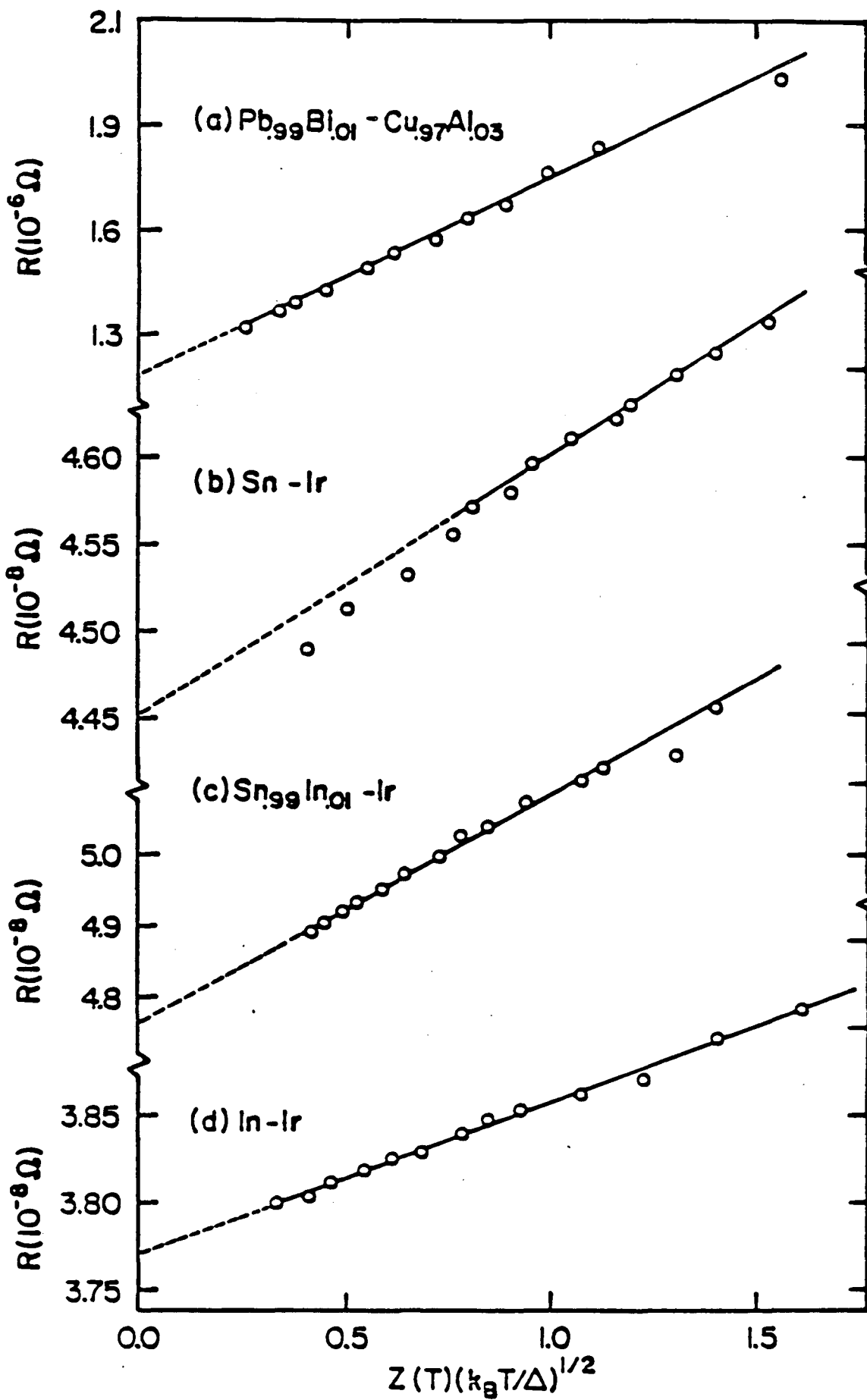


Fig. 16

XBL 808-11232

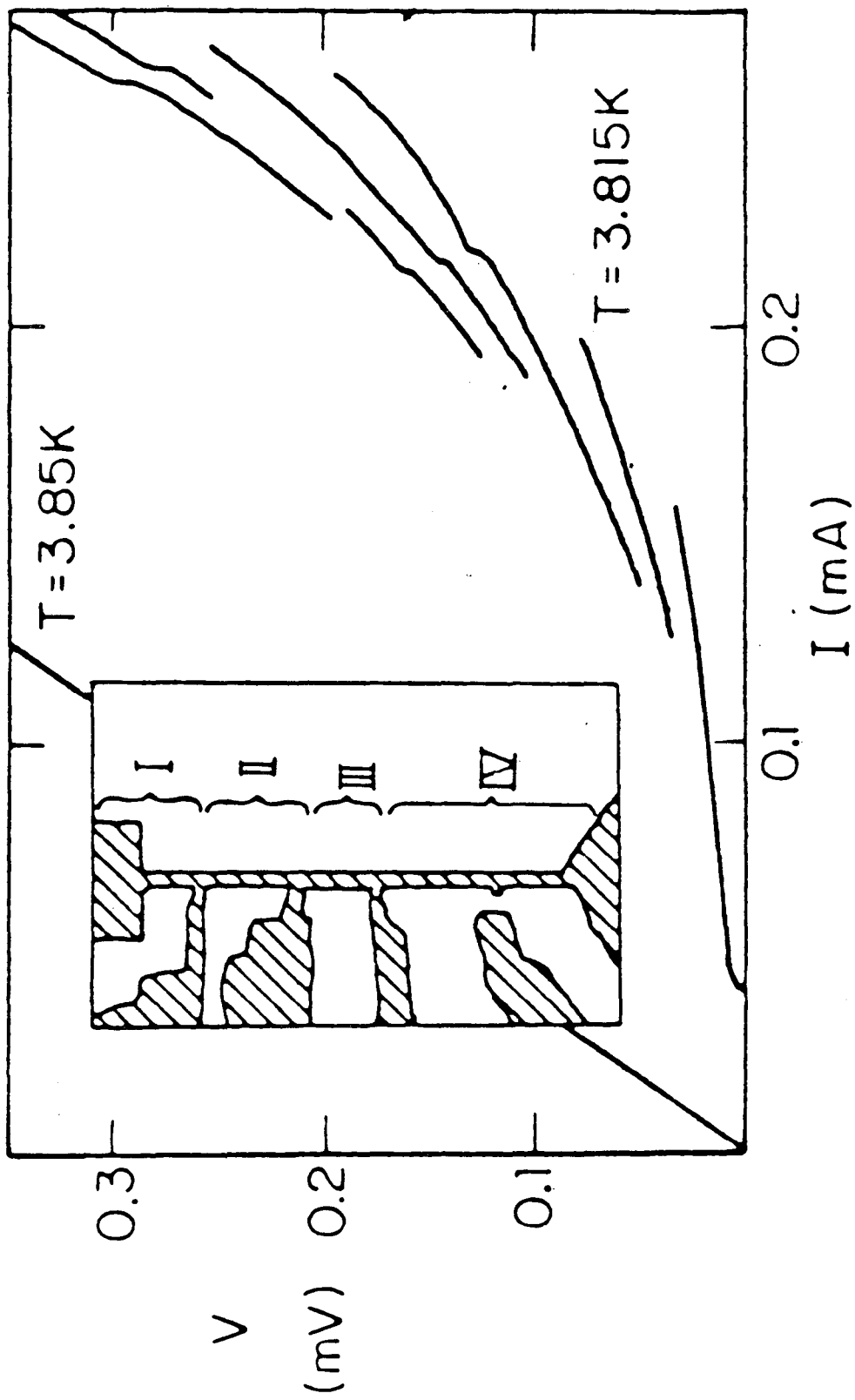
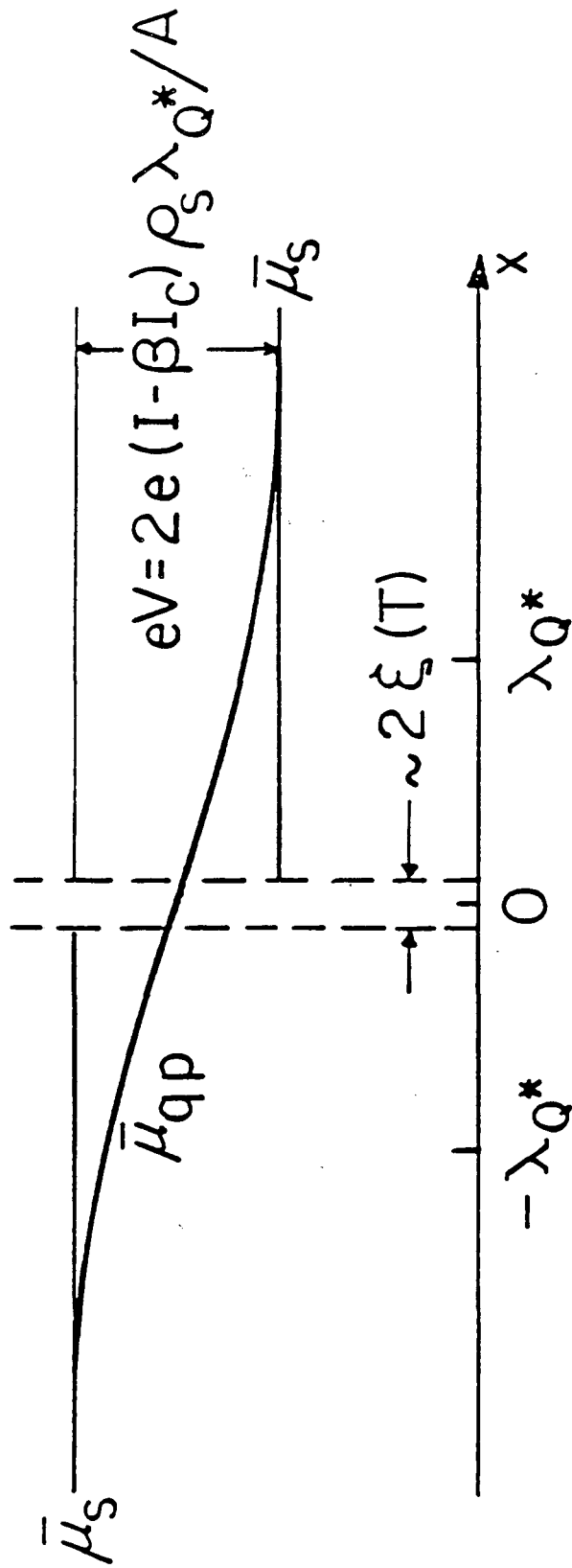


FIG. 17



XBL84I-6525

FIG. 18

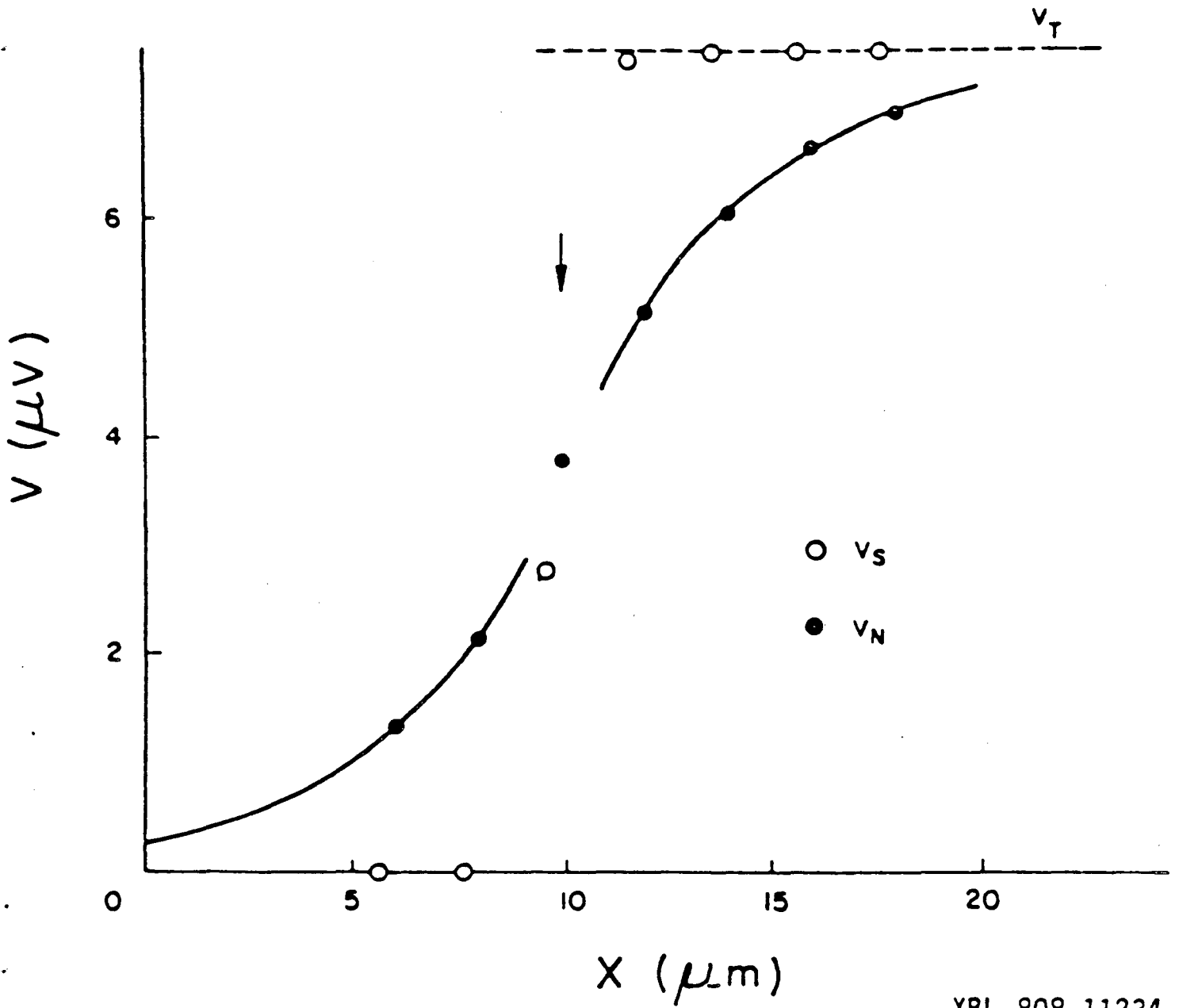


Fig. 19

XBL 808-11234

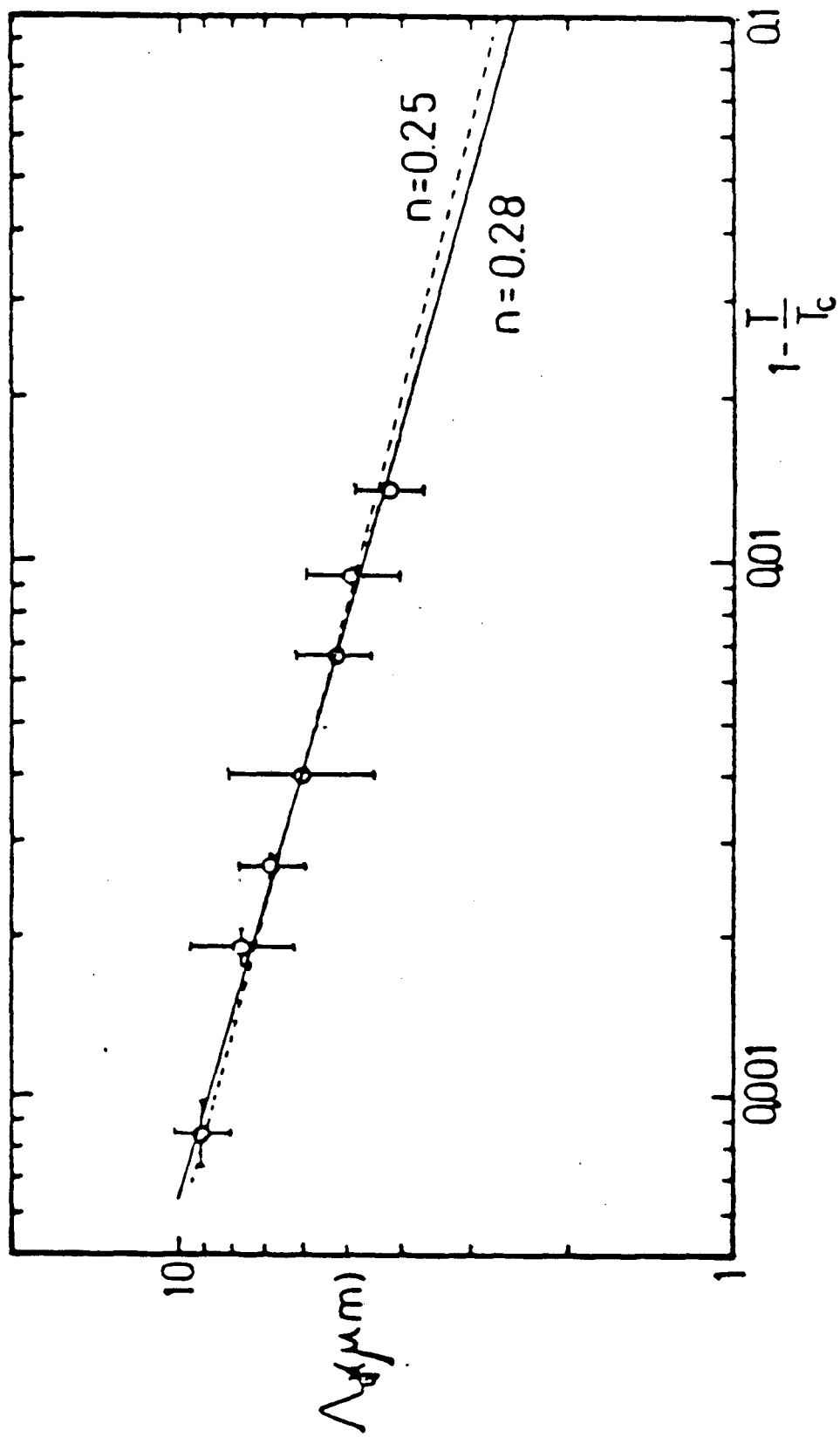


Fig. 20

XBL 841-17

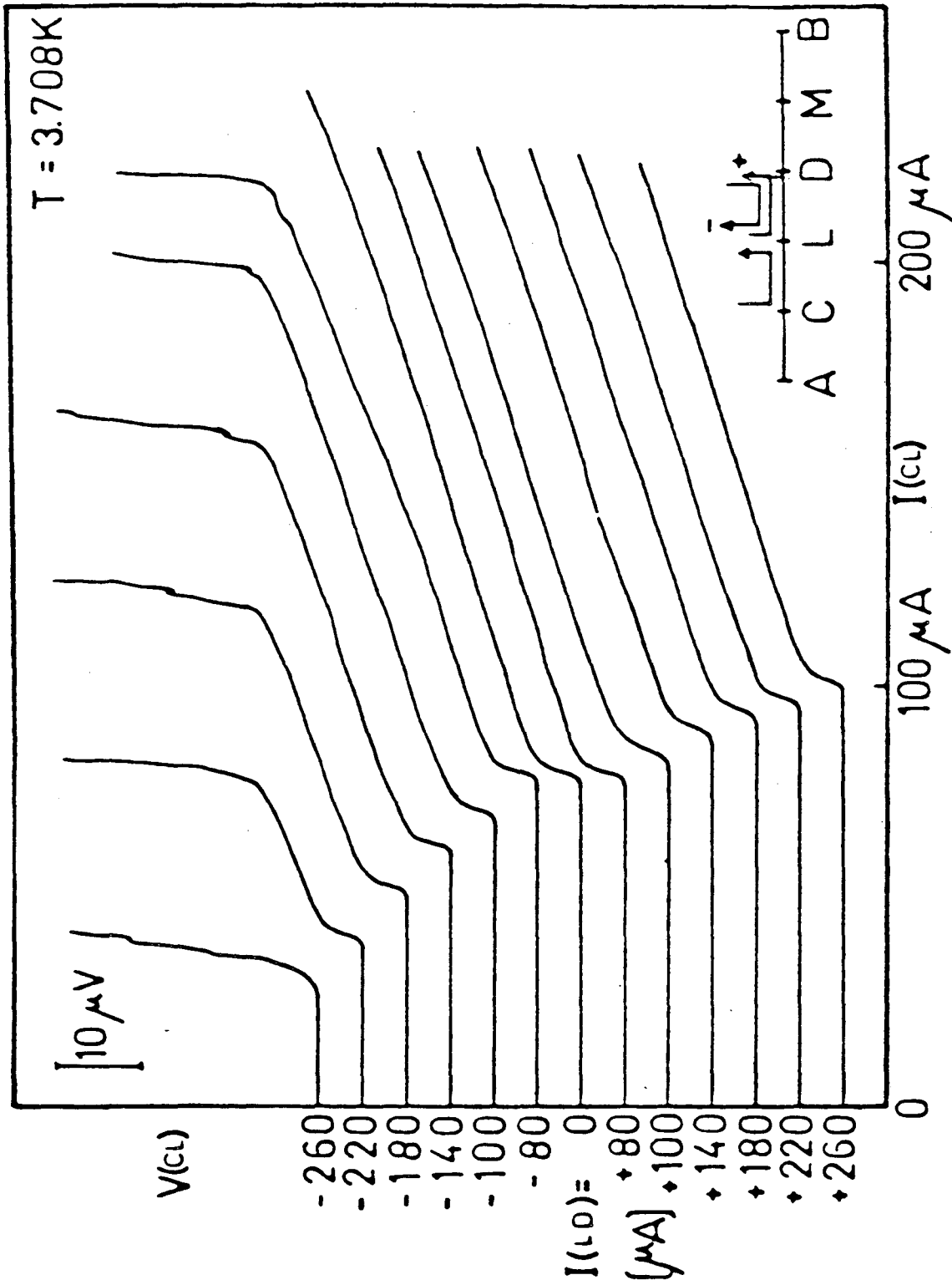


FIG. 21

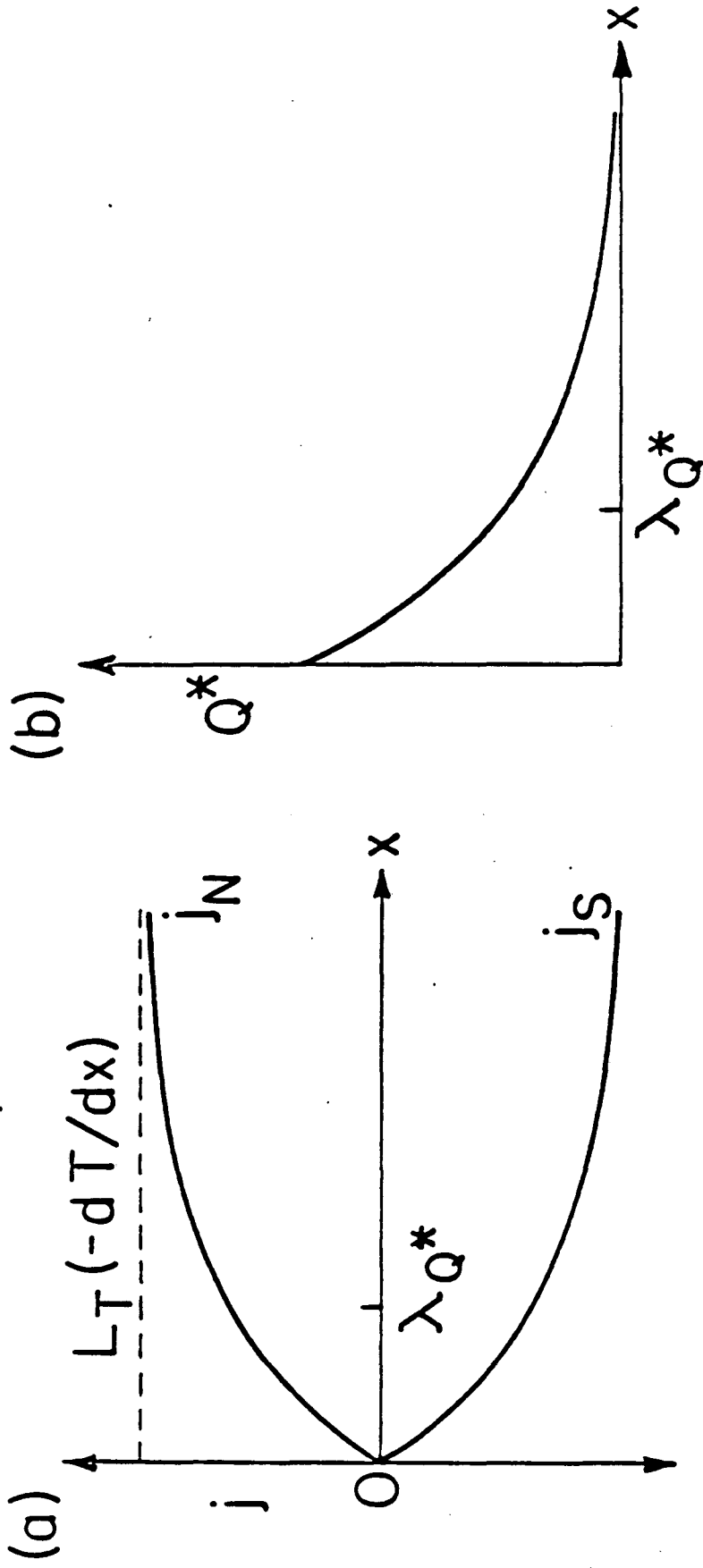


Fig. 22

XBL 836-5953

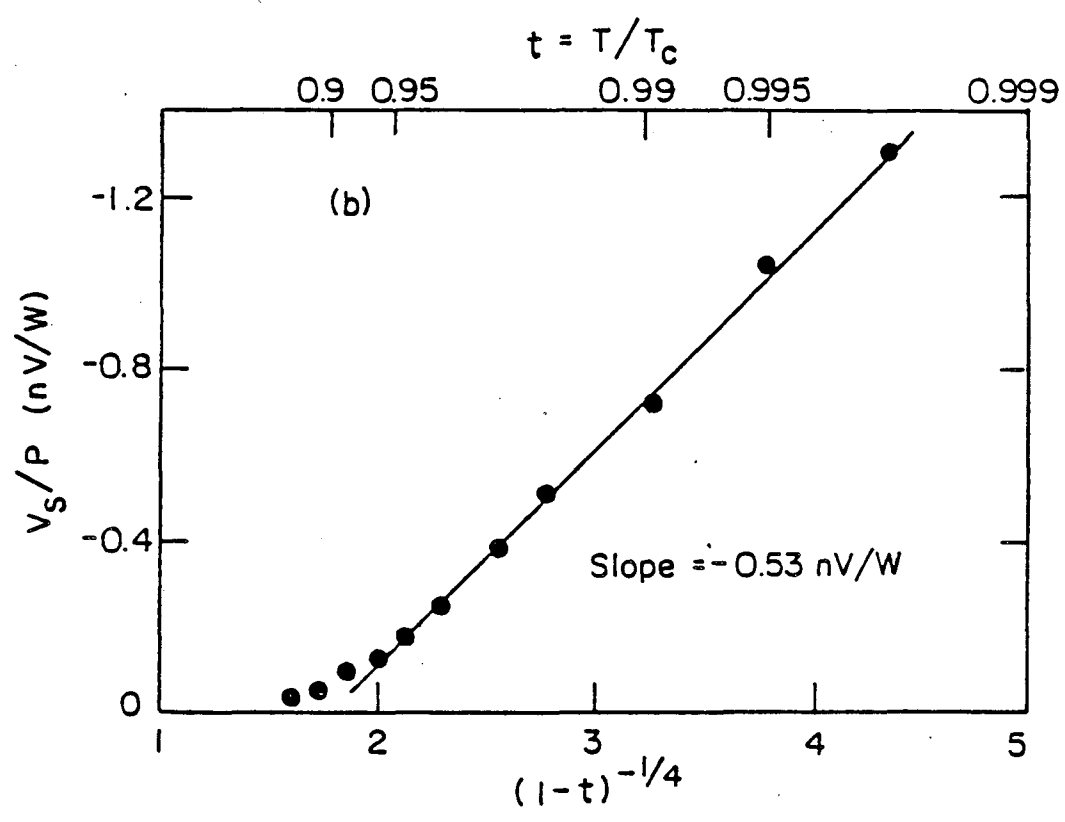
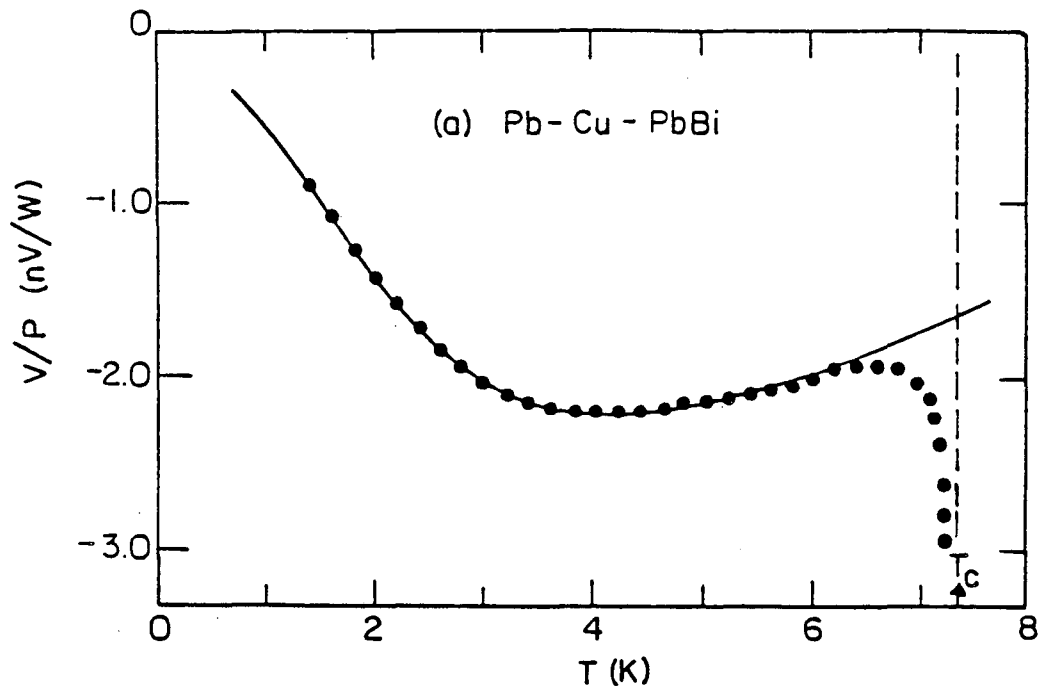


Fig. 23

XBL8012-13424

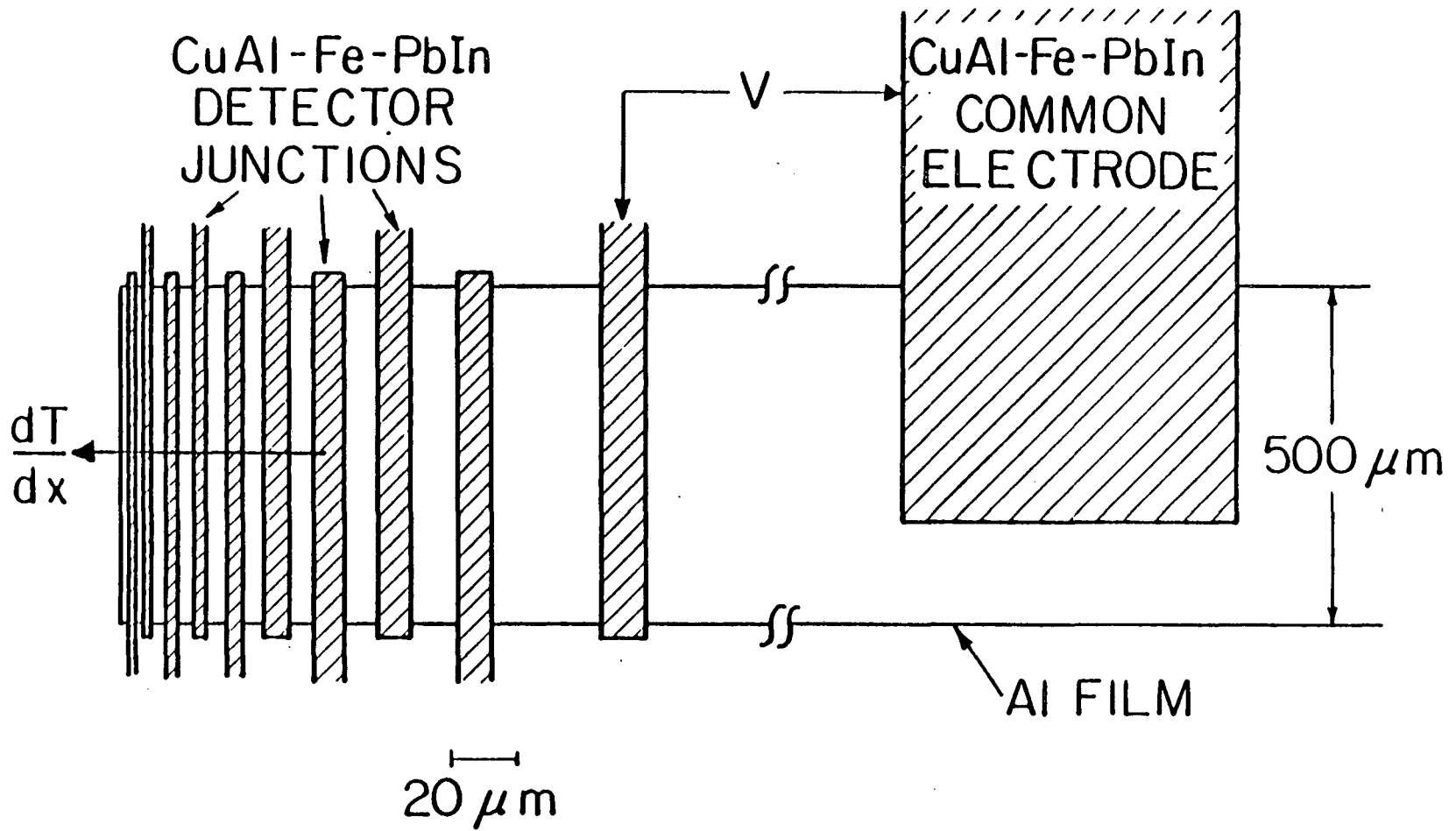


Fig. 24

XBL836-5955A

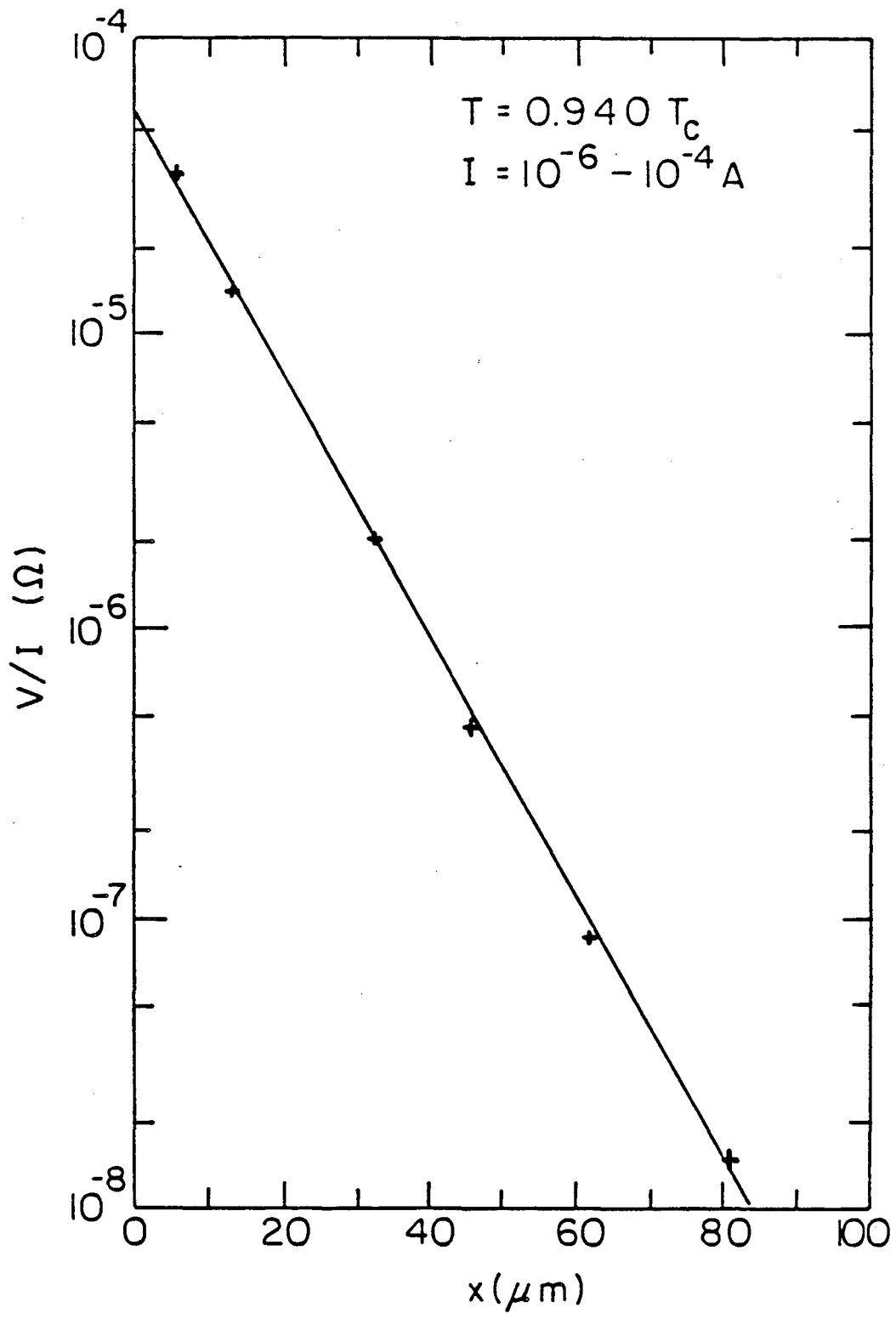


Fig. 25

XBL 837-6057

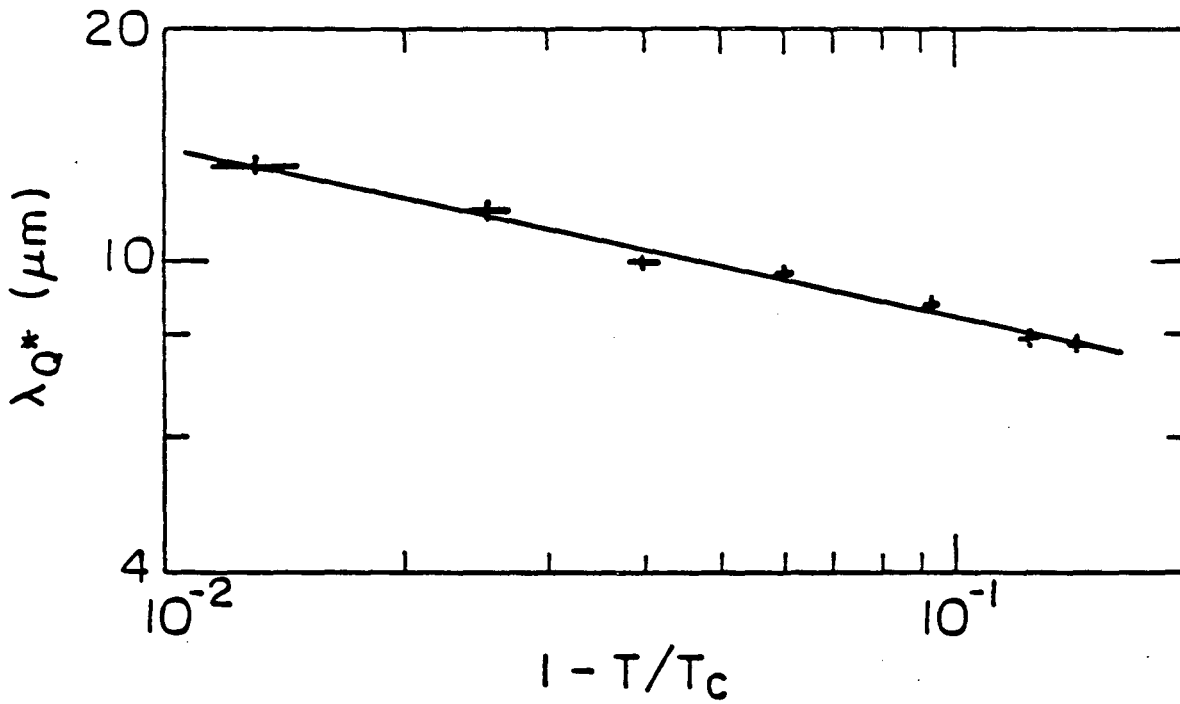


Fig. 26

XBL 837-6056

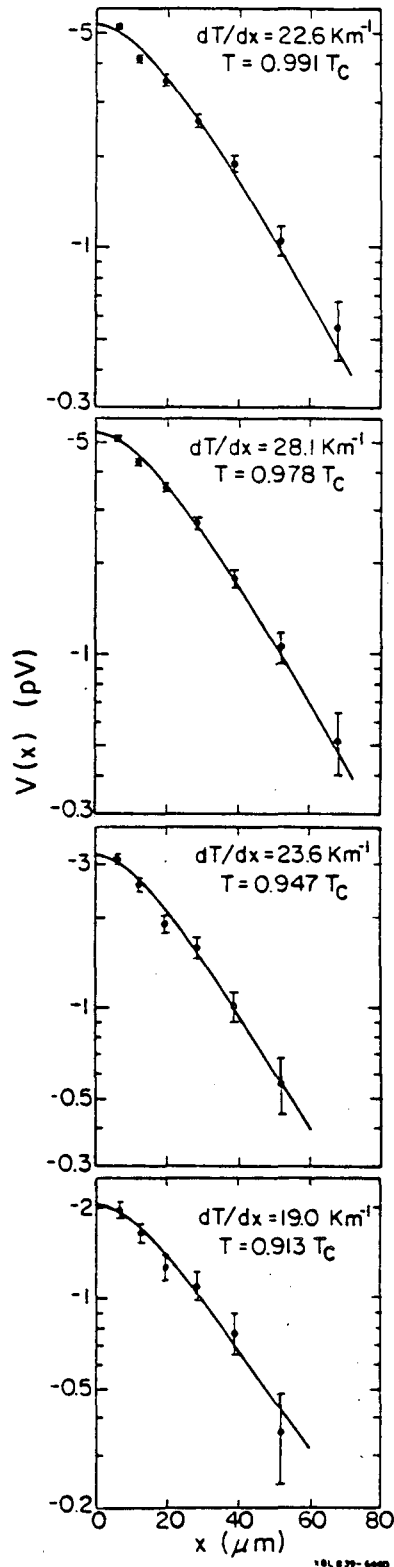


Fig. 27

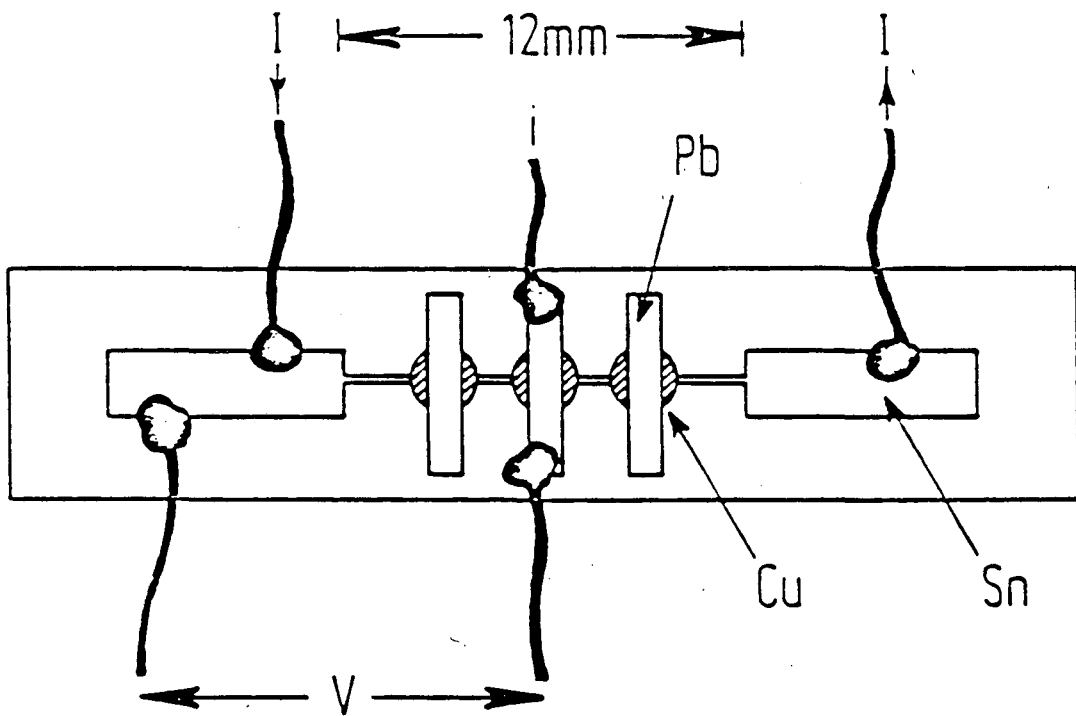


Fig. 28

XBL 7911-12877

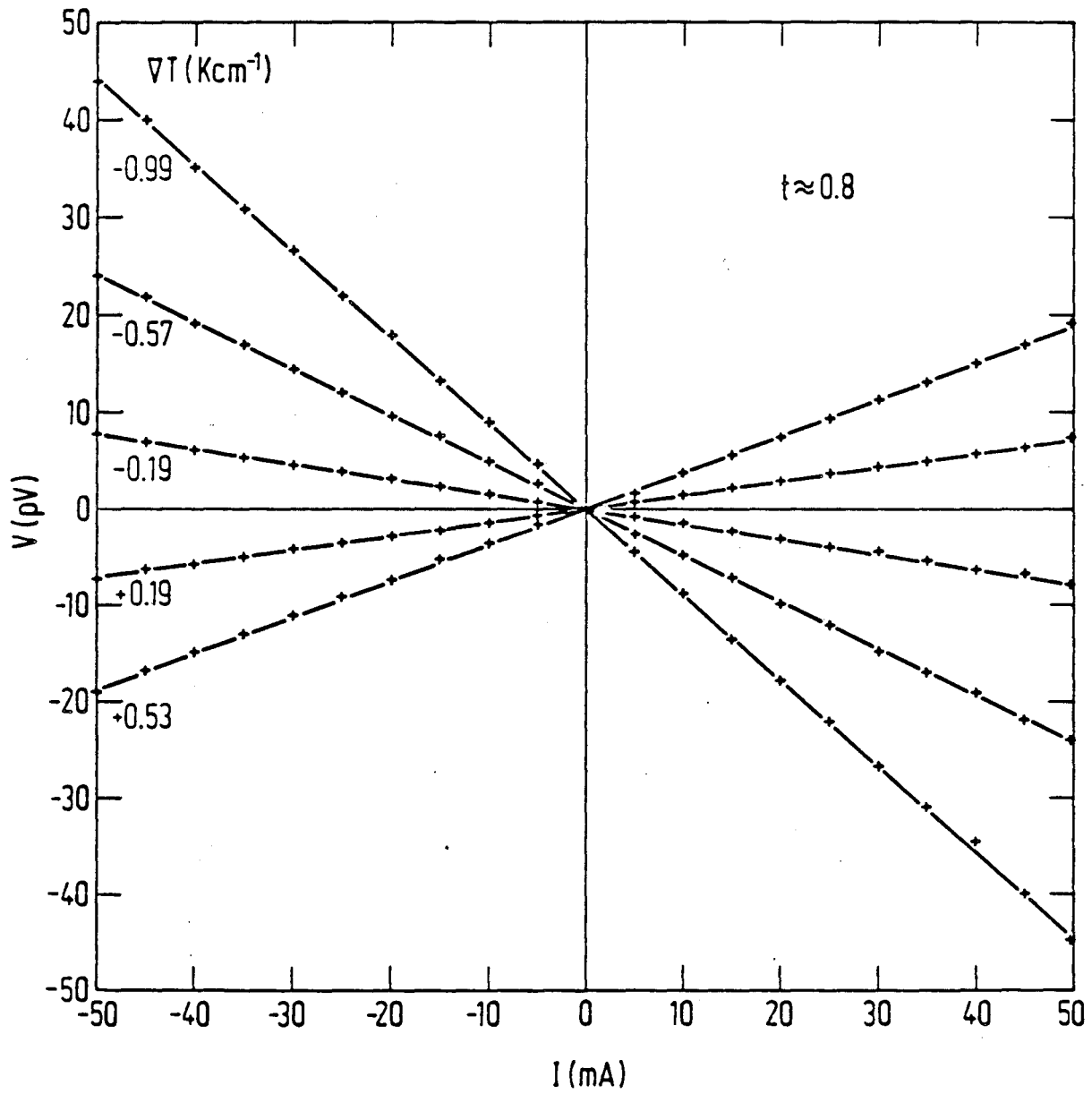


Fig. 29

XBL 7911-12875

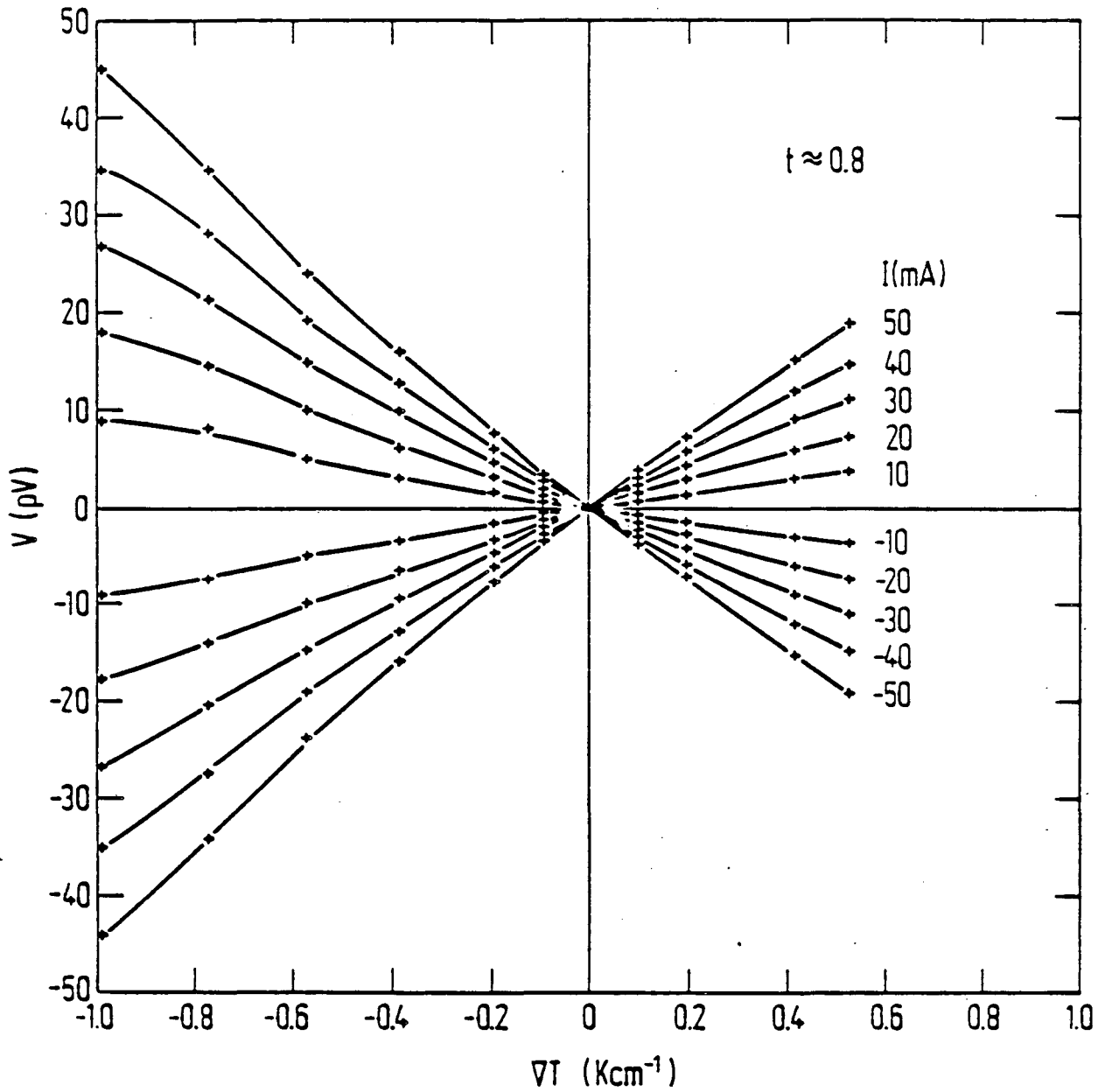


Fig. 30

XBL 7911-12876

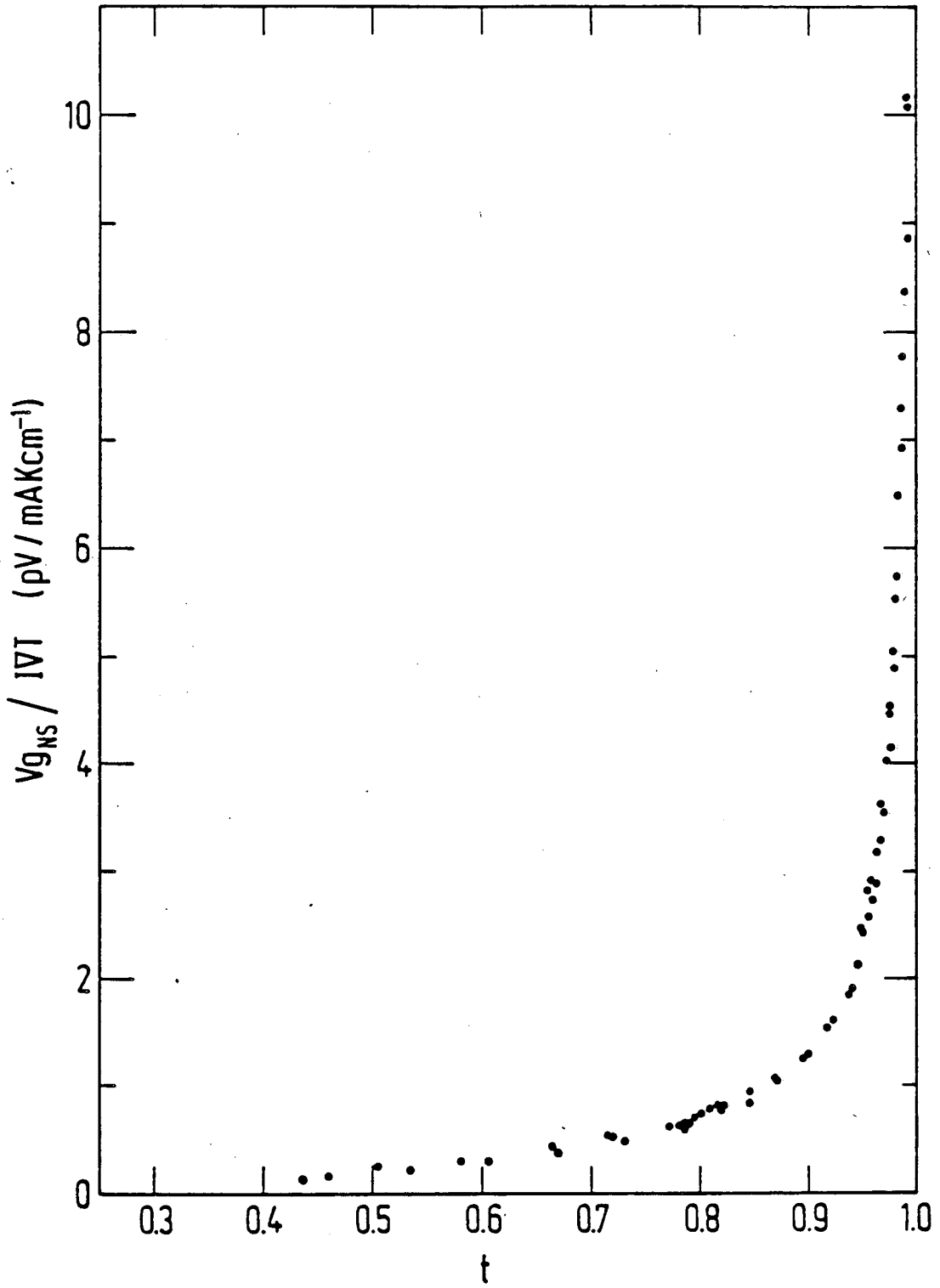


Fig. 31

XBL 808-11431

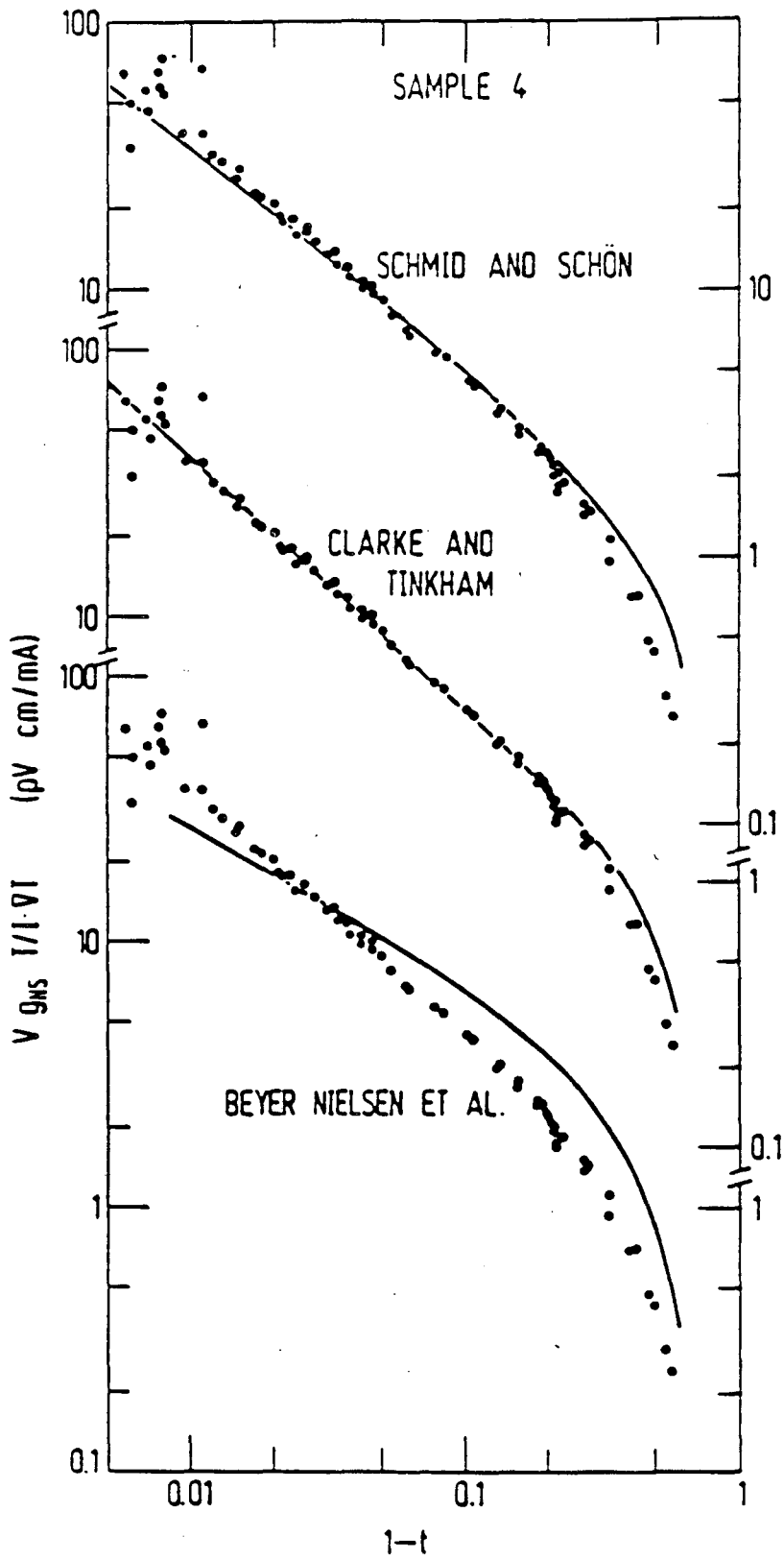


Fig. 32

XBL 909-11976

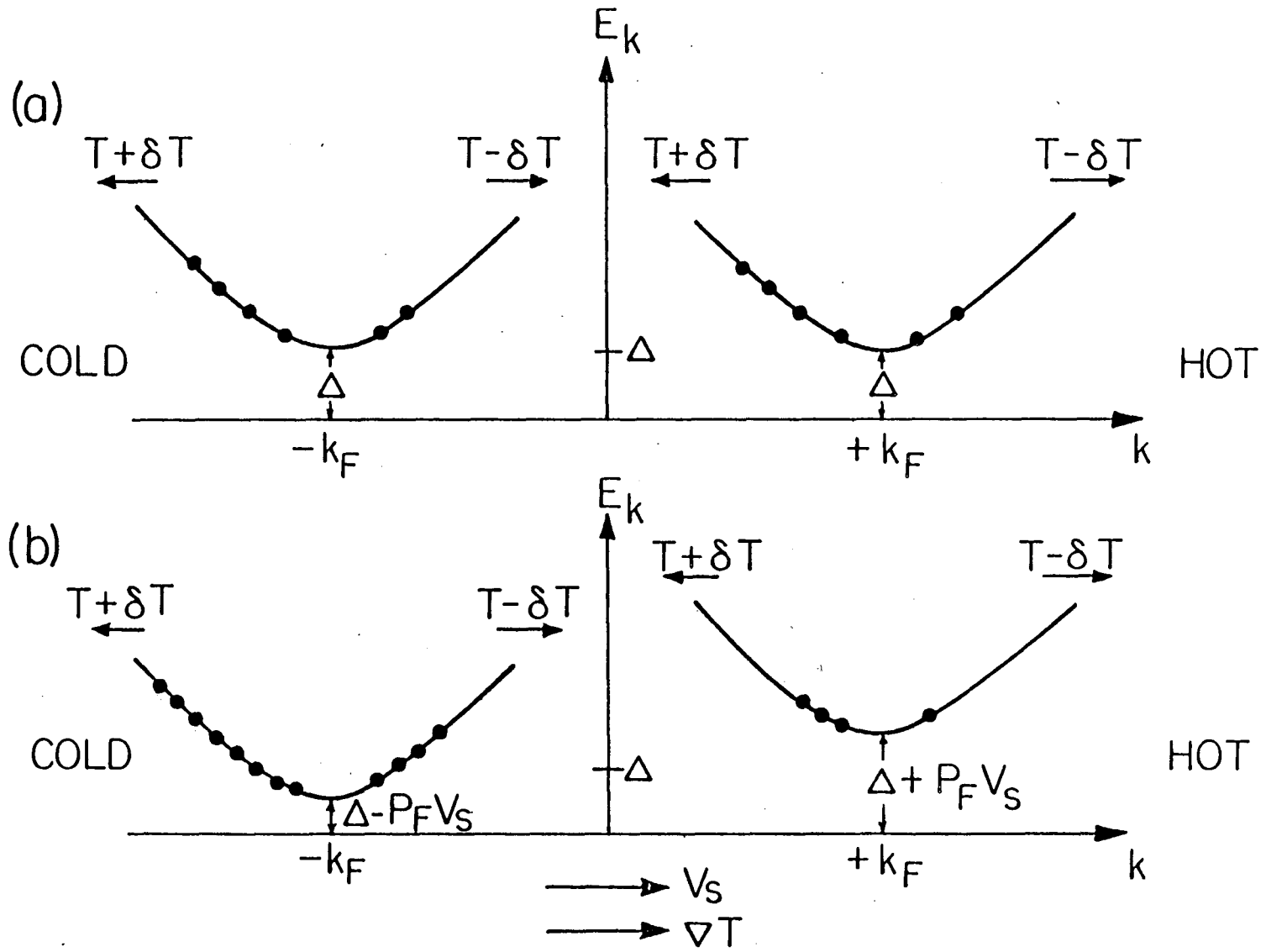


Fig. 33

XBL 808-5712

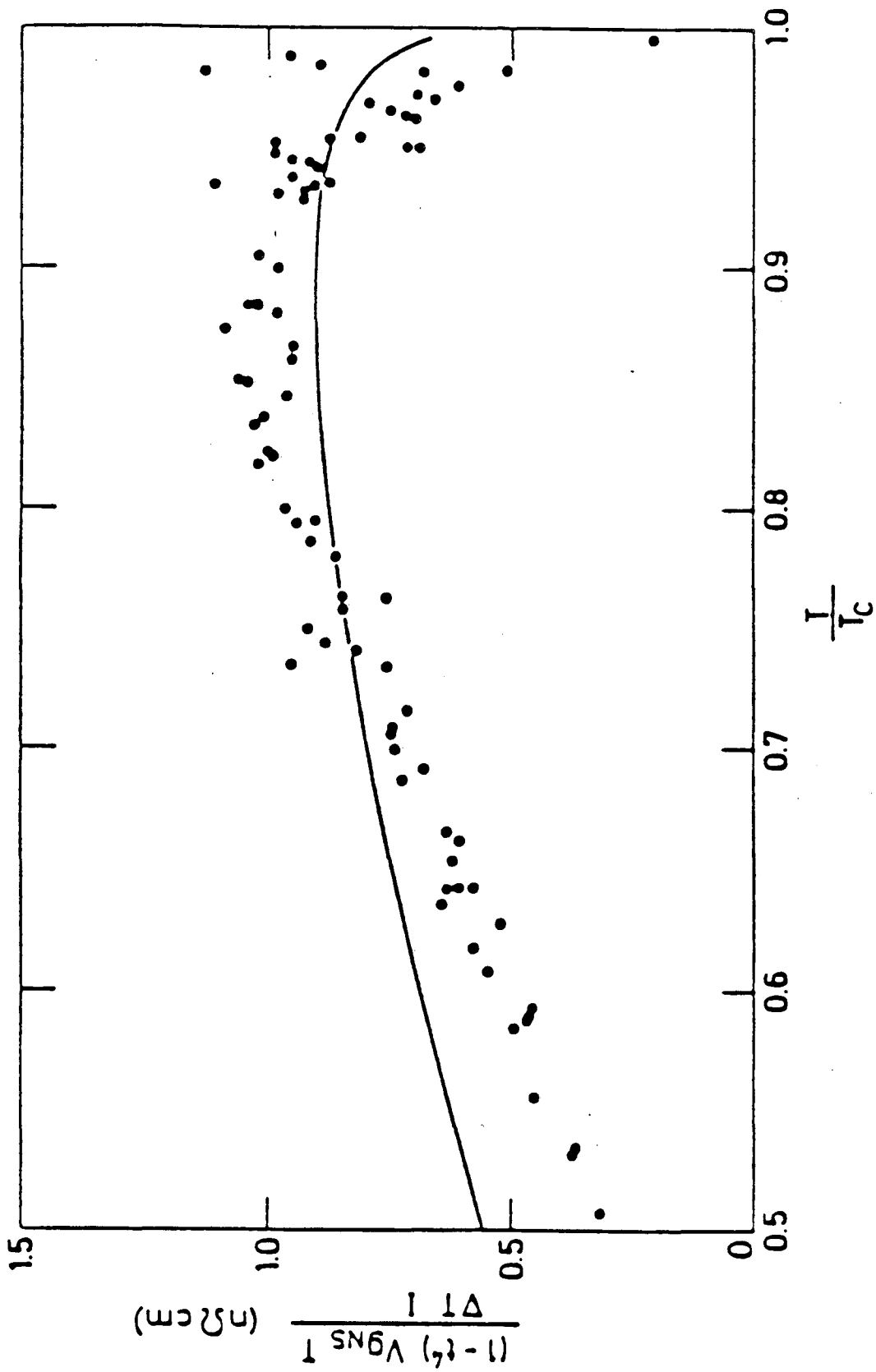


FIG. 34

XBL 841-19

U.S. Govt.

Printed in U.S.A.

This report was done with support from the Department of Energy. Any conclusions or opinions expressed in this report represent solely those of the author(s) and not necessarily those of The Regents of the University of California, the Lawrence Berkeley Laboratory or the Department of Energy.

Reference to a company or product name does not imply approval or recommendation of the product by the University of California or the U.S. Department of Energy to the exclusion of others that may be suitable.

TECHNICAL INFORMATION DEPARTMENT
LAWRENCE BERKELEY LABORATORY
UNIVERSITY OF CALIFORNIA
BERKELEY, CALIFORNIA 94720